

Optimization of Concretes and Repair Materials for Corrosion Resistance

PUBLICATION NO. FHWA-RD-99-096

SEPTEMBER 1999



PB99-175564



U.S. Department of Transportation

Federal Highway Administration

Research, Development, and Technology
Turner-Fairbank Highway Research Center
6300 Georgetown Pike
McLean, VA 22101-2296

REPRODUCED BY:
U.S. Department of Commerce
National Technical Information Service
Springfield, Virginia 22161

NTIS



FOREWORD

The deterioration of various reinforced concrete (R/C) bridge components containing conventional black steel reinforcement is a critical problem facing U.S. highway agencies. A major cause of concrete deterioration (cracking, delamination, and spalling) is the corrosion of the embedded steel reinforcement, initiated by chloride ions from deicing salts and salt water spray, that have penetrated the concrete cover. FHWA initiated this research project in 1993 directed at: (1) the quantitative identification of the corrosive conditions fostering concrete bridge deterioration and (2) the identification of concrete materials that consistently provide superior performance when used for bridge deck overlays.

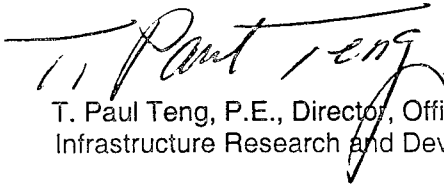
The overall scope of the project includes laboratory testing of concretes in well-controlled environments. In task A, corrosion rates and potentials were measured as a function of the environmental variables of temperature, relative humidity, and chloride concentration. The environmental corrosion map indicated that corrosion is negligible at low (43 percent) relative humidity or at low temperature (4 °C [40 °F]), even at relatively high chloride concentrations. The corrosion rate increased significantly at temperatures greater than 21 °C (70 °F) and 75 percent relative humidity.

In task B, corrosion rates and potentials were measured as a function of selected concrete properties, including water-cement ratio, air content, aggregate type, mineral admixture, and cement type. In addition to the corrosion properties, the concrete properties of chloride permeability, resistivity, and compressive strength were measured as a function of these concrete variables. General linear regression models were developed to predict performance based on these concrete variables. The effect of aggregate type was significant, with the inert (quartz) aggregates providing greater corrosion resistance and lower chloride permeability. Silica fume increased corrosion resistance, but the other mineral admixtures decreased corrosion resistance compared to no admixture. However, all mineral admixtures decreased chloride permeability. Cement type also gave mixed results for corrosion and chloride permeability.

A general optimization model was developed that provided a first estimate prediction of performance life of a concrete structure based on the climatic conditions, salting procedures, and concrete mix variables. The model indicated that a wide range of performance could be obtained by varying the concrete mix variables. Life extension was obtained by either low-chloride-permeability concrete, or corrosion-resistant concrete, or both.

This report provides insight to the effects of the environment and concrete mix components on the corrosion rates of reinforcing steel in concrete. It will be of interest to materials and bridge engineers, reinforced concrete specialists, manufacturers of admixtures and those concerned with the specification and performance of reinforced concrete bridge structures.

PROTECTED UNDER INTERNATIONAL COPYRIGHT
ALL RIGHTS RESERVED.
NATIONAL TECHNICAL INFORMATION SERVICE
U.S. DEPARTMENT OF COMMERCE


T. Paul Teng, P.E., Director, Office of
Infrastructure Research and Development

NOTICE

This document is disseminated under the sponsorship of the Department of Transportation in the interest of information exchange. The United States Government assumes no liability for its contents or use thereof. This report does not constitute a standard, specification, or regulation.

The contents of this report reflect the views of the authors, who are responsible for the facts and accuracy of the data presented herein. The contents do not necessarily reflect the official policy of the Departments of Transportation.

The United States Government does not endorse products or manufacturers. Trade or manufacturers' names appear herein only because they are considered essential to the object of this document.

Technical Report Documentation Page

1. Report No. FHWA-RD-99-096	2. Government Accession No.	3. Recipient's Catalog No.	
4. Title and Subtitle OPTIMIZATION OF CONCRETES AND REPAIR MATERIALS FOR CORROSION RESISTANCE		5. Report Date September 1999	
		6. Performing Organization Code	
7. Author(s) Neil G. Thompson and David R. Lankard		8. Performing Organization Report No. R203-01	
		10. Work Unit No. (TRAIS) 3D4d	
9. Performing Organization Name and Address CC Technologies Laboratories, Inc., 6141 Avery Road, Dublin, OH 43016-8761		11. Contract or Grant No. DTFH61-93-C-00028	
12. Sponsoring Agency Name and Address Office of Infrastructure R&D, Federal Highway Administration 6300 Georgetown Pike, McLean, VA 22101-2296		13. Type of Report and Period Covered Final Report	
		14. Sponsoring Agency Code	
15. Supplementary Notes Contracting Officer's Technical Representative (COTR): Y. Paul Virmani, HRD 1			
16. Abstract <p>A major cause of this concrete deterioration (cracking, delamination, and spalling) is the corrosion of embedded steel reinforcement, initiated by chloride ions from deicing salts and salt water spray that have penetrated the concrete cover. The research was structured to address the three principal rate phenomena that control corrosion-induced deterioration of concrete bridge components: (1) chloride permeation rate, (2) corrosion rate of the steel bar, and (3) deterioration/damage rate.</p> <p>Low chloride permeability is critical to achieving the desired life of a concrete structure. A predictive model was developed to determine the effect of concrete properties on chloride permeability. The concrete properties that had a significant effect were in order of greatest effect: mineral admixture, coarse aggregate, water-cement ratio, cement chemistry, and fine aggregate. The mineral admixture had nearly twice the effect of other concrete variables on the chloride permeability. The addition of any of the mineral admixtures tested tended to decrease the chloride permeability. Silica fume was the most effective.</p> <p>Corrosion rate is dependent on the environmental variables temperature, relative humidity, and chloride concentration and, over the range tested, each variable is equally important in establishing the corrosion rate of steel. Concrete mix designs also have a significant influence on corrosion resistance of a concrete structure. A predictive model was developed to estimate the corrosion of steel as a function of concrete mix design. The concrete mix components that had a significant effect on corrosion behavior were, in order of greatest effect: mineral admixture, fine aggregate, water-cement ratio, cement chemistry, coarse aggregate, and air content. The mineral admixture had nearly twice the effect of other concrete mix variables on the corrosion behavior of steel. Only silica fume decreased the corrosion rate to lower values than having no mineral admixture.</p> <p>Based on a limited data sample, the rate of damage (cracking/spalling) is related to the amount of corrosion product that can diffuse into the concrete matrix (i.e., the less diffusion into the concrete matrix, the greater the rate of damage). A good correlation was shown between cumulative corrosion prior to cracking and modulus of elasticity of the concrete.</p> <p>A six-step optimization model was proposed for predicting the life of a concrete structure and permitting economic analysis and optimization of resources. The model is based on prediction models developed in this research and requires input of the following by the bridge designer: (1) concrete mix components/parameters, (2) climatic conditions, and (3) frequency of salt applications.</p>			
17. Key Words Concrete, corrosion, chloride permeability, life prediction, compressive strength, modulus of elasticity, flexural strength, resistivity, temperature, relative humidity, mineral admixture, water-cement ratio.		18. Distribution Statement No restrictions. This document is available to the public through the National Technical Information Service, Springfield, VA 22161.	
19. Security Classif. (of this report) Unclassified	20. Security Classif. (of this page) Unclassified	21. No. of Pages 169	22. Price

SI* (MODERN METRIC) CONVERSION FACTORS

APPROXIMATE CONVERSIONS TO SI UNITS

APPROXIMATE CONVERSIONS FROM SI UNITS

Symbol	When You Know	Multiply By	To Find	Symbol	When You Know	Multiply By	To Find	Symbol
LENGTH								
in	inches	25.4	millimeters	mm	millimeters	0.039	inches	in
ft	feet	0.305	meters	m	meters	3.28	feet	ft
yd	yards	0.914	meters	m	meters	1.09	yards	yd
mi	miles	1.61	kilometers	km	kilometers	0.621	miles	mi
AREA								
in ²	square inches	645.2	square millimeters	mm ²	square millimeters	0.0016	square inches	in ²
ft ²	square feet	0.093	square meters	m ²	square meters	10.764	square feet	ft ²
yd ²	square yards	0.836	square meters	m ²	square meters	1.195	square yards	yd ²
ac	acres	0.405	hectares	ha	hectares	2.47	acres	ac
mi ²	square miles	2.59	square kilometers	km ²	square kilometers	0.386	square miles	mi ²
VOLUME								
fl oz	fluid ounces	29.57	milliliters	mL	milliliters	0.034	fluid ounces	fl oz
gal	gallons	3.785	liters	L	liters	0.264	gallons	gal
ft ³	cubic feet	0.028	cubic meters	m ³	cubic meters	35.71	cubic feet	ft ³
yd ³	cubic yards	0.765	cubic meters	m ³	cubic meters	1.307	cubic yards	yd ³
MASS								
oz	ounces	28.35	grams	g	grams	0.035	ounces	oz
lb	pounds	0.454	kilograms	kg	kilograms	2.202	pounds	lb
T	short tons (2000 lb)	0.907	megagrams (or "metric ton")	Mg (or "t")	megagrams (or "metric ton")	1.103	short tons (2000 lb)	T
TEMPERATURE (exact)								
°F	Fahrenheit temperature	5(F-32)/9 or (F-32)/1.8	Celsius temperature	°C	Celsius temperature	1.8C + 32	Fahrenheit temperature	°F
ILLUMINATION								
fc	foot-candles	10.76	lux	lx	lux	0.0929	foot-candles	fc
fl	foot-Lamberts	3.426	candela/m ²	cd/m ²	candela/m ²	0.2919	foot-Lamberts	fl
FORCE and PRESSURE or STRESS								
lbf	poundforce	4.45	newtons	N	newtons	0.225	poundforce	lbf
lbf/in ²	poundforce per square inch	6.89	kilopascals	kPa	kilopascals	0.145	poundforce per square inch	lbf/in ²

NOTE: Volumes greater than 1000 l shall be shown in m³.

* SI is the symbol for the International System of Units. Appropriate rounding should be made to comply with Section 4 of ASTM E380.

TABLE OF CONTENTS

	Page
CHAPTER 1. INTRODUCTION	1
CHAPTER 2. BACKGROUND.....	3
CHAPTER 3. TASK A – CORROSIVE ENVIRONMENT STUDY	7
EXPERIMENTAL APPROACH: TASK A - CORROSIVE ENVIRONMENT	
STUDY	7
Specimen Design	7
Preliminary Tests	9
Test Specimen Fabrication	9
Test Matrix	10
Chloride Incorporation	12
Humidity Control in Environmental Test Chambers	12
Measured Dependent Variables	12
RESULTS: TASK A – CORROSIVE ENVIRONMENT STUDY	13
Subtask A.1 – Mortar A2 and Conventional Reinforcing Steel	14
Subtask A.2 – Mortar A2 and Prestressed Steel Tendons	18
Subtask A.3 – Concrete A5 and Conventional Reinforcing Steel	19
Subtask A.4 – Mortar B2 and Conventional Reinforcing Steel	20
DISCUSSION: TASK A – CORROSIVE ENVIRONMENT STUDY	22
Mapping of Corrosion Rate Versus Environment	22
SUMMARY: TASK A – CORROSIVE ENVIRONMENT STUDY	26
CHAPTER 4. TASK B – CONCRETE CHEMICAL AND PHYSICAL	
PROPERTIES	27
EXPERIMENTAL APPROACH: TASK B – CONCRETE CHEMICAL AND	
PHYSICAL PROPERTIES.....	27
Environmental Variables.....	27
Material Variables	27
Concrete Mix Proportion Variables	31
Experimental Design.....	32
Measured Dependent Variables	34
RESULTS: TASK B – CONCRETE CHEMICAL AND PHYSICAL	
PROPERTIES	36
Water-Cement Ratio	36
Air Content.....	37
Coarse Aggregate	38
Fine Aggregate	40
Mineral Admixture.....	41
Cement	43
Statistical Model	45
DISCUSSION: TASK B – CONCRETE CHEMICAL AND PHYSICAL	
PROPERTIES	49

TABLE OF CONTENTS (Continued)

Effects of Independent Variables.....	49
Correlation Among Dependent Variables	50
Optimization for Corrosion Resistance	57
SUMMARY: TASK B – CONCRETE AND PHYSICAL PROPERTIES	60
CHAPTER 5. TASK C – LONG-TERM PERFORMANCE STUDIES	63
EXPERIMENTAL APPROACH: TASK C – LONG-TERM PERFORMANCE STUDIES.....	63
Selection of Task C Concretes	63
Test Specimen Design	64
Standard Concretes	66
Repair/Patch Concretes	67
Environment	70
Exposure	70
Measurements.....	71
RESULTS: TASK C – LONG-TERM PERFORMANCE STUDIES	74
Concrete Property Data.....	74
Corrosion Behavior – Standard Concretes.....	76
Corrosion Behavior – Repair/Patch Concretes.....	99
DISCUSSION: TASK C – LONG-TERM PERFORMANCE STUDIES	106
Comparison to Task B Model Predictions	106
Concrete Damage	110
SUMMARY: TASK C – LONG-TERM PERFORMANCE STUDIES	111
CHAPTER 6. TASK D – IMPLEMENTATION.....	113
STEP 1 – DETERMINE AVERAGE CLIMATIC CONDITIONS	114
STEP 2 – CORROSIVE NATURE OF AVERAGE CLIMATE	116
STEP 3 – SELECT CONCRETE MIX.....	116
STEP 4 – PREDICTION OF CORROSION AND CHLORIDE PERMEATION	117
Corrosion Rate Prediction	117
Chloride Permeation	120
STEP 5 – LIFE PREDICTION	123
Phase I – Corrosion Initiation	124
Phase II – Corrosion Propagation Until Initial Damage	124
STEP 6 – ECONOMIC ANALYSIS.....	125
SUMMARY: TASK D – IMPLEMENTATION	126
CHAPTER 7. CONCLUSIONS	127
CHLORIDE PERMEATION RATE.....	127
CORROSION RATE.....	127
DAMAGE.....	128
CONCRETE OPTIMIZATION MODEL	129
RECOMMENDATIONS	129

TABLE OF CONTENTS (Continued)

Page

APPENDIX A – CORROSION RATE, CORROSION POTENTIAL, AND CHLORIDE CONCENTRATIONS FOR TASK B EXPERIMENTS.....	131
APPENDIX B – COUPLED CURRENTS FOR SELECTED TASK C CONCRETES (nos.1, 3, 31, 37 and 38)	135
APPENDIX C – COMPLETE LPR CORROSION RATE AND POTENTIAL DATA FOR ALL SPECIMENS FOR TASK C STANDARD CONCRETES.....	139
APPENDIX D – RESULTS OF INDIVIDUAL POST-TEST EXAMINATIONS OF TASK C CONCRETES.....	149
APPENDIX E – COMPLETE LPR CORROSION RATE AND POTENTIAL DATA FOR ALL SPECIMENS FOR TASK C REPAIR MATERIALS	151

LIST OF FIGURES

	Page
Figure 1. Specimen design for short-term corrosion tests using #18 normal reinforcing steel.....	7
Figure 2. Layout for prestressing steel specimen (section view)	8
Figure 3. Effect of temperature on corrosion rate and corrosion potential for mortar A-2	15
Figure 4. Effect of relative humidity on corrosion rate and corrosion potential for mortar A-2.	15
Figure 5. Effect of chloride concentration on corrosion rate and corrosion potential for mortar A-2	16
Figure 6. Effect of temperature on corrosion rate at 43 percent relative humidity	16
Figure 7. Effect of mortar versus concrete and conventional reinforcement (C/R) versus prestressing steel reinforcement (PS/R) on corrosion rate and corrosion potential for all data averaged.	19
Figure 8. Comparison of actual chloride concentrations measured at the steel-cement interface for tests in mortar A-2 (conventional reinforcing steel), mortar A-2-PST (post-tensioning reinforcing steel), and concrete A-5 (conventional reinforcing steel)	20
Figure 9. Effect of temperature on corrosion rate and corrosion potential for mortar B-2.....	21
Figure 10. Effect of relative humidity on corrosion rate and corrosion potential for mortar B-2	21
Figure 11. Effect of chloride concentration on corrosion rate and corrosion potential for mortar B-2	21
Figure 12. Environmental map of corrosion rate for mortar A-2.....	23
Figure 13. Environmental maps of corrosion rate for mortar B-2	23
Figure 14. Environmental maps of corrosion rate for concrete A-5.....	24
Figure 15. Environmental maps of corrosion rate for a type I portland cement-based concrete adjusted for comparison of mortar A-2 and concrete A-5 data.	25
Figure 16. Logarithm of corrosion rate versus potential for the portland cementconcretes tested in task B	51
Figure 17. Photographs of typical corrosion in the aggressive environment in task B.....	52
Figure 18. Logarithm of corrosion rate versus potential for the portland cement concretes tested In Task A And B combined (individual test specimen data is given).....	53
Figure 19. Rapid chloride permeability versus 1/resistivity for task B portland cement concrete.	54
Figure 20. Corrosion rate versus 1/resistivity in the aggressive environment for task B portland cement concrete.	55
Figure 21. Corrosion rate versus 1/resistivity in the moderate environment for task B portland cement concrete	55
Figure 22. Corrosion rate versus chloride concentration for mix nos. 28 and 3 in task B	56

LIST OF FIGURES (Continued)

Figure 23. Corrosion rate versus chloride concentration for all Portland cements in task B	57
Figure 24. Schematic of task C standard slab specimen	65
Figure 25. Schematic of task C repair/patch slab specimen	66
Figure 26. Percentage of water loss during initial drying exposure for task C concretes	71
Figure 27. Schematic showing chloride analysis locations.	72
Figure 28. Coupled current measurement using zero resistance ammeter (ZRA)	73
Figure 29. LPR corrosion rate measurement for the center steel bar	73
Figure 30. Averaged coupled current versus time for concrete no. 24.	78
Figure 31. Coupled current versus time for individual cycled exposure specimens for concrete no. 24.	78
Figure 32. Coupled current versus time for individual continuously wet exposure specimens for concrete no. 24	79
Figure 33. Averaged coupled current versus time for concrete no. 15R	79
Figure 34. Averaged coupled current versus time for concrete no. 11.	80
Figure 35. Averaged coupled current versus time for concrete no. 29.	80
Figure 36. Averaged coupled current versus time for concrete no. 22	81
Figure 37. Coupled currents for concrete no. 11 (slab 11D) during A wet-dry cycle	81
Figure 38. Humidity for concrete no. 11 (slab 11D) during a wet-dry cycle	82
Figure 39. Temperature for concrete no. 11 (slab 11D) during A wet-dry cycle.	82
Figure 40. Photograph of concrete slab 22F showing cracking over center steel bar and cracking of side (right steel bar)	88
Figure 41. Photograph of concrete slab 11C showing cracking over right steel bar and none over the center steel bar.	89
Figure 42. Photograph of steel bars from concrete no. 15R, slab A.	91
Figure 43. Cross-sectional view of steel bar in slab 15R-B showing cracking in the concrete matrix, but not extending to the slab surface	95
Figure 44. Close-up of cross-section shown in figure 43	96
Figure 45. Cross-sectional view for slab 15R-B shows diffusion of corrosion product into concrete matrix	96
Figure 46. Cross-sectional view of steel bar in slab 22-B with cracks highlighted (the top crack extends to the slab surface)	97
Figure 47. Close-up of cross-section from figure 46 showing diffusion of steel corrosion product into the porous coarse aggregate	97
Figure 48. Close-up of cross-section from figure 46 showing limited diffusion of steel corrosion product along the fracture plane surfaces	98
Figure 49. Averaged coupled current versus time for standard slab repair material no. 40	99
Figure 50. Averaged coupled current versus time for standard slab repair material no. 41	100
Figure 51. Averaged coupled current versus time for repair slab material no. 40	101

LIST OF FIGURES (Continued)

Figure 52. Averaged coupled current versus time for repair slab material no. 41.....	101
Figure 53. Averaged coupled current versus time for repair slab material no. 42.....	102
Figure 54. Averaged coupled current versus time for repair slab material no. 43.....	102
Figure 55. Photograph of repair slab 43D showing typical cracking.....	104
Figure 56. Plot of chloride permeability (task B) versus chloride concentration (task C).....	108
Figure 57. Plot of corrosion rate for task B model predictions versus task C data.....	109
Figure 58. Flow diagram for concrete optimization.....	113
Figure 59. Environmental map for corrosion as a function of temperature and relative humidity.....	114
Figure 60. Four classes of conditions based on ability to sustain corrosion.....	115
Figure 61. Chloride permeability model prediction versus chloride concentration per cycle.....	122
Figure 62. Coupled current versus time for concrete no. 1.....	135
Figure 63. Coupled current versus time for concrete no. 3.....	136
Figure 64. Coupled current versus time for concrete no. 31.....	136
Figure 65. Coupled current versus time for concrete no. 37.....	137
Figure 66. Coupled current versus time for concrete no. 38.....	137

LIST OF TABLES

Table 1. List of variables that influence corrosion of steel in concrete.....	3
Table 2. Mortar and concrete compositions for task A tests.....	11
Table 3. Comparison of shrp and germann methods of chloride analysis.....	13
Table 4. Corrosion rate statistical regression analyses for mortar A-2.....	17
Table 5. Corrosion potential statistical regression analyses for mortar A-2.....	18
Table 6. Comparison of corrosion rates for concrete A-5 and mortar A-2.....	25
Table 7. Summary of material variables considered in the research.....	28
Table 8. Cements used in task B.....	29
Table 9. Fine aggregates used in task B.....	30
Table 10. Coarse aggregates (ASTM C33-90, no. 8 gradation) used in task B.....	31
Table 11. Example of three concrete mix designs for task B.....	32
Table 12. Experimental matrix of mix designs for task B.....	33
Table 13. Summary of water-cement ratio data for the concrete property variables: rapid chloride permeability, resistivity, and compressive strength.....	36
Table 14. Summary of water-cement ratio data for the corrosion variables: corrosion rate, potential, and chloride concentration.....	37
Table 15. Summary of air content data for the concrete property variables: rapid chloride permeability, resistivity, and compressive strength.....	37
Table 16. Summary of air content data for the corrosion variables: corrosion rate, potential, and chloride concentration.....	38

LIST OF TABLES (Continued)

Table 17.	Summary of coarse aggregate data for the concrete property variables: rapid chloride permeability, resistivity, and compressive strength.....	39
Table 18.	Summary of coarse aggregate data for the corrosion variables: corrosion rate, potential, and chloride concentration	40
Table 19.	Summary of fine aggregate data for the concrete property variables: rapid chloride permeability, resistivity, and compressive strength.....	40
Table 20.	Summary of fine aggregate data for the corrosion variables: corrosion rate, potential, and chloride concentration	41
Table 21.	Summary of mineral admixture data for the concrete property variables: rapid chloride permeability, resistivity, and compressive strength.....	42
Table 22.	Summary of mineral admixture data for the corrosion variables: corrosion rate, potential, and chloride concentration	43
Table 23.	Summary of cement data for the concrete property variables: rapid chloride permeability, resistivity, and compressive strength.....	44
Table 24.	Summary of cement data for the corrosion variables: corrosion rate, potential, and chloride concentration.....	45
Table 25.	General linear model for main effect terms for rapid chloride permeability after 90 days.	47
Table 26.	General linear model for main effect terms for compressive strength after 90 days.....	47
Table 27.	General linear model for main effect terms for corrosion rate (mpy) in the moderate environment	48
Table 28.	General linear model for main effect terms for corrosion rate (mpy) in the aggressive environment.	49
Table 29.	Summary of effects for the independent variables on the measured dependent variables.....	50
Table 30.	Levels of each independent variable ranked according to corrosion resistance for corrosion rate (moderate and aggressive environments) and rapid chloride permeability	58
Table 31.	Optimizing concrete deterioration resistance based on the concretes tested in task B.....	60
Table 32.	Concretes selected for task C.....	63
Table 33.	Ranking of concretes selected for task C	64
Table 34.	Concrete mix designs selected for task C concretes	67
Table 35.	Example of mix designs for concrete nos. 31, 37, and 38	69
Table 36.	Repair/patch concrete mix designs selected for task C	70
Table 37.	Compressive strength data for task C concretes	74
Table 38.	Flexural strength data for the task C concretes	75
Table 39.	Modulus of elasticity for the task C concretes.....	76
Table 40.	Resistivity of the task C concretes.....	76
Table 41.	Average corrosion rates and potentials for the coupled bar (center) in task C	83
Table 42.	Average corrosion rate and potential data for the three steel bars in each of the slabs where corrosion had initiated	84

LIST OF TABLES (Continued)

Table 43. Comparison of LPR and coupled current corrosion rates for task C concretes	85
Table 44. Time to corrosion initiation for the task C concretes	86
Table 45. Time to cracking for the task C concretes.....	87
Table 46. Final chloride concentrations for task C concretes	90
Table 47. Summary of measured corrosion variables compared to post-test visual examination	92
Table 48. Constituents of concretes evaluated in the petrographic examination.....	93
Table 49. Corrosion activity of reinforced concrete slabs in task C study.....	94
Table 50. Corrosion rate and potential for standard slab repair materials	103
Table 51. Corrosion rates and potentials for the steel bars in the repair slabs.....	104
Table 52. Chloride concentrations for standard slab repair materials.....	106
Table 53. Chloride concentrations for the repair slabs	106
Table 54. Comparison of normalized data for rapid chloride permeability model predictions (table 32) and chloride concentration at the steel surface from task C (table 46)	107
Table 55. Comparison of corrosion rate from task B model predictions with task C data	109
Table 56. Comparison of cumulative corrosion prior to cracking to mechanical properties	111
Table 57. Example calculation for step 4	117
Table 58. Corrosion rate index calculation for base concrete and design concrete example (see table 28).....	119
Table 59. Prediction model for rapid chloride permeability	121
Table 60. Corrosion rate predictions for several example concretes	125
Table 61. Phases I and II life predictions for example concretes.....	126
Table 62. Concrete nos. 1, 2, 3, 4, 5R, 6, and 7	131
Table 63. Concrete nos. 8, 9, 10, 11, 12, 13, and 15R.....	132
Table 64. Concrete nos. 16, 17, 18, 19, 20, 21, and 22	133
Table 65. Concrete nos. 23, 24, 25, 26, 27, 28, 29, and 30	134
Table 66. Concrete no. 1	139
Table 67. Concrete no. 3	140
Table 68. Concrete no. 11	141
Table 69. Concrete no. 15R.....	142
Table 70. Concrete no. 22	143
Table 71. Concrete no. 24	144
Table 72. Concrete no. 29	145
Table 73. Concrete no. 31	146
Table 74. Concrete no. 37	147
Table 75. Concrete no. 38	148
Table 76. Percentage of corrosion coverage for task C concretes.	149
Table 77. Concrete surface condition of task C concretes	150
Table 78. Repair material no. 40 standard slab.....	151

LIST OF TABLES (Continued)

Table 79. Repair material no. 41 standard slab.....	151
Table 80. Repair material no. 42 standard slab.....	152
Table 81. Repair material no. 43 standard slab.....	152
Table 82. Repair material no. 40 repair slab.....	153
Table 83. Repair material no. 41 repair slab.....	153
Table 84. Repair material no. 42 repair slab.....	154
Table 85. Repair material no. 43 repair slab.....	154

CHAPTER 1. INTRODUCTION

This is the Final Report on FHWA project "Corrosion Protection Systems for Bridges in Corrosive Environments" (FHWA Contract No. DTFH61-93-C-00028). Previously published report "Improved Concretes for Corrosion Resistance" (Publication No. FHWA-RD-96-207, May 1997) provided details on tasks A and B of the above-referenced FHWA project. This report reviews tasks A and B and provides details of tasks C and D, as well as the final analysis and conclusions on the overall project.

The deterioration of various reinforced concrete (R/C) bridge components containing conventional black steel reinforcement is the most important problem facing U.S. highway agencies. A major cause of this concrete deterioration (cracking, delamination, and spalling) is the corrosion of the embedded steel reinforcement, initiated by chloride ions from deicing salts and salt-water spray that have penetrated the concrete cover. A similar problem exists for prestressing steel in prestressed concrete (PS/C) bridge components exposed to deicing salts and marine environments. For PS/C bridge components, in addition to the corrosion-induced concrete deterioration, corrosion-induced hydrogen embrittlement of prestressing steel may eventually compromise the structure's safety and its ability to carry the normal structural loads.

The historical approach to this problem has involved small-area patching on all bridge components, and complete overlays on bridge decks. These conventional rehabilitation methods have involved a wide variety of repair strategies, and dozens of different repair materials. No single repair (patch) material has evolved as the optimum solution to the problem.

In response to this situation, the Federal Highway Administration (FHWA), in 1992, issued a Broad Agency Announcement (no. DTFH61-92-R-000137) to solicit research proposals aimed at improving rehabilitation technology for corrosion-induced deterioration of bridges. FHWA initiated this research project directed at the quantitative identification of the corrosive conditions fostering concrete bridge deterioration, and at the identification of concrete materials that consistently provide superior performance when used for bridge deck overlays and for the repair of other concrete bridge members. It was also envisioned that this work would lead to the identification of concretes that are cost-effective for the construction of new bridge members, in addition to successfully resisting corrosion-induced concrete deterioration in the presence of well-defined corrosive conditions.

The present research project was initiated during January 1993, in answer to this need. The research approach was structured to address the three principal rate phenomena that control corrosion-induced deterioration of concrete bridge components. These phenomena are identified as:

1. Diffusion of chloride ions to the level of the reinforcing steel (chloride diffusion rate).
2. Corrosion of the reinforcing steel once passivity has been destroyed by the presence of the chloride ion (rate of corrosion).
3. Cracking/spalling distress in the concrete as a result of the build-up of steel corrosion

products (rate of deterioration).

The experimental phase of this project had as its goals: (1) quantify the effects of environmental variables on the corrosion of reinforcing steel in concrete and (2) quantify the effects of concrete mix variables on the corrosion-induced deterioration of concrete. To accomplish this, the experimental program is divided into three tasks:

- Task A - Corrosive Environment Study.
- Task B - Concrete Chemical and Physical Properties.
- Task C - Long-Term Corrosion Performance.

In task A, laboratory experiments were conducted to characterize the corrosive environment and to establish boundary conditions for moisture content, chloride content, and temperature levels for corrosion initiation and propagation.

Task B focused on identification of the chemical and physical characteristics of concretes as they relate to the rate of corrosion of embedded reinforcing steel. Corrosive environments used in task B were selected on the basis of results obtained in the task A work.

Task C provided simulation and measurement of all three of the phenomena that control corrosion-induced deterioration of concrete structures. These include the chloride diffusion rate in the concrete, the rate of corrosion of the steel once corrosion is initiated, and the rate of deterioration of the concrete during the build-up of corrosion products. The primary focus of task C was to validate the prediction models of tasks A and B using larger scale slab specimens.

Task D provided the final analysis of the research findings. Task D consolidated the research of tasks A, B, and C, along with economic considerations to define the optimum concrete based on environment, concrete constituents and properties, expected life, and economics.

CHAPTER 2. BACKGROUND

Over the past 60 years or so, an enormous amount of energy has been expended in laboratory and field studies of reinforced concrete to characterize the nature of the corrosion-induced damage phenomenon, and to identify preventative and remedial solutions. Despite this effort, it is still not possible to identify the “ideal” concrete to provide “optimum” performance in a particular corrosive environment situation.

What has been learned in the previous and ongoing research investigations is that there are many material, design, and environmental variables that can affect both the corrosion process itself, and the extent of damage resulting from the corrosion process. Table 1 provides a list of these variables.

Table 1. List of variables that influence corrosion of steel in concrete.

Material Variables	Environmental Variables	Design Variables
Concrete Chemistry	Aggressive Anions	Depth of Cover
pH of Pore Water	Cl ⁻	Cracking
Cl ⁻ /OH ⁻ Ratio of Pore Water	SO ₄ ⁻²	Size of Rebar
Cl ⁻ Binding Ability	Temperature Cycles	Spacing of Rebar
Concrete Physical/Mechanical Properties	Relative Humidity	Drainage of Structure
Permeability	Moisture Content	
Porosity	Environmental Cycling	
Compressive Strength	Loading	
Bond Strength		
Flexural Strength		
Modulus of Elasticity		
Electrical Resistance		
Concrete Mix Proportion Variables		
Water-Cement Ratio		
Air Content		
Hardened Concrete Free Water Content		

It is widely known and accepted that reinforcing steel in Portland cement concrete will exhibit negligible corrosion such that cracking and spalling distress is never manifested unless one of three conditions occur: (1) chloride contamination, (2) carbonation, or (3) cracking of the concrete. It is only when one or more of these three conditions occur that corrosion of reinforcing steel can initiate and be sustained. Intrusion of chloride-bearing solutions to the level of reinforcing steel can break down the normal passive film on the steel and result in localized corrosion. Carbonation of the concrete to the level of the reinforcing steel decreases the pH of the concrete (normally 12.5 to 13.5) and results in active corrosion. Corrosion products have a greater volume than the steel. Therefore, corrosion caused damage (cracking and spalling) of the concrete by creating expansion forces associated with the reinforcing steel, placing the top layer of concrete

in tension. Cracking of the concrete due to mechanical forces can hasten the onset of corrosion by providing oxygen, water, and chlorides with direct access to the reinforcing steel.

Because of the dominant role played by chloride in the corrosion process, the vast majority of research designed to make concrete more “protective” focuses on changes to the concrete that can reduce the rate of chloride ingress. Once chloride reaches the level of reinforcing steel in concrete, corrosion is inevitable if oxygen and moisture are available. However, following the initiation of corrosion, both the rate of corrosion and the subsequent rate of damage arising from the corrosion process depend upon many factors that, at present, are not well understood.

Much of the treatment of the steel corrosion problem in the literature is concerned with material and design variables that will increase the time required for chloride ions to reach the level of reinforcing steel. A lesser amount of the literature is concerned with chemical factors that influence the onset and rate of corrosion once the chloride has reached the steel level. A detailed review of the literature was presented in the interim report (FHWA-RD-96-207) and is summarized below.

The literature review was focused on the three main rate processes that control the time of onset of corrosion, as well as the deterioration of the concrete to the point that the structure requires repair or is no longer serviceable. These rate processes include: (1) the chloride diffusion rate, (2) the corrosion rate, and (3) the rate of corrosion-induced damage. The review of the literature, in this context, leads to the following conclusions and observations:

- Historically, the greatest research effort has been on a study of factors affecting the chloride diffusion rate.
- Within the last 10 to 15 years, there has been a significant increase in studies focused on factors affecting the rate of corrosion once chloride reaches the level of the reinforcing steel.
- The rate of corrosion-induced damage in reinforced concrete has been largely neglected in the literature. This is due, in part, to the difficulty in reproducing field conditions in laboratory environments, and to the long times required for damage to occur and progress.
- Concrete compositional variables that influence the diffusion rate of chloride ions into concrete have been well studied and well defined. Concretes showing high levels of resistance to chloride ion penetration have been prepared using low water-cement ratios and mineral admixtures. Low water-cement ratios are achieved through the use of high-range water reducers (superplasticizers). Of the mineral admixtures that are available, silica fume provides the greatest and most consistent reduction in chloride ion penetration rates into concrete.

- Factors that have been shown to affect the corrosion of embedded reinforcing steel in concrete, once chloride ions reach the steel, include: (1) pore water chemistry, (2) concrete ionic conductivity, (3) concrete microstructure, and (4) temperature and relative humidity. A primary variable controlling rate of corrosion is the Cl^-/OH^- ratio of the pore water solution.
- For most reinforced concrete structures that are exposed to extraneous sources of chloride (deicing salts, seawater), the chloride source may be viewed as inexhaustible. It has been well established that the Cl^-/OH^- ratio of the pore water in the concrete surrounding the steel controls the rate of corrosion (the higher this ratio, the higher the rate of corrosion). However, with an inexhaustible supply of chloride ion, it appears useless to control concrete compositional variables that maximize the hydroxyl concentration in the pore water.
- With an inexhaustible supply of chloride ions, it is necessary to concentrate concrete compositional studies on factors that affect the rate of corrosion once high chloride levels are achieved (i.e., oxygen diffusion to the steel reinforcement, the ionic conductivity of the concrete surrounding the reinforcement, and other compositional variables [e.g., cement chemistry, cement content, admixture type, aggregate properties]).
- The phenomenon of pitting corrosion of reinforcing steel in chloride-contaminated concrete is a well-known, but little studied, phenomenon. A systematic study of the influence of local concrete microstructure relative to this phenomenon should be fruitful. Even in the limited studies conducted to date in this area, there is disagreement as to what concrete microstructure features promote pitting corrosion.

CHAPTER 3. TASK A — CORROSIVE ENVIRONMENT STUDY

The purpose of task A was to establish boundary conditions for the environmental parameters of moisture, chlorides, and temperature on the corrosion rate of reinforcing steel embedded in concrete.

EXPERIMENTAL APPROACH: TASK A — CORROSIVE ENVIRONMENT STUDY

Specimen Design

Figure 1 shows the type of specimen configuration used in task A. This specimen design is rather novel, but it facilitates evaluation of both corrosion product phases and interfacial chemistry of the concrete/cement phase.

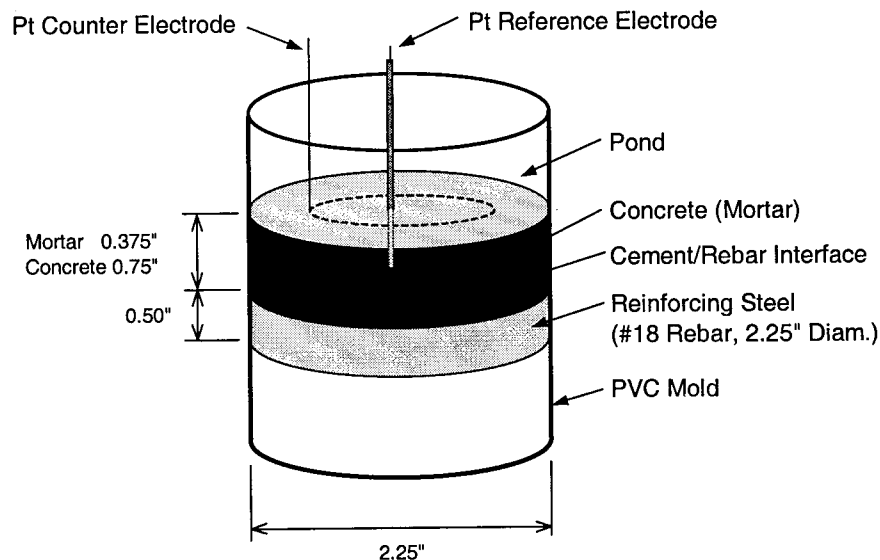


Figure 1. Specimen design for short-term corrosion tests using #18 normal reinforcing steel. [1 in = 2.54 cm]

For a majority of the task A tests, it was decided that a mortar would be used. A normal concrete mix contains cement, water, and coarse and fine aggregates. A mortar is essentially the same but without the coarse aggregates. In all reinforced concrete materials, the interface surface of the concrete in contact with the reinforcing steel is composed principally of the fine particulate materials in the concrete (minus 100-mesh material). This includes the hydrated portland cement phases, any finely divided particulate additives such as silica fume, slag, or flyash, and a small contribution of fine particulate material from the fine aggregate or the coarse aggregate phase. Only rarely do actual fine or coarse aggregate particles greater than 0.15 mm (0.006 in) come in contact with the reinforcing steel.

The specimen design was such that the concrete (mortar) environment was in contact with the cross-sectional face of the reinforcing steel bar rather than the circumferential area. The steel specimen was a #18 (57-mm-(2.25-in-diameter) steel bar about 12.7 mm (0.5 in) long. Except for the cross-sectional interface, which was in contact with the mortar and had a uniform surface finish, all other areas of the steel were sealed with an epoxy compound. The steel specimen was snugly fitted into a plastic mold (a polyvinyl chloride [PVC] pipefitting) and a 9.5-mm (0.375-in) layer of mortar was cast onto the cross-sectional area (for concrete specimens, a 19-mm [0.75-in] cover was used). A reference electrode and a counter electrode, both made of platinized niobium wire, were incorporated into the mortar so that they were isolated from each other and the steel.

The specimen design for the prestressing steel was slightly different from the conventional steel bar specimens. Since large-diameter prestressing steel was not available, strand tendons had to be used. The cross-sectional area consisted of a bundle of seven 7-strand tendons tied together. Again, as in the case of the conventional steel bar specimens, a 9.5 mm (0.37-in) layer of mortar is cast onto the cross-sectional surface incorporating the wire tendons. A layout of the prestressing steel tendons is shown in figure 2.

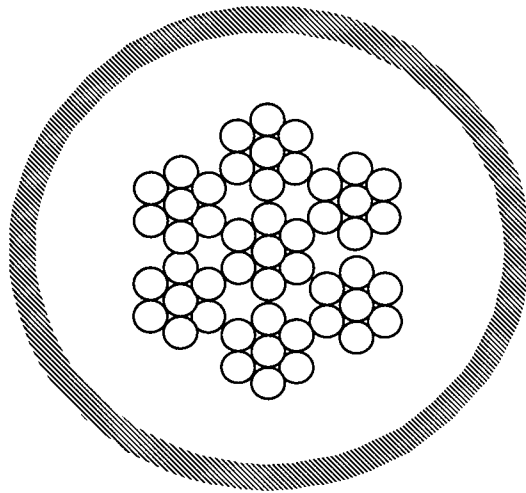


Figure 2. Layout for prestressing steel specimen (section view).

Preliminary Tests

Using the specimen design discussed above, preliminary tests were performed to examine certain aspects of the design and subsequent test procedures:

- Optimum Cover. Tests indicated that a mortar thickness of 6.4 mm (0.25 in) would survive the planned drying cycle free of defects. However, because it was more difficult to incorporate the test electrodes in the specimen, it was decided to use a thickness of
- 9.5 mm (0.375 in). For concrete specimens, the size of the coarse aggregates dictates the minimum thickness, that is, 19 mm (0.75 in) or twice the diameter of the largest aggregate size.
- Loss of Moisture. The non-evaporable water in the concrete (or mortar) is considered as being 20 percent of the cement weight. The moisture loss tests indicated that the evaporable water in the mortar is not easily removed at ambient temperatures. At a higher temperature (38 °C, [100 °F]) and with the application of simultaneous vacuum, the moisture removal was markedly improved. For the 6.4- mm (0.25-in) sample, about 90 percent of the evaporable water could be removed under heat and vacuum. An even higher temperature of 60 °C (140 °F) resulted in further moisture loss. However, the specimens developed a few cracks at this higher temperature. Hence, the treatment for removal of the evaporable water from the specimens was decided to be 38 °C (100 °F) with simultaneous vacuum.
- Rate of Chloride Ingress. To incorporate chloride into the mortar specimens, it was decided to use chloride solution ponding on the cured and dried specimens instead of initially mixing the chloride with the mortar. With ponding, the chloride is introduced into the mortar matrix by a process of diffusion, which simulates a real-life situation. Theoretical calculations were made to estimate the chloride concentration of the ponding solution that would be required to achieve a certain level of chloride in the mortar (based on weight percent of mortar and the replacement of free water with chloride solution). The mortar samples were first dried at 38 °C (100 °F) under vacuum for about 48 h prior to ponding with the chloride solutions. Ponding was carried out at 38 °C (100 °F) to facilitate the chloride uptake by the samples. Fourteen days of ponding was required to achieve 90 percent of the theoretically calculated chloride concentration in the mortar.

Test Specimen Fabrication

A total of 198 samples were fabricated for the short-term tests that were all instrumented for corrosion potential and corrosion rate measurements under the different experimental conditions (see test matrix section). It was decided to make additional specimens for chloride analysis under each set of test conditions at the beginning and during the progress of the tests. It was estimated that 102 additional specimens would

be required. Thus, a total of 300 specimens were made using two types of mortar, one type of concrete, and two types of reinforcing steel.

Both the reference and counter electrodes were fabricated from platinized niobium wire (niobium wire with 100-micron platinum coating). The steel surface in contact with the mortar was given an 80-grit finish. Except for the face in contact with the mortar (or concrete), the exposed parts of the steel were covered with a thin coating of coal tar epoxy. Recall that #18 steel bar, with a diameter of 57.2 mm (2.25 in), was used as the conventional reinforcing steel and that it is the cross-sectional surface of the steel bar that is in contact with the mortar. The total surface area of the steel in contact with the mortar was 2,548 mm² (3.98 in²).

The prestressed specimens contained seven 7-wire strands (figure 2). The steel wires used in this study had a diameter of 4.8 mm (0.187 in). To ensure that there was electrical continuity between the individual wires and throughout the composite bundle, a conductive coating was painted on the backside of the specimen. A small screw with a soldered wire was then installed into the bundle for subsequent electrical connection to the specimen. Finally, this surface was coated with coal tar epoxy. The cross-section surface, which received the mortar, was given an 80-grit finish. Altogether there are 49 wires in the composite bundle. The total surface area of the prestressed steel in contact with the mortar was 871 mm² (1.35 in²).

All specimens were given a 28-day cure at room temperature by ponding with saturated calcium hydroxide solution.

Test Matrix

The variables included in the task A test matrix were:

- Mortar/concrete composition.
- Reinforcing steel type.
- Ambient environment.

The mortar/concrete variables tested included two mortars (A-2 and B-2) and one concrete (A-5). Table 2 presents the mortar and concrete compositions. The only difference in mortar A-2 and concrete A-5 is that concrete A-5 contains coarse aggregate. The primary difference in mortars A-2 and B-2 was the pH (A-2 had a pH of 12 to 13 and B-2 had a pH of 9 to 10).

Table 2. Mortar and concrete compositions for task A tests.

Composition ID	Cement	Sand	Coarse Aggregate	Water-Cement Ratio
Mortar A-2	Medusa Type-I Portland Cement	Sidley Quartz	None	0.45
Mortar B-2	Lumnite Calcium Aluminate	Sidley Quartz	None	0.45
Concrete A-5	Medusa Type-I Portland Cement	Sidley Quartz	Sidley Quartz #8	0.45

The two types of reinforcing steel included in the test matrix were conventional reinforcing steel bars and prestressed tendons (7-wire).

The environmental variables included in the test matrix were:

- Chloride concentration.
- Relative Humidity.
- Temperature.

The levels of the environmental variables were selected to provide a realistic range to which bridge structures are exposed. Three levels were selected for each of the environmental variables. The levels were designed to provide low, moderate, and high conditions for each variable.

The levels selected were:

- Chloride concentration at 0.6, 1.8, and 6 kg/m³ (1, 3, and 10 lb/yd³).
- External relative humidity at 43, 75, and 98 percent.
- Temperature at 4, 21, and 38 °C (40, 70, and 100 °F).

A full factorial matrix of these three variables, each at three levels, gives a matrix of 27 test conditions. Triplicate specimens were tested for each environmental condition.

A full matrix of tests was performed for two mortars (A-2 and B-2) using conventional reinforcing steel specimens. For the concrete (A-5), tests were performed in triplicate for a single temperature (21 °C [70 °F]), two humidities (75 percent and 98 percent), and three chlorides (0.6, 1.8, and 6 kg/m³ [1, 3, and 10 lb/yd³]). For the pre-stressing steel tendons, tests were performed for the same conditions as concrete A-5.

Chloride Incorporation

The specimens were thoroughly dried after the 28-day curing cycle to facilitate chloride uptake. The following sequence was followed to prepare the samples before exposing them to the various environmental conditions:

1. Dry samples at 38 °C (100 °F) in a controlled temperature room for 7 days.
2. Apply epoxy concrete sealant (Sikagard) to joint between mortar and plastic mold.
3. Dry under vacuum at 38 °C (100 °F) for 2 additional days.
4. Pond with 6 mL of the desired chloride solution for 14 days at 38 °C (100 °F). Ponding was carried out within an hour after completing step 3.
5. Rinse off any excess chloride solution from the specimen surface after the 14-day ponding period, pat dry with tissue, and place them in the environmental chambers.

Weight checks after the drying cycle indicated that samples lost approximately 90 to 95 percent of the theoretical evaporable water. Control samples pulled down at intermediate times during and following ponding indicated that the desired chloride levels at the steel surface were achieved.

Humidity Control in Environmental Test Chambers

Humidity control in the environmental test chambers was achieved with the help of a layer of saturated salt solution placed at the bottom of the chamber. This method of humidity control is well established (ASTM E104 – “Maintaining Constant Relative Humidity by Means of Aqueous Solutions”). Each of the test chambers (444 mm by 356 mm by 165 mm [17.5 in by 14 in by 6.5 in]) was filled with 1 L of the required salt solution, which gave an approximate 19-mm (0.75-in) layer of the solution at the bottom. The samples (24 in each chamber) were supported on a plastic grid above the surface of the solution. The actual humidity and temperature in each chamber was measured with a Thermo-hygrometer and were found to be within 2 to 3 percent (or degrees) of the desired values.

Measured Dependent Variables

The measured dependent variables in task A included:

- Corrosion potential.
- Corrosion rate.
- Chloride concentration at the steel surface.

The potential of each specimen with respect to a copper/copper sulfate electrode (CSE) was measured periodically during the exposure period.

Two measurement systems were used to more accurately determine the polarization resistance: the PR Monitor 4500 by CC Technologies Systems, Inc. and the Solartron Models 1255 and 1286 electrochemical impedance spectroscopy (EIS) measurement system. The PR Monitor 4500 performed a solution resistance measurement

to correct the polarization resistance. In several of these specimens, the solution resistance was quite high compared to the polarization resistance, which made accurate determination of the polarization resistance difficult. The two measurement systems gave comparable results for corrosion rates.

Chloride concentrations in the mortar (concrete) test specimens were measured with a portable test kit manufactured by Germann Instruments. The accuracy of the test kit was confirmed during this project by conducting parallel analysis using the method developed by the Strategic Highway Research Program (SHRP). The comparative results, given in table 3 for eight different mortar samples, show that there is very good correlation between the Germann and the SHRP methods.

Table 3. Comparison of SHRP and Germann methods of chloride analysis.

Sample No.	% Chloride**	
	SHRP Method*	Germann Method
1	0.23	0.19
2	0.11	0.12
3	0.28	0.34
4	0.77	0.88
5	0.82	0.91
6	0.74	0.78
7	0	0
8	0.74	0.8

* Standard solutions of 1.25, 0.60, 0.30, 0.03, and 0.01 percent were used to calibrate probe.

** Based on dry concrete weight.

RESULTS: TASK A — CORROSIVE ENVIRONMENT STUDY

The following results are summarized from the interim report (FHWA-RD-96-207). Task A was divided into four subtasks, corresponding to the mortars (or concrete) and/or type of reinforcing steels evaluated:

- Subtask A.1 - Mortar A-2 and Conventional Reinforcing Steel.
- Subtask A.2 - Mortar A-2 and Prestressed Steel Tendons.
- Subtask A.3 - Concrete A-5 and Conventional Reinforcing Steel.
- Subtask A.4 - Mortar B-2 and Conventional Reinforcing Steel.

Subtasks A.1 and A.4 utilized the full factorial matrix of independent variables with triplicate specimens:

- Temperature at 4, 21, and 38 °C (40, 70, and 100 °F).
- Relative Humidity at 43, 75, and 98 percent.
- Chloride concentration at 0.6, 1.8, and 6 kg/m³ (1, 3, and 10 lb/yd³).

Subtasks A.2 and A.3 utilized a full factorial matrix, but with the following independent variables with triplicate specimens:

- Temperature at 38 °C (70 °F).
- Relative Humidity at 75 and 98 percent.
- Chloride concentration at 0.6, 1.8, and 6 kg/m³ (1, 3, and 10 lb/yd³).

Subtask A.1 — Mortar A-2 and Conventional Reinforcing Steel

Individual Independent Variable Analysis

In the following analysis, all of the data for a single level of a particular independent variable was averaged and the three different levels for that variable were compared. Figure 3 shows the effect of temperature on corrosion rate and corrosion potential for mortar A-2. Figure 3a shows that as temperature increases, corrosion rate increases. The average of a 1.4 mpy (0.035-mm/yr) corrosion rate at the high temperature includes data for all three relative humidities and all three chloride concentrations tested. It is interesting to note that an increase in temperature makes the corrosion potential more positive (figure 3b plots negative potential). This is the opposite effect expected based on the corrosion rate shown in figure 3a. This indicates one of the problems in attempting to establish a relationship between potential and corrosion rate. There are several variables that affect this relationship that must be taken into account.

Figure 4 shows the effect of relative humidity on corrosion rate and corrosion potential. Figure 4a shows that corrosion rate increases with increasing relative humidity, with a large increase from 75 to 98 percent. Figure 4b shows that there is not a large effect of relative humidity on corrosion potential. These data do not address fully saturated conditions (ponded) that can limit oxygen content within the concrete and affect the corrosion potential.

Figure 5 shows the effect of chloride concentration on corrosion rate and corrosion potential. Figure 5a shows that at 0.6 kg/m³ (1 lb/yd³), the corrosion rate is negligible, at 1.8 kg/m³ (3 lb/yd³), corrosion can occur (although the average for all conditions tested is relatively low); and at 6 kg/m³ (10 lb/yd³), a large increase in the average corrosion rate is observed. At 6 kg/m³ (10 lb/yd³), relatively high corrosion rates were observed in all conditions tested, with the exception of low temperature and low humidity. The corrosion potential becomes more negative with increasing chloride concentration. It should be noted that in these tests, the chloride concentrations measured during post-test examination

were relatively close to the targeted chloride concentrations. The following are the averages for each chloride level:

0.6 kg/m³ – Average was 0.9 kg/m³.
 1.8 kg/m³ – Average was 2.5 kg/m³.
 6.0 kg/m³ – Average was 6.4 kg/m³.

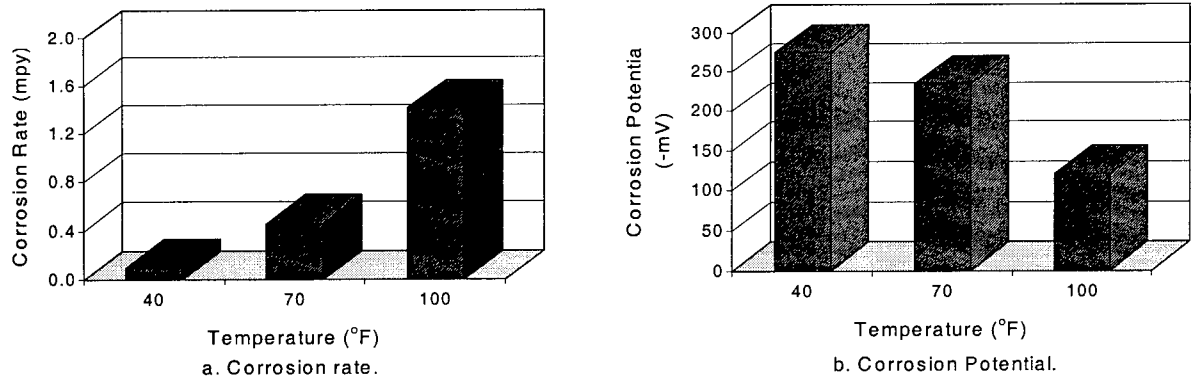


Figure 3. Effect of temperature on corrosion rate and corrosion potential for mortar A-2. [Note: 1 mpy = 0.0254 mm/yr; 40 °F = 4 °C, 70 °F = 21 °C, and 100 °F = 38 °C.]

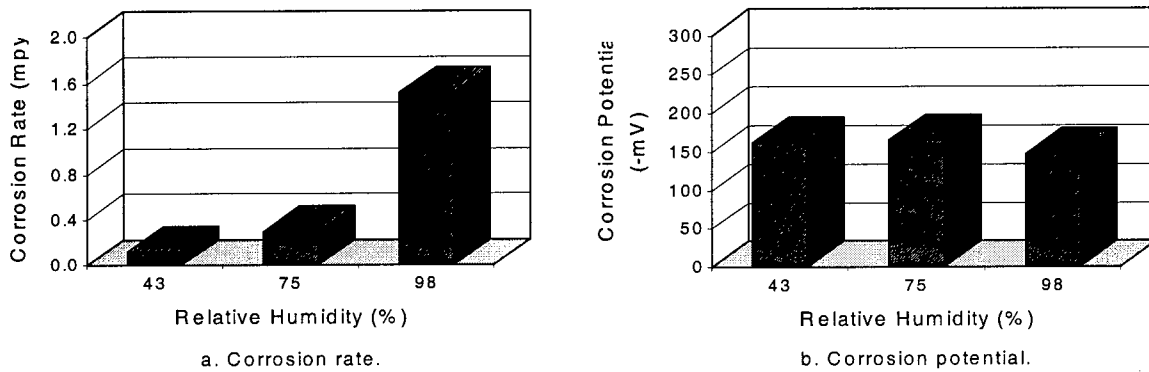


Figure 4. Effect of relative humidity on corrosion rate and corrosion potential for mortar A-2. [Note: 1 mpy = 0.0254 mm/yr.]

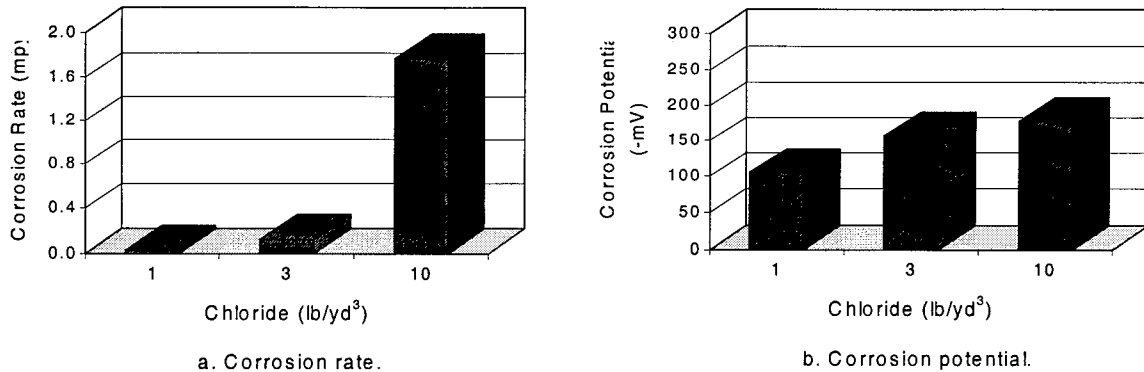


Figure 5. Effect of chloride concentration on corrosion rate and corrosion potential for mortar A-2. [Note: 1 mpy = 0.0254 mm/yr; 0.6 kg/m³ = 1 lb/yd³, 1.8 kg/m³ = 3 lb/yd³, and 6 kg/m³ = 10 lb/yd³.]

One of the interesting effects is that for non-saturated conditions, the corrosion rate is at a maximum at an intermediate temperature and then decreases at high temperatures. This effect was previously reported in the literature by Lopez et al. and observed in the present tests as well.¹ Figure 6 shows a graph of corrosion rate versus temperature at 1.8 kg/m³ (3 lb/yd³) and 6 kg/m³ (10 lb/yd³) chloride and 43 percent relative humidity. This effect of maximum corrosion rate at an intermediate temperature is likely due to a decrease in available pore water solution at the higher temperature even though the humidity remains constant. Although the root cause was not determined, the finding could be significant in understanding and predicting corrosion rate in a variety of environmental conditions. Also, the data show that corrosion can occur at a relatively low humidity (43 percent).

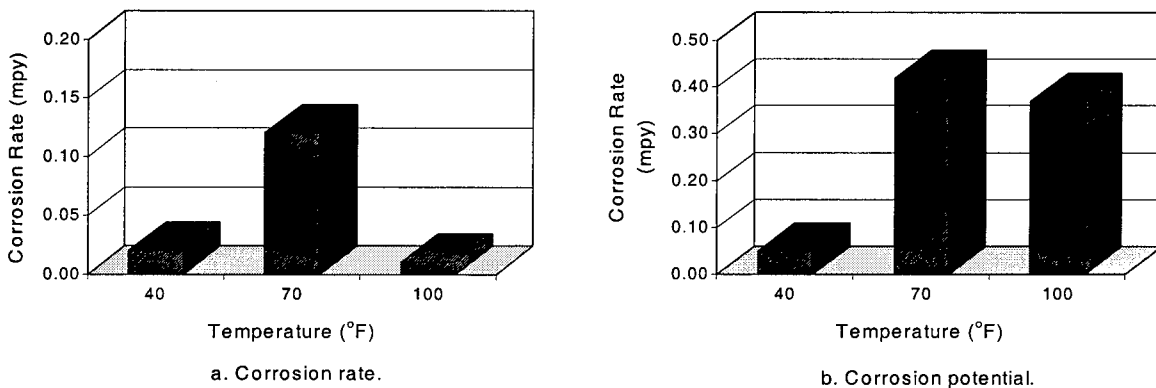


Figure 6. Effect of temperature on corrosion rate at 43 percent relative humidity. [Note: 1 mpy = 0.0254 mm/yr; 40 °F = 4 °C, 70 °F = 21 °C, and 100 °F = 38 °C; 1 lb/yd³ = 0.6 kg/m³.]

¹W. Lopez et al., "Influence of Temperature on the Life of Rebars," *Cement and Concrete Research*, Vol. 23, 1993, pp. 1130-1140.

General Linear Model

A statistical regression model was developed to permit prediction of the corrosion rate and potential as a function of temperature, relative humidity, and chloride concentration based on the data presented above. Models were performed using both; actual and targeted chloride concentrations. Similar results were achieved with both, however, improved error analysis was achieved using the targeted chloride. Therefore, the targeted chloride levels were used in the analysis presented below. The model included the main-effect terms for temperature, relative humidity, and chloride concentration; quadratic terms for each of the main effects; and interaction terms of the main effects. Table 4 gives the estimate of the coefficient for each parameter predicted and the probability that the parameter is significant for the corrosion rate model. Regardless of the significance of the parameter, all parameters were included in the model. Table 5 gives the results for the corrosion potential model. The general linear model equation for predicting corrosion rate (CR) in mpy (1 mpy = 0.0254 mm/yr) or the potential (E_{cor}) in mV versus CSE is given below.

$$CR = a + \underbrace{b \cdot T + b \cdot R + b \cdot C}_{\text{[main effect terms]}} + \underbrace{b \cdot T^2 + b \cdot R^2 + b \cdot C^2}_{\text{[quadratic terms]}} + \underbrace{b \cdot C \cdot R + b \cdot C \cdot T + b \cdot R \cdot T}_{\text{[interaction terms]}} \quad (1)$$

Where a is the intercept, b is the estimate of the coefficient, T is the temperature in $^{\circ}\text{F}$ ($^{\circ}\text{C} = 5(^{\circ}\text{F} - 32)/9$), C is the chloride concentration in lb/yd^3 ($1 \text{ lb/yd}^3 = 0.6 \text{ kg/m}^3$), and R is the percent relative humidity.

Table 4. Corrosion rate statistical regression analyses for mortar A-2 [Note: 1 mpy = 0.0254 mm/yr; $^{\circ}\text{C} = 5(^{\circ}\text{F} - 32)/9$; and $1 \text{ lb/yd}^3 = 0.6 \text{ kg/m}^3$.]

Parameter		Estimate of Coefficient	Probability of Significance
Intercept	a	1.24E+01	99.99%
Temperature ($^{\circ}\text{F}$)	T	-1.35E-01	98.05%
Relative Humidity (%)	R	-2.07E-01	99.74%
Chloride (lb/yd^3)	C	-1.14E+00	99.86%
	T^2	3.52E-04	65.28%
	R^2	8.68E-04	94.47%
	C^2	2.16E-02	61.37%
	C x T	7.23E-03	99.99%
	C x R	8.14E-03	99.99%
	R x T	1.03E-03	99.96%
R-square	61.9%		

Table 5. Corrosion potential statistical regression analyses for mortar A-2.
[Note: 1 mpy = 0.0254 mm/yr; °C = 5(°F-32)/9; and 1 lb/yd³ = 0.6 kg/m³.]

Parameter		Estimate of Coefficient	Probability of Significance
Intercept	a	-63.5700	22.6%
Temperature (°F)	T	-4.9081	76.7%
Relative Humidity (%)	R	6.9026	84.7%
Chloride (lb/yd³)	C	-44.3689	92.5%
	T²	0.0255	65.6%
	R²	-0.0973	99.7%
	C²	-0.0365	1.6%
	C x T	0.0676	43.6%
	C x R	0.1592	77.7%
	R x T	0.0499	98.5%
R-square	71.3%		

For corrosion rate, all parameters were significant at a 90 percent or greater confidence level except the quadratic terms of temperature and chloride concentration. An R-square value of 62 percent indicates that the model developed is capable of predicting approximately 62 percent of the experimental variation observed. For corrosion potential, only the main-effect term for chloride concentration, the quadratic term for relative humidity, and the interaction term of relative humidity/temperature were significant at a 90 percent or greater confidence level. An R-square value of 71 percent indicates that the model developed is capable of predicting approximately 71 percent of the experimental variation observed. The development of these data and equations provides the necessary tools to develop a prediction model for determining corrosion rate and potential as a function of environment.

Subtask A.2 — Mortar A-2 and Prestressed Steel Tendons

In these tests, only a single temperature (21 °C [70] °F), two humidities (75 and 98 percent), and all three chloride concentrations (0.6, 1.8, and 6 kg/m³ [1, 3, and 10 lb/yd³]) were tested. In comparison to conventional reinforcing bar, the rates for each condition are lower for the prestressing steel. Figure 7 shows a comparison of the average corrosion rates and potentials for the two types of reinforcing steel. Under similar conditions it is seen that the prestressed reinforcing strands have a lower corrosion rate than conventional reinforcing steel. However, the prestressed steel exhibited the same corrosion trends as the conventional reinforcing steel. It should be noted that due to the high strength of the prestressed steel, it is expected that structural damage from hydrogen embrittlement would occur from a lower corrosion rate for the prestressed steel than for the conventional reinforcing steel. The corrosion potential data show that the prestressed steel and the conventional steel have similar corrosion potentials.

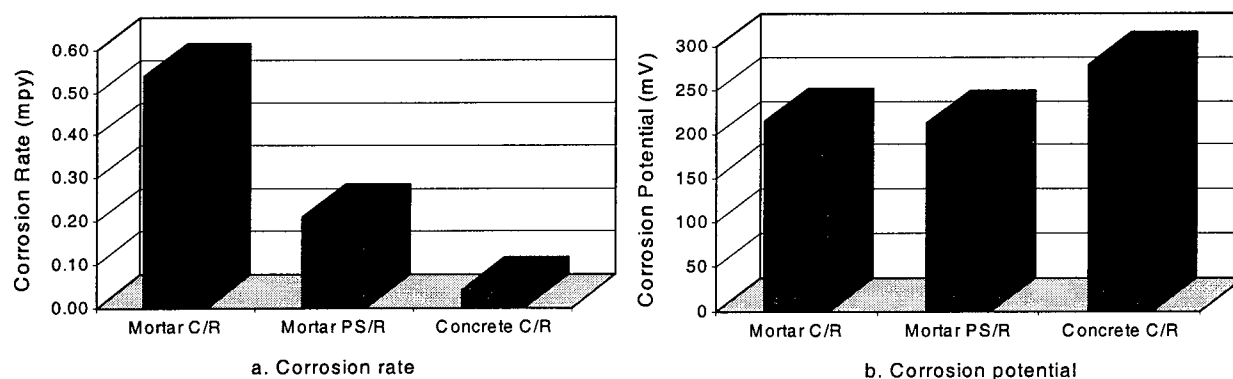


Figure 7. Effect of mortar versus concrete and conventional reinforcement (C/R) versus prestressing steel reinforcement (PS/R) on corrosion rate and corrosion potential for all data averaged. [Note: 1 mpy = 0.0254 mm/yr]

Subtask A.3 — Concrete A-5 and Conventional Reinforcing Steel

The same matrix of tests was performed as for the prestressed steel tests discussed above. In comparison to mortar A-2, the corrosion rates for each condition were significantly lower for concrete A-5. Figure 7 shows a comparison of the average corrosion rates and potentials for conventional reinforcing (C/R) bar in the concrete A-5 and in mortar A-2.

Under similar conditions, it is seen that the conventional reinforcing steel in the concrete has a much lower corrosion rate than the mortar. The reason for this cannot be verified, but the conductivity of the mortar is greater than the concrete. Although this explanation is not a completely satisfactory cause for the large effect observed, a higher conductivity would be expected to support a higher corrosion rate.

Figure 8 compares the actual measured values of chloride concentration to the desired target values for the three series of tests performed. The values shown are for the average of all comparative conditions. In general, the chloride levels achieved are in agreement with the targeted chloride concentrations.

There is no fundamental reason for a difference in the mortar A-2 and mortar A-2-PST (prestressed steel tendon) data since the only difference was the type of steel; otherwise, the mortar was the same and specimen construction was the same. However, the measured chloride concentration for mortar A-2-PST is consistently lower than mortar A-2 (figure 8). This, in-part, explains the lower corrosion rates for the prestressing steel versus the conventional steel. Differences in the steel composition and metallurgy also may be responsible for differences in corrosion behavior observed.

The specimens for concrete A-5 had a greater cover thickness than the mortar specimens. The concrete A-5 data for the 0.6 kg/m³ (1 lb/yd³) and 1.8 kg/m³ (3 lb/yd³) targeted chloride concentrations are lower than the mortar A-2, but the concrete A-5 data

for the 6 kg/m³ (10 lb/yd³) targeted chloride concentration is greater than the mortar A-2 (figure 8). Therefore, the chloride concentration does not explain the difference in the corrosion rate data observed for the concrete versus the mortar.

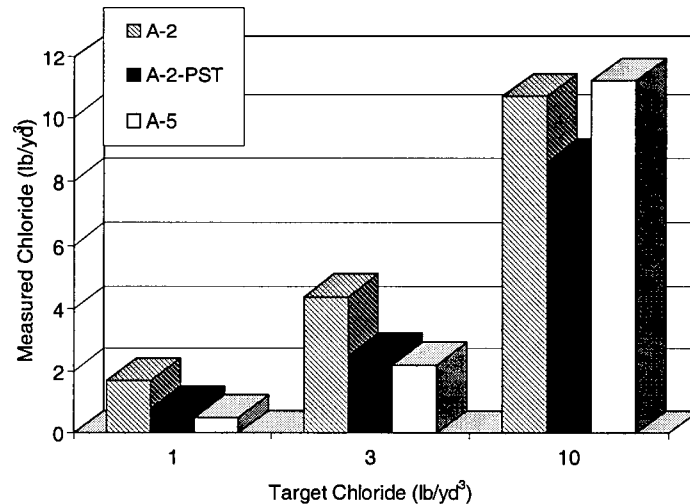
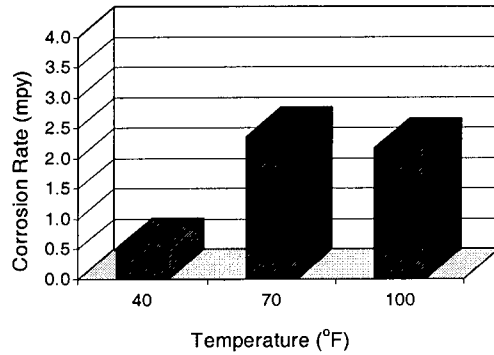


Figure 8. Comparison of actual chloride concentrations measured at the steel-cement interface for tests in mortar A-2 (conventional reinforcing steel), mortar A-2-PST (post-tensioning reinforcing steel), and concrete A-5 (conventional reinforcing steel). [Note: 1 lb/yd³ = 0.6 kg/m³.]

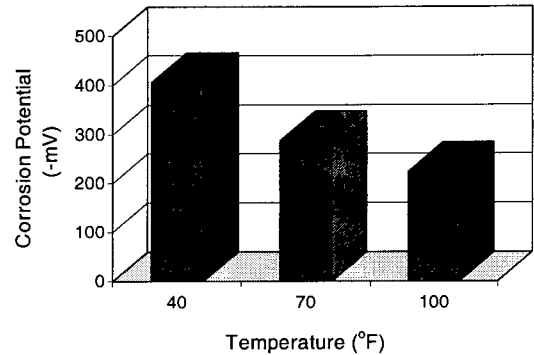
Subtask A.4 — Mortar B-2 and Conventional Reinforcing Steel

A similar full factorial matrix of experiments was performed for mortar B-2 as discussed above for mortar A-2 (three levels each of temperature, relative humidity, and chloride concentration). In the following analysis, all of the data for a single level of a particular independent variable was averaged and the three different levels for that variable were compared. Figures 9, 10, and 11 show the effect of temperature, relative humidity, and chloride concentration, respectively, on corrosion rate and corrosion potential for mortar B-2. In general, the corrosion rates are much greater for mortar B-2 than for A-2, although similar trends were observed. This higher corrosion rate for mortar B-2 is attributed to its lower pH (9 to 10) as compared to mortar A-2 (12 to 13).

Figure 9a shows the same trend discussed for mortar A-2 for non-saturated moisture levels. That is, at intermediate temperatures, corrosion rate is at a maximum and decreases at high temperatures. A closer examination of the data indicates that the trend shown in figure 9a is not the case for the high chloride level at 75 or 98 percent relative humidity, but is the case for most other conditions.

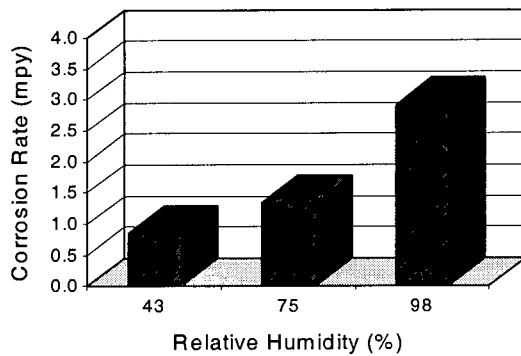


a. Corrosion rate

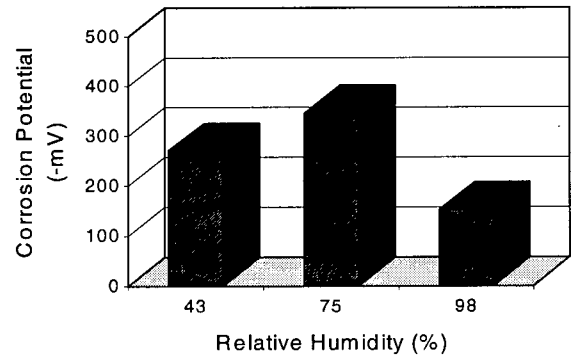


b. Corrosion potential

Figure 9. Effect of temperature on corrosion rate and corrosion potential for mortar B-2. [Note: 1 mpy = 0.0254 mm/yr; 40 °F = 4 °C, 70 °F = 21 °C, and 100 °F = 38 °C.]

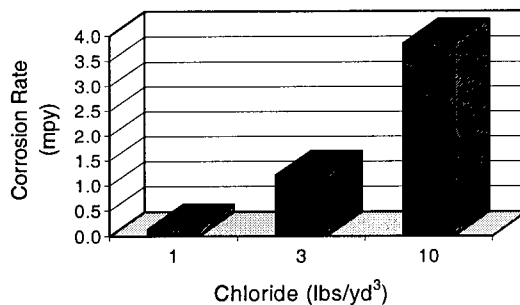


a. Corrosion rate

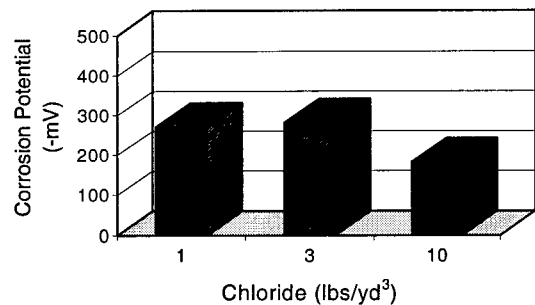


b. Corrosion potential

Figure 10. Effect of relative humidity on corrosion rate and corrosion potential for mortar B-2. [Note: 1 mpy = 0.0254 mm/yr.]



a. Corrosion rate



b. Corrosion potential

Figure 11. Effect of chloride concentration on corrosion rate and corrosion potential for mortar B-2. [Note: 1 mpy = 0.0254 mm/yr; 0.6 kg/m³ = 1 lb/yd³, 1.8 g/m³ = 3 lb/yd³, and 6 g/m³ = 10 lb/yd³.]

A statistical regression model was developed to permit prediction of the corrosion rate and potential as a function of temperature, relative humidity, and chloride concentration for mortar B-2. This model was presented in the interim report and is not repeated here.

DISCUSSION: TASK A — CORROSIVE ENVIRONMENT STUDY

Mapping of Corrosion Rate versus Environment

A primary focus of task A was to determine the effect of environmental variables on corrosion and to establish the boundary conditions necessary for corrosion. Task A examined two mortars in detail (Type I portland cement [mortar A-2] and calcium aluminate cement [mortar B-2]) and selected conditions for a concrete (concrete A-5) with the same cement as mortar A-2. Figures 12 and 13 show a corrosion rate as a function of environment for mortars A-2 and B-2, respectively. It is clear that the lower pH of the calcium aluminate cement produced a profound effect on the range in which corrosion is possible and significantly increased the rate of corrosion for a specific environment. For the calcium aluminate cement, significant corrosion occurred even for several conditions tested for the 0.6 kg/m^3 (1-lb/yd^3) chloride concentration. For the portland cement, only two conditions produced any measurable corrosion at 0.6 kg/m^3 (1-lb/yd^3) chloride concentration. For those two conditions, the corrosion rate was at the very low end of the corrosion range given.

Figure 14 shows the environmental map for the corrosion rate of steel in concrete A-5. Corrosion rate data is available only for the 21°C (70°F) condition at the intermediate and high humidity levels. As was pointed out earlier, the corrosion rates for steel in the concrete are significantly lower than measured in the mortar using the same cement.

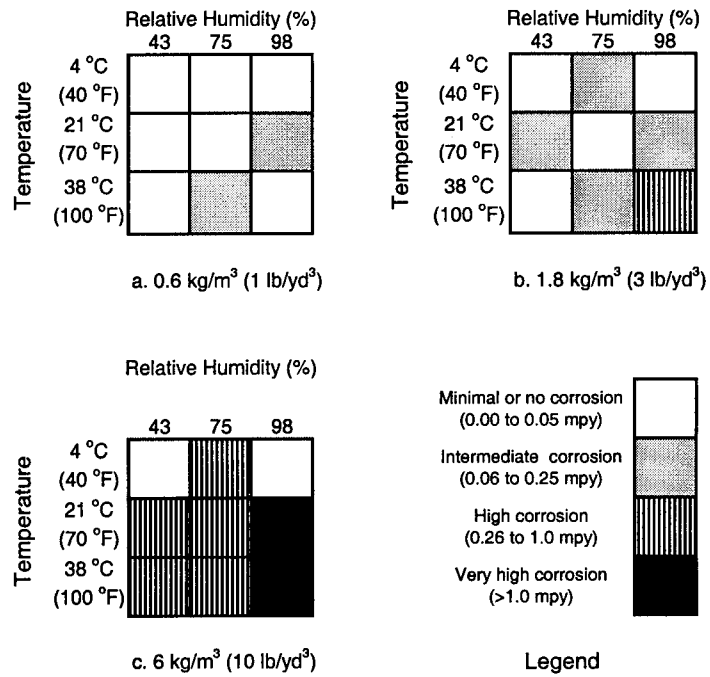


Figure 12. Environmental map of corrosion rate for mortar A-2.

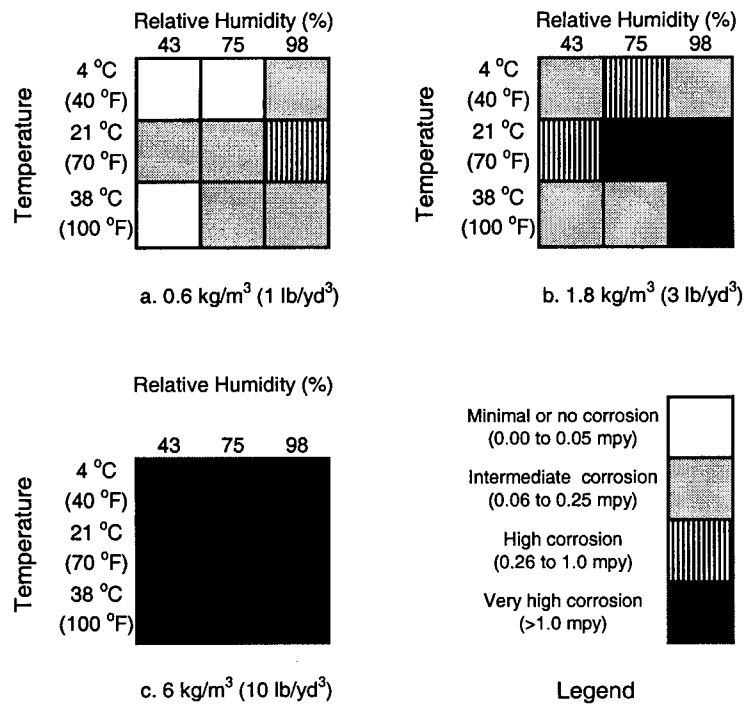


Figure 13. Environmental maps of corrosion rate for mortar B-2.

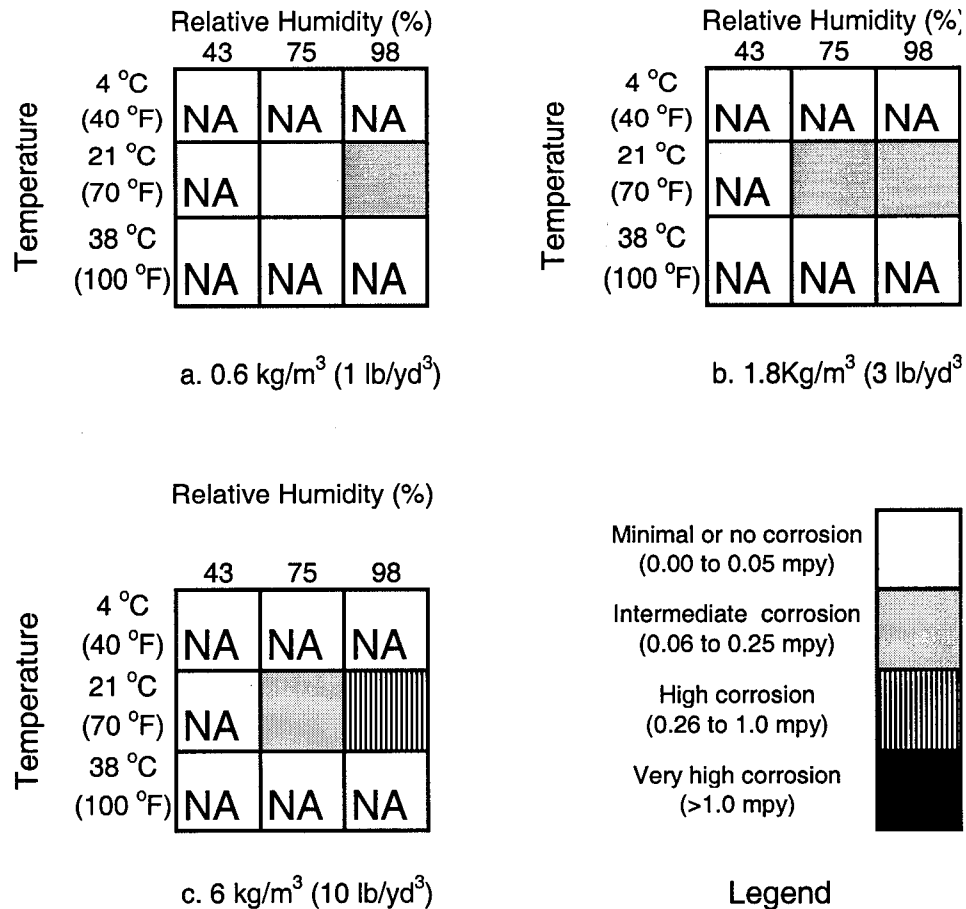


Figure 14. Environmental maps of corrosion rate for concrete A-5.
[Note: NA – Data Not Available for That Condition].

Regardless of the reason for the effect of lower corrosion rates for the concrete, the data can be used to create a more complete environmental map for typical concrete. In reviewing the data, the following assumptions were made: (1) for the 0.6 and 1.8- kg/m³ (1- and 3-lb/yd³) data, the corrosion rate of the concrete is 5 times (5x) less than measured for the mortar; and (2) for the 6.0 kg/m³ (10-lb/yd³) data, the corrosion rate of the concrete is 10 times (10x) less than measured for the mortar. These values are estimates (see table 6) and any additional fine adjustments are not warranted based on the range of corrosion rate data developed for different concrete mixes using portland Type I cement in task B. Based on the above assumptions and the data from figure 12, figure 15 shows the projected environmental map for a Type I portland cement-based concrete. At a chloride concentration of 0.6 kg/m³ (1 lb/yd³), corrosion is expected to be minimal for all environmental conditions. At a chloride concentration of 1.8 kg/m³ (3 lb/yd³), the only environmental conditions that indicate corrosion are for high temperature (38 °C [100 °F]) and high humidity (98 percent). At a chloride concentration of 6.0 kg/m³ (10 lb/yd³), corrosion is minimal at low humidity (43 percent), with generally increasing corrosion at higher temperature and higher humidity.

Table 6. Comparison of corrosion rates for concrete A-5 and mortar A-2
[1 mpy = 0.0254 mm/yr].

Temperature (°C)	Relative Humidity (%)	Chloride (kg/m ³)	Corrosion Rate		Ratio A-2/A-5
			Concrete A-5	Mortar A-2	
			mpy	mpy	
21	75	0.6	0.01	0.03	3.0
21	98	0.6	0.05	0.09	1.8
21	75	1.8	0.02	0.05	2.5
21	98	1.8	0.02	0.08	4.0
21	75	6.0	0.04	0.85	21
21	98	6.0	0.10	2.2	22

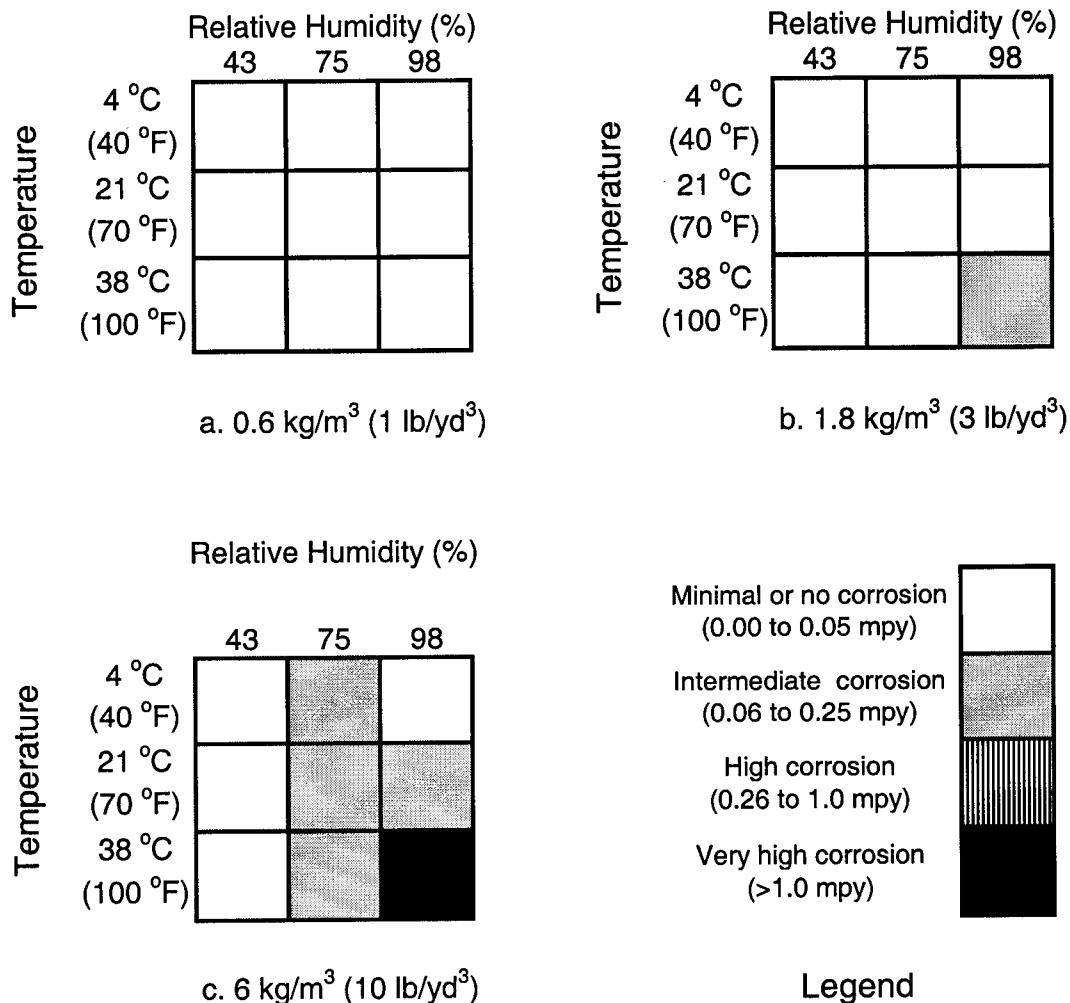


Figure 15. Environmental maps of corrosion rate for a type I portland cement-based concrete adjusted for comparison of mortar A-2 and concrete A-5 data.

SUMMARY: TASK A – CORROSIVE ENVIRONMENT STUDY

In task A, corrosion behavior of reinforcing steel in concrete was defined as a function of temperature, relative humidity, and chloride concentration (figure 15). The following summarizes the environmental effects for the concrete tested (Medusa Type I portland cement, quartz fine and coarse aggregate, and 0.45 w-c):

- At a chloride concentration of 0.6 kg/m^3 (1 lb/yd^3), corrosion of reinforcing steel in concrete is negligible for all environmental conditions.
- At a chloride concentration of 1.8 kg/m^3 (3 lb/yd^3), moderate corrosion of reinforcing steel in concrete occurs for the combined condition of high relative humidity (98percent) and high temperature (38°C [100°F]).
- At a chloride concentration of 6 kg/m^3 (10 lb/yd^3), corrosion of reinforcing steel in concrete is negligible at low relative humidity (43 percent). Corrosion of reinforcing steel in concrete is maximum at a combined condition of high relative humidity (98 percent) and high temperature (38°C [100°F]). Corrosion of reinforcing steel in concrete is moderate at moderate relative humidity (75 percent) and low temperature (4°C [40°F]).

A significantly greater corrosion rate was observed for reinforcing steel in mortar than in concrete of the same cement, cement to fine aggregate ratio, and water-cement ratio.

For similar environmental conditions, a significantly greater corrosion rate of reinforcing steel was observed in a mortar of lower pH calcium aluminate cement than for a higher pH portland cement.

The results of task A provided critical inputs for tasks B and D:

- Two environments were selected for testing in task B.
- The environmental conditions and subsequent corrosion rates of reinforcing steel in concrete were used in the corrosion rate prediction model developed in task D.

CHAPTER 4. TASK B — CONCRETE CHEMICAL AND PHYSICAL PROPERTIES

The purpose of task B was to investigate the chemical and the physical characteristics of concretes as they relate to the corrosion behavior of embedded reinforcing steel.

EXPERIMENTAL APPROACH: TASK B — CONCRETE CHEMICAL AND PHYSICAL PROPERTIES

The independent variables examined in task B can be classified into the following:

- Environmental variables.
- Material variables.
- Concrete mix design variables.

Environmental Variables

Based on the results of the task A work, two environments were selected to be used in the task B tests. The environments were selected to provide: (1) moderately aggressive corrosive conditions (moderate environment) and (2) highly aggressive corrosive conditions (aggressive environment). These environments were:

- Moderate environment: 21 °C (70 °F), 75 percent relative humidity (RH) 1.8 kg/m³ (3 lb/yd³) chloride.
- Aggressive environment: 38 °C (100 °F), 98 percent RH, 6 kg/m³ (10 lb/yd³) chloride.

As in task A, chlorides were diffused into the concrete following curing of the specimens. Relative humidity was maintained through the use of selected salt solutions maintained at the bottom of test chambers. Therefore, the relative humidity was that of the outside air surrounding the concrete (or mortar) specimens. Temperature was maintained ± 2 °C (4 °F) during the exposure period.

Material Variables

The selection of materials and mixture proportions for the concretes was guided by the results of previous studies and by experience with concretes used for the repair and construction of bridges. Although both mortars and concretes were used in task A, only concretes were used in task B.

Material variables considered include:

1. Cement type.
2. Mineral admixture type.
3. Fine aggregate type.
4. Coarse aggregate type.

A summary of the material variables considered in the research is presented in table

7.

Table 7. Summary of material variables considered in the research.

Variable	Range of Variables
Cement Type	A. Type I portland cement - high alkali B. Calcium aluminate cement - intermediate pH C. Type I portland cement - low alkali D. Type I portland cement - high C3A E. Type III portland oil-well cement - no C3A F. Magnesium phosphate cement - low pH
Mineral Admixture	1. Silica fume 2. Class F flyash 3. Class C flyash 4. Granulated blast furnace slag 5. None
Fine Aggregate	1. Pure quartz (SiO_2) sand 2. Natural sand with high levels of carbonate rock
Coarse Aggregate	1. A dense, inert, impermeable quartz 2. A permeable limestone

Cements

Six different cements were selected for use in the research, (see table 8). They include four portland cements (A, C, D, and E), a calcium aluminate cement (B), and a magnesium phosphate cement (F). The cements were chosen to provide a wide but realistic range in tricalcium aluminate (C_3A) content, alkali (Na_2O , K_2O) content, and pH.

The variation in C_3A content of the portland cements provides variation in the amount of chloride ion that is chemically bonded. The calcium aluminate cement is expected to bind large quantities of chlorides, while magnesium phosphate cement may exhibit no chloride binding qualities at all.

An increase in alkali content in the portland cements is expected to exert an influence on the corrosion events. This includes: (1) an increase in the conductivity of the electrolyte phase in the saturated concrete and (2) an increase in the OH^- levels in the electrolyte phase (pore water phase).

The two non-portland cements provide two significantly lower levels of pH values in the concrete matrix phase. With the calcium aluminate cement, the pH value is 9 to 10, while in the magnesium phosphate cement, the value is 5 to 6.

The type III portland cement 'E' had the greatest Blaine fineness ($4200 \text{ cm}^2/\text{g}$). The other portland cements used in this study (A, C, and D) had Blaine fineness of 3940, 3570, and $3413 \text{ cm}^2/\text{g}$, respectively.

Table 8. Cements used in task B.

Cement Identification	Cement Description	C3A Content	Alkali as Na ₂ O	pH Range
A	Type I portland cement containing a high level of alkali (Medusa Cement Company, Type I portland cement from the Charlevoix, MI, plant)	9.8	1.03	12-13
B	Calcium aluminate cement (Lumnite cement from the Lehigh portland Cement Company, Buffington Plant, Gary, IN)	*	NA **	9-10
C	Type I portland cement with a low alkali content (Holnam Type I portland cement, Holly Hill, SC, plant)	7	0.10	12-13
D	Type I portland cement with a high C3A content (Holnam Type I portland cement from the Artesia, MS, plant)	12.3	0.40	12-13
E	Type III portland cement with a low C3A level (Lone Star Industries, Class C oil-well cement from Maryneal, TX, plant)	0	0.23	12-13
F	Magnesium phosphate cement	NA	NA	5-6

* Calcium aluminate phases include CA, CA₂, and C₁₂A₇.

** NA

Mineral Admixtures

Mineral admixtures that were selected as partial replacements for the cements include:

1. Silica fume.
2. Class F flyash.
3. Class C flyash.
4. Granulated blast furnace slag.

The silica fume and Class F flyash function principally as pozzolanic materials, while the Class C flyash and granulated blast furnace slag function as cementitious materials in addition to participating in pozzolanic reactions. Depending upon the level of pozzolanic activity, the availability of OH⁻ is expected to decrease in concretes containing the pozzolanic additives.

For all of the additives, the in-situ creation of additional calcium silicate hydrate (CSH) and other cement hydrates will reduce the porosity and permeability of the matrix phase in the concretes. This has the effect of reducing the diffusion rate of chloride ions in the concrete. The additional cementitious material also is expected to provide an increase in strength and elastic modulus in the concrete.

Fine Aggregates

Typically, the fine aggregate used in concretes for bridge structures can be thought of as an inert material. However, as the pH of the matrix phase surrounding a corroding steel bar changes, the solubility of some fine aggregate constituents may change. This is

an important consideration since the finest particle size materials in the fine aggregate phase may end up in the interface material that is actually in contact with the reinforcing steel.

The two fine aggregates used in this task represent reasonable extremes in porosity and chemical activity. Both aggregates are natural sands, obtained from Ohio sources. They include (see table 9) quartz sand and mixed siliceous/calcareous sand derived from glacial deposits. The silica sand is pure quartz sand (SiO_2 >99.0 percent) derived from a quartz conglomerate source. The glacial deposit-derived sand contains about 50 percent carbonate rock types (dolomitic limestone/limestone), with the bulk of the remaining sample dominated by sedimentary and igneous rock types. Both meet the gradation requirements of ASTM C 33-90, the Standard Specification for Concrete Aggregates.

Table 9. Fine aggregates used in task B.

Fine Aggregate Source	Type Of Sand	Source Location	*SSD Specific Gravity	Water Absorption (%)	Fineness Modulus
Sidley	Quartz Conglomerate	Painesville Ohio	2.65	0.33	2.78
Frank Road	Glacial Deposit	Columbus Ohio	2.7	2.18	2.86

*Saturated Service Dry

Coarse Aggregates

The coarse aggregate also is typically considered to be inert in a portland cement concrete with a pH of 12.4 to 13.5. The coarse aggregate is not expected to exert a significant influence on the overall chemistry at the interface between the concrete and the steel bar. However, it is known that the permeability of some concrete aggregates is greater than that of good-quality hydrated cement paste. Aggregate permeability may be an important factor influencing the migration rate of chloride ions into the concrete and the ionic conductivity of the concrete.

The two coarse aggregates used in task B were quartz aggregate from an Ohio source (same source as the quartz sand), and limestone from a Florida source. Both coarse aggregates meet the gradation requirements of ASTM C 33-90, no. 8 gradation (3/8 in [9.5 mm] maximum size). The coarse aggregates, described in table 10, were chosen to represent meaningful extremes in porosity and water absorption values.

Table 10. Coarse aggregates (ASTM C33-90, no. 8 gradation) used in task B.

Coarse Aggregate Source	Aggregate Type	Source Location	SSD Specific Gravity	Water Absorption (%)
Sidley	Quartz (Gravel)	Painesville, OH	2.62	0.59
Harper Brothers	Limestone (Crushed)	Ft. Myers, FL (Alico Pit)	2.38	9.79

Concrete Mix Proportion Variables

Because of the relatively large number of material variables evaluated in the research, it was necessary to limit the concrete mix proportion variables. At the same time, it was necessary to provide reasonable variations in the cement content of the concretes to reflect both past and expected future practice. This was handled in the present research by varying water-cement ratio (water-cement ratio [w-c] used in this report relates to all cementitious material in the mix) while by volume maintaining the volume of the cementitious phase at a constant value (30 percent). Water-cement ratios of 0.3, 0.4, and 0.5 were used in these concretes. In addition, air contents were adjusted at 2 percent, 5 percent, and 8 percent.

An example of concrete mix design is shown in table 11. In this example, the water-cement ratio is 0.40, and the entrained air content is 7 percent. The cementitious phase in this example is comprised of portland cement, ground granulated blast furnace slag, and water. When summed, these components represent 30 percent by volume.

In this project, the variation in water-cement ratio over a relatively wide but realistic range provided variations in the porosity and permeability of the cementitious matrix phase of the concretes. By maintaining the cementitious phase at a constant level (30 percent by volume) and varying the water-cement ratio, it was possible to provide a large (but realistic) range in cement content. In the concretes, the proportion of fine and coarse aggregates was maintained at 1:1. Variations in air content were achieved at the expense of the combined aggregate phases.

Table 11. Example of three concrete mix designs for task B.

Concrete No. 1 (Tasks B & C)						
Concrete Constituents	Batch Weights		Density		Volume Ratio Component to Concrete	
	kg/m ³	lb/yd ³	kg/m ³	lb/ft ³	m ³ /m ³	ft ³ /yd ³
Cement A	358	603	3,152	196.6	0.114	3.07
Class C Flyash	119	201	2,770	172.8	0.043	1.16
Quartz Sand	894	1,507	2,651	165.4	0.337	9.11
Quartz Aggregate	885	1,491	2,621	163.5	0.338	9.12
Water	143	241	1,000	62.4	0.143	3.86
Air					0.025	0.68
Totals	2,399	4,043			0.999	27.00

Theoretical cement paste (cement + mineral admixture + water) content = 30% vol

Theoretical unit weight = 2,401 kg/m³ (149.8 lb/yd³)

Water-cementitious material ratio = 0.3

Air content = 2.5% vol

Concrete No. 9 (Task B)						
Concrete Constituents	Batch Weights		Density		Volume Ratio Component to Concrete	
	kg/m ³	lb/yd ³	kg/m ³	lb/ft ³	m ³ /m ³	ft ³ /yd ³
Cement D	268	452	3,152	196.6	0.085	2.30
GGBF Slag	144	243	2,881	179.7	0.050	1.35
Quartz Sand	834	1,406	2,651	165.4	0.315	8.50
Quartz Aggregate	825	1,390	2,621	163.5	0.315	8.50
Water	165	278	1,000	62.4	0.165	4.46
Air					0.070	1.89
Totals	2,236	3,769			0.999	27.00

Theoretical cement paste (cement + mineral admixture + water) content = 30% vol

Theoretical unit weight = 2,238 kg/m³ (139.6 lb/yd³)

Water-cementitious material ratio = 0.4

Air content = 7% vol

Concrete No. 26 (Task B)						
Concrete Constituents	Batch Weights		Density		Volume Ratio Component to Concrete	
	kg/m ³	lb/yd ³	kg/m ³	lb/ft ³	m ³ /m ³	ft ³ /yd ³
Cement E	272	458	3,152	196.6	0.086	2.33
Class C Flyash	90	152	2,770	172.8	0.033	0.88
Quartz Sand	870	1,467	2,680	167.2	0.325	8.77
Quartz Aggregate	851	1,435	2,621	163.5	0.325	8.78
Water	181	305	1,000	62.4	0.181	4.89
Air					0.050	1.35
Totals	2,264	3,817			0.999	27.00

Theoretical cement paste (cement + mineral admixture + water) content = 30% vol

Theoretical unit weight = 2,222 kg/m³ (141.4 lb/yd³)

Water-cementitious material ratio = 0.5

Air content = 5% vol

Experimental Design

The experimental design included 29 trial concrete mix designs, which incorporate all the material and concrete proportion variables previously discussed (further details of the design are provided in the interim report [FHWA-RD-96-207]). Table 12 gives the experimental matrix of mix designs for task B.

Table 12. Experimental matrix of mix designs for task B.

Concrete No.	Water-Cement Ratio	Air Content, %	Fine Aggregate	Coarse Aggregate	Mineral Additive	Cement Identification ^(e)	Admixture Dosage, oz/cwt ^(a)		
							Superplasticizer ^(b)	Air-Entraining Admixture ^(c)	Set Retarder ^(d)
1	0.3	2	Q	Q	FA - C	A	18.0	None	4.0
2	0.3	8	Q	LS	FA - F	A	18.0	2.0	6.0
3	0.3	8	G	Q	FA - C	C	10.0	2.5	3.0
4	0.5	5	Q	Q	Slag	B	None	0.75	None
5R	0.5	2	Q	Q	MS	D	15.0	None	None
6	0.3	5	Q	Q	None	E	16.0	0.75	None
7	0.4	5	Q	Q	MS	F	None	0.5	Boric Acid
8	0.5	8	Q	Q	None	F	None	1.0	Boric Acid
9	0.4	8	Q	Q	Slag	D	None	3.75	None
10	0.4	8	Q	Q	FA - C	B	None	1.5	6.0
11	0.5	2	Q	Q	FA - F	E	None	None	None
12	0.4	8	G	LS	MS	E	18.0	7.0	None
13	0.4	5	Q	Q	None	C	None	1.5	None
14*	0.3	5	G	Q	Slag	F	---	---	---
15R	0.5	8	G	Q	MS	C	10.0	8.0	None
16	0.3	2	G	Q	None	B	36.0**	None	Citric Acid
17	0.5	5	G	LS	FA - C	D	None	0.3	None
18	0.3	5	Q	LS	MS	B	18.0	1.0	6.0
19	0.5	2	Q	LS	Slag	C	None	None	None
20	0.5	2	G	LS	FA - F	F	None	None	Boric Acid
21	0.4	5	G	Q	FA - F	B	None	2.5	None
22	0.4	2	G	LS	None	D	None	None	None
23	0.4	5	G	Q	Slag	A	13.0	2.5	None
24	0.3	8	Q	LS	Slag	E	13.0	0.75	None
25	0.4	2	Q	LS	FA - C	F	None	None	Boric Acid
26	0.5	5	G	Q	FA - C	E	None	0.6	None
27	0.4	5	Q	LS	FA - F	C	None	0.75	None
28	0.4	2	G	Q	MS	A	18.0	None	3.0
29	0.5	8	Q	LS	None	A	6.0	2.0	None
30	0.3	5	Q	Q	FA - F	D	18.0	1.0	4.0

(a) oz/100 lb of cement + mineral additive (1 oz/100lb=1 mL/1.54 kg).

(b) Boremco Company's Might 150 superplasticizer.

(c) Sika Corporation's AEA-15 air-entraining agent.

(d) Sika Corporation's Plastiment set-retarding admixture.

(e) See table 8 for cement descriptions.

Q: Sidley quartz coarse (3/8 in)/fine aggregate (1 in = 25.4 mm)

G: Glacial sand

LS: Limestone (Florida - 3/8 in) (1 in = 25.4 mm)

FA - C: Class C flyash

FA - F: Class F flyash

Slag: Koch Mineral ground granulated blast furnace slag

MS: Elkem Materials EMS960 microsilica

*: Concrete 14 was not prepared because of an incompatibility between constituents of the cementitious phase

** MISO and Darvan 811D

The greatest difficulty in maintaining the desired design levels of the independent variables was for entrained air. Most of this difficulty was for magnesium phosphate cement. The primary reason for this is the fact that air-entraining admixtures used in the present investigation were developed for Portland cement, and do not perform the same function in magnesium phosphate cement.

The statistical experimental design was developed using the software package ECHIP for the independent variables below:

1. Water to cement ratio – three levels: 0.3, 0.4, and 0.5.
2. Air entrainment – three levels: 2 percent, 5 percent, and 8 percent.
3. Fine aggregates – two types: Glacial Deposit (G) and Quartz (Q) (table 9).
4. Coarse aggregates – two types: Quartz (Q), Limestone (LS) (table 10).

5. Admixtures – five types: None, Flyash-F (FA-F), Microsilica (MS), Slag, Flyash-C (FA-C).
6. Cement type - six types: A, B, C, D, E, and F (table 8).

In task B, there were too many independent variables (six) with too many levels (six for cement type) to perform sufficient tests to either: (1) perform a full factorial matrix of tests or (2) determine a model containing interaction and quadratic terms. Therefore, a “main effect terms only” statistical design was generated. The design allowed estimation of the six main effect terms for the variables listed above (water-cement ratio, air, etc.).

ECHIP was used to find an optimal design for the experimental matrix, subject to using a base design limited to 30 conditions (30 concrete mix designs). Supplied with the number of independent variables and the levels of each, ECHIP designed an experimental matrix that maximizes the information to be captured for a main effects only model.

The experimental matrix was limited to 29 conditions due to problems in achieving a good concrete set for one of the mix combinations. The design included duplicates for the concrete property testing and triplicates for the corrosion rate testing.

Measured Dependent Variables

The following dependent variables were measured for each of the concrete mix designs:

1. Rapid Chloride Permeability.
2. Compressive Strength.
3. Electrical Resistivity.
4. Corrosion Rate.
5. Corrosion Potential.
6. Final Chloride at the Steel Surface.

Rapid Chloride Permeability

AASHTO Designation T277-93, “The Standard Method of Test for Rapid Determination of the Chloride Permeability of Concrete,” was used to measure chloride ion permeability. For this test, 102-mm- (4-in-) diameter by 203-mm- (8-in-) long cylinders were cast for the experimental concretes. The specimen for the test is a 51-mm- (2-in-) thick slice sawcut from the cylinders. Duplicate specimens were run following a 28-day curing period and following a 90-day curing period (100 percent humidity room).

Compressive Strength

ASTM C 109-92, “The Standard Test Method for Compressive Strength of Hydraulic Cement Mortars,” was used to measure the compressive strength for each experimental concrete. For this test, 51-mm (2-in) cubes were cast. Triplicate specimens were tested following a 7-day, 28-day, 90-day, and 365-day curing period.

Electrical Resistivity

The electrical resistivity of the concretes was measured using a Nilsson Electric laboratory model 4-PIN soil resistance meter. For this test, the concrete was cast in a 100-mm polypropylene beaker (Nalgene 1201-0100). The cups are fitted with two 1.6- (0.062-) diameter titanium wires. The distance between the wires was 25.4 mm (1 in). The specimens were stored in a 100 percent relative humidity room for the entire test period. Electrical resistivity was measured on triplicate specimens immediately after casting the specimen and at 1, 7, 28, 90, 180, and 365 days.

Corrosion Rate and Potential

The same specimen design and fabrication procedures were used in the task B investigation as were used in task A (see figure 1). In task B, all of the tests were performed with concrete and the concrete cover was maintained at 19 mm (0.75 in). This gave a concrete cover that was a factor of two greater than the maximum aggregate size. Conventional reinforcing steel was the only steel tested in task B.

Although the primary independent variables of interest in task B were concrete mix variables, it was of interest to evaluate these variables in different environmental conditions. Based on the task A results, moderate and aggressive environments were selected. The moderate environment was 21 °C (70 °F), 75 percent relative humidity, and 1.8 g/m³ (3 lb/yd³) of chloride. The aggressive environment was 38 °C (100 °F), 98 percent relative humidity, and 6 g/m³ (10 lb/yd³) of chloride. The full matrix of 29 concretes was tested in each of the two environments. Triplicate samples were tested in each condition.

The test procedures used in task B were the same as developed and used in task A. Following curing of a minimum of 28 days, the specimens were: (1) dried, (2) ponded to be diffused in chlorides, and (3) exposed to one of the two environmental conditions listed above. Corrosion rate and potential measurements were made as described in task A.

Final Chloride at the Steel Surface

At the completion of the corrosion tests, the chloride concentration in the 1.6 mm (0.062 in) of concrete in contact with the steel surface was measured. Chloride concentration in the concrete was measured as described above for the task A tests. The ability to measure chloride in the concrete very close to the steel surface was one of the reasons for selecting the overall specimen design.

RESULTS: TASK B — CONCRETE CHEMICAL AND PHYSICAL PROPERTIES

Task B work was divided into two subtasks: (1) Concrete Property Data and (2) Corrosion Performance Data. For presentation purposes, these data are combined and presented for each independent variable in the test matrix. The concrete property data were given in the interim report (FHWA-RD-96-207). The corrosion performance data is given in Appendix A.

Water-Cement Ratio

Table 13 shows the mean values of rapid chloride permeability, electrical resistivity, and compressive strength at 28- and 90-day exposures for concretes prepared with water-cement ratios of 0.3, 0.4, and 0.5. The mean values presented in the table are the means of all the concretes (from the matrix of 29 concretes) that had a water-cement ratio set at the particular level given.

Table 13. Summary of water-cement ratio data for the concrete property variables: rapid chloride permeability, resistivity, and compressive strength [1,000 psi = 6.895 MPa].

w/c Ratio	Rapid Cl Permeability		Resistivity		Compressive Strength	
	28 days (C)	90 days (C)	28 days (ohm-cm)	90 days (ohm-cm)	28 days (psi)	90 days (psi)
0.3	2,276	1,468	34,000	67,000	8,244	9,049
0.4	3,317	2,107	37,000	52,000	6,677	7,397
0.5	4,589	3,382	14,000	30,000	4,764	5,439

Rapid chloride permeability decreases as a function of decreasing water-cement ratio. This is an expected result since the total porosity in the cement paste phase decreases as a function of decreasing water-cement ratio. In the test procedure used here (ASTM C 1202), it is the ionic conductivity of the concrete that is being measured. A reduction in total pore volume results in a corresponding reduction in the current carrying medium (i.e., pore water containing dissolved ions). Also, the 90-day rapid chloride permeability is consistently less than the 28-day data.

The effect of the water-cement ratio on concrete electrical resistivity at 28 days and 90 days is shown in table 13. At 90 days, electrical resistivity decreased with higher water-cement ratio as expected.

Mean values of 28-day and 90-day compressive strength are shown in table 13. Compressive strength increases as a function of decreasing water-cement ratio. This is a well-known and expected result.

Table 14 shows the mean values of corrosion rate, potential, and actual chloride

concentration achieved for the aggressive and moderate environments for concretes prepared with water-cement ratios of 0.3, 0.4, and 0.5. The target chloride concentrations for the aggressive and moderate environments were 1.8 kg/m³ (3 lb/yd³) and 6.0 Kg/m³ (10 lb/yd³), respectively. Although statistically significant, the magnitude of the effect of water-cement ratio on the moderate environment is not large for corrosion rate. For the aggressive environment, the higher the water-cement ratio, the higher the corrosion rate. This effect is probably related to the availability of the reactants water and oxygen. Also, the mean value of chloride concentration was greater at w/c=0.5, which also could cause the higher corrosion rate. There were similar trends in corrosion potential, but the variations were not statistically significant at a 90 percent or greater confidence level.

Table 14. Summary of water-cement ratio data for the corrosion variables: corrosion rate, potential, and chloride concentration [1 mpy = 0.0254 mm/yr; 1 lb/yd³ = 0.6 kg/m³].

w/c Ratio	Moderate Environment			Aggressive Environment		
	Corrosion Rate (mpy)	Corrosion Potential (mV, CSE)	Chloride Concentration (lb/yd ³)	Corrosion Rate (mpy)	Corrosion Potential (mV, CSE)	Chloride Concentration (lb/yd ³)
0.3	0.14	-145	2.0	2.0	-301	6.2
0.4	0.08	-158	1.5	2.8	-339	6.2
0.5	0.19	-188	2.3	3.9	-384	8.8

Air Content

Table 15 gives the mean values of rapid chloride permeability, electrical resistivity, and compressive strength at 28- and 90-day exposures for concretes prepared with air contents of 2, 5, and 8 percent. At 28 days, the highest rapid chloride permeability value is shown by concretes containing 5 percent air, and the lowest value is shown by concretes containing the highest air content. At 90 days, there is virtually no difference in the rapid chloride permeability values as affected by air content in the 2 to 8 percent range.

Table 15. Summary of air content data for the concrete property variables: rapid chloride permeability, resistivity, and compressive strength [1,000 psi = 6.895 MPa].

Air Content (%)	Rapid Cl Permeability		Resistivity		Compressive Strength	
	28 days (C)	90 days (C)	28 days (ohm-cm)	90 days (ohm-cm)	28 days (psi)	90 days (psi)
2	3,437	2,284	45,000	53,000	7,079	7,860
5	4,482	2,426	10,000	45,000	6,673	7,855
8	2,763	2,227	31,000	53,000	5,933	6,171

The expected contribution of air void content to the chloride permeability (as measured in this test) depends upon whether or not the air voids are filled with water during the test. If the air voids became water-filled during the specimen preparation step, it is expected that they would act as conduits for increased chloride permeability and, hence would provide a higher charge passed. If the air voids were not water-filled at the time of testing, the air voids would not contribute to increased chloride permeability.

The effect of air content on concrete electrical resistivity correlates well to that measured for chloride permeability (inversely related). There is no significant difference in electrical resistivity as affected by air content (within the range of 2 percent to 8 percent), with electrical resistivity values ranging between 45,000 ohm-cm and 53,000 ohm-cm after 90 days.

It should be noted that the result discussed above (chloride permeability and resistivity are not affected by air content) is contrary to general belief.

The effect of air content on the 28-day and 90-day compressive strength is given in table 15. The highest values of compressive strength were shown for the concretes with air contents of 2 and 5 percent, with the 8 percent air content condition being slightly lower. In general, air content had only minimal effect on the concrete properties measured.

Table 16 gives the mean values of corrosion rate, potential, and chloride concentration for the aggressive and moderate environments for concretes prepared with air contents of 2, 5, and 8 percent. For the moderate environment, there is no statistically significant effect of air content in the range of 2 to 8 percent. For the aggressive environment, a decrease in corrosion rate and corrosion potential (more negative) with an increase in air content was observed. This relationship is in conflict with conventional understanding. Also, note that the chloride concentration was similar for the three air contents in the aggressive environment. Typically, a more negative potential indicates a greater probability for corrosion. One possible explanation is that in these tests where macrocell corrosion is not present, the highly active steel surface behaves in a manner that is typical for activation polarization systems (corrosion rate decreases with more negative potentials). This explanation is discussed in a later section.

Table 16. Summary of air content data for the corrosion variables: corrosion rate, potential, and chloride concentration
[1 mpy = 0.0254 mm/yr; 1 lb/yd³ = 0.6 g/m³].

Air Content (%)	Moderate Environment			Aggressive Environment		
	Corrosion Rate (mpy)	Corrosion Potential (mV, CSE)	Chloride Concentration (lb/yd ³)	Corrosion Rate (mpy)	Corrosion Potential (mV, CSE)	Chloride Concentration (lb/yd ³)
2	0.18	-141	2.2	3.7	-254	7.0
5	0.09	-151	2.1	2.5	-357	7.3
8	0.15	-198	1.6	2.4	-412	7.0

Coarse Aggregate

Table 17 gives the mean values of rapid chloride permeability, electrical resistivity,

and compressive strength at 28- and 90-day exposures for concretes prepared with two different coarse aggregates: (1) quartz aggregate with an absorption value less than 1 percent and (2) limestone with an absorption value greater than 9 percent. Both aggregates are 9.5mm (0.375 in) maximum size (ASTM C 33, no. 8 Gradation).

Table 17. Summary of coarse aggregate data for the concrete property variables: rapid chloride permeability, resistivity, and compressive strength [1,000 psi = 6.895 MPa].

Coarse Aggregate	Rapid Cl Permeability		Resistivity		Compressive Strength	
	28 days (C)	90 days (C)	28 days (ohm-cm)	90 days (ohm-cm)	28 days (psi)	90 days (psi)
Limestone	4,784	3,401	26,000	40,000	5,700	6,450
Quartz	2,338	1,224	31,000	59,000	7,400	8,150

The high-absorption limestone aggregate results in significantly higher rapid chloride permeability at both 28 days and 90 days than the quartz aggregate. This is an expected result if it is assumed that the aggregates are saturated during the rapid chloride permeability test. If this is the case, it is expected that the effect of aggregate absorption (porosity) on rapid chloride permeability will remain constant throughout the concrete's curing history, as long as the concrete is in a saturated condition.

Concretes containing the quartz aggregate show slightly to moderately higher values of electrical resistivity. This is in agreement with the inverse relationship to chloride permeability.

The highest values of compressive strength were provided by the quartz aggregate (table 17). At 90 days, concretes containing the quartz coarse aggregate showed a mean compressive strength of 56.1 MPa (8,145 psi), compared to 44.4 MPa (6,445 psi) for concretes containing the limestone coarse aggregate. The greater porosity and lower intrinsic strength of the limestone aggregate is responsible for this result.

Table 18 gives the mean values of corrosion rate, potential, and chloride concentration for the aggressive and moderate environments for concretes prepared with coarse aggregate types of limestone and quartz. For the moderate environment, no effect of coarse aggregate was observed. For the aggressive environment, a lower corrosion rate was measured for the quartz aggregate. A more negative corrosion potential was also observed for the quartz aggregate. As for the air content data, the

more negative corrosion potential resulted in a lower average corrosion rate. No significant effect was observed for chloride concentration as a function of coarse aggregate.

Table 18. Summary of coarse aggregate data for the corrosion variables: corrosion rate, potential, and chloride concentration [1 mpy = 0.0254 mm/yr; 1 lb/yd³ = 0.6 kg/m³].

Coarse Aggregate	Moderate Environment			Aggressive Environment		
	Corrosion Rate (mpy)	Corrosion Potential (mV, CSE)	Chloride Concentration (lb/yd ³)	Corrosion Rate (mpy)	Corrosion Potential (mV, CSE)	Chloride Concentration (lb/yd ³)
Limestone	0.16	-152	1.9	3.6	-282	6.8
Quartz	0.12	-174	1.9	2.2	-400	7.3

Fine Aggregate

Table 19 gives the mean values of rapid chloride permeability, electrical resistivity, and compressive strength at 28- and 90-day exposures for concretes prepared with two different fine aggregates: (1) a relatively impermeable quartz aggregate and (2) a glacial sand composed of a variety of rock types, including limestone, dolomitic limestone, quartz, and siltstones. The porosity of the glacial sand, as indicated by water absorption, is moderately higher than that of the quartz sand (2.2 vs. 0.3 percent).

Table 19. Summary of fine aggregate data for the concrete property variables: rapid chloride permeability, resistivity, and compressive strength [1,000 psi = 6.895 MPa].

Fine Aggregate	Rapid Cl Permeability		Resistivity		Compressive Strength	
	28 days (C)	90 days (C)	28 days (ohm-cm)	90 days (ohm-cm)	28 days (psi)	90 days (psi)
Glacial	4,148	2,956	25,000	41,000	6,200	7,200
Quartz	2,974	1,668	33,000	58,000	6,950	7,850

As with the coarse aggregates, the mean values of rapid chloride permeability (C) are lower for concretes containing the quartz fine aggregate, relative to those containing the glacial sand. The effect of fine aggregate type is less significant than the effect of coarse aggregate type on rapid chloride permeability. This result is not unexpected since the difference in porosity (absorption) is not nearly as great for the fine aggregate as it is for the coarse aggregate.

Concretes containing the quartz aggregate show slightly to moderately higher values of electrical resistivity (table 19). This data is similar to for the coarse aggregate.

The highest value of compressive strength was provided by the quartz fine aggregate (table 19). The data for the fine aggregate is similar to that observed for the coarse aggregate. The glacial sand has a higher porosity and a lower intrinsic strength than the quartz sand.

Table 20 gives the mean values of corrosion rate, potential, and chloride concentration for the aggressive and moderate environments for concretes prepared with fine aggregate types of glacial sand and quartz sand. The effects of fine aggregate on the corrosion rate were more pronounced than for the coarse aggregate. The quartz sand had the lower corrosion rate in both of the environments. This more significant effect of the fine aggregate, as compared to the coarse aggregate, is probably due to the fine aggregate being incorporated into the concrete-steel interface to a greater extent than the coarse aggregate. The effect on corrosion potential was minimal. Although not large, the effect on chloride concentration is consistent with that on corrosion rate (lower chloride concentration corresponds to lower corrosion rate).

Table 20. Summary of fine aggregate data for the corrosion variables: corrosion rate, potential, and chloride concentration [1 mpy = 0.0254 mm/yr; 1 lb/yd³ = 0.6 kg/m³].

Fine Aggregate	Moderate Environment			Aggressive Environment		
	Corrosion Rate (mpy)	Corrosion Potential (mV, CSE)	Chloride Concentration (lb/yd ³)	Corrosion Rate (mpy)	Corrosion Potential (mV, CSE)	Chloride Concentration (lb/yd ³)
Glacial Sand	0.23	-177	2.2	4.0	-330	7.6
Quartz Sand	0.05	-150	1.7	1.8	-353	6.5

Mineral Admixture

Table 21 gives the mean values of rapid chloride permeability, electrical resistivity, and compressive strength for concretes prepared with mineral admixtures of silica fume, Class C flyash, Class F flyash, ground granulated blast furnace (GGBF) slag, and no admixture. The microsilica was used at a constant rate of 10 percent (by weight) of total cementitious material. Both the Class C and Class F flyash were used at a constant rate of 25 percent (by weight) of total cementitious material. The GGBF slag was used at a constant rate of 35 percent (by weight) of total cementitious material.

Table 21. Summary of mineral admixture data for the concrete property variables: rapid chloride permeability, resistivity, and compressive strength [1,000 psi = 6.895 MPa].

Mineral Admixture	Rapid Cl Permeability		Resistivity		Compressive Strength	
	28 days (C)	90 days (C)	28 days (ohm-cm)	90 days (ohm-cm)	28 days (psi)	90 days (psi)
Silica Fume	1,966	1,129	43,000	96,000	7,576	8,575
None	4,231	3,992	22,000	40,000	7,139	7,550
Class C Flyash	3,453	1,433	53,000	58,000	6,475	6,887
GGBF Slag	2,971	1,864	11,500	26,500	6,299	7,269
Class F Flyash	5,183	3,143	14,000	27,000	5,321	6,194

The most significant influence of mineral admixture on rapid chloride permeability is shown in the 90-day value where concretes prepared with silica fume, Class C flyash, and slag all have a mean rapid chloride permeability value of less than 2,000 C (table 20). The mean 90-day rapid chloride permeability value of the concretes containing no mineral admixture is 3,992 C. The use of Class F flyash provided only a slight reduction in rapid chloride permeability at 90 days (3143 C).

The contribution of the mineral admixture to reductions in rapid chloride permeability is related to either its pozzolanic activity, or to its ability to contribute additional cementitious material. Silica fume provided the most dramatic reduction in rapid chloride permeability at both 28 days and 90 days, despite the fact that it was used at only a 10 percent cement-replacement level. The small particle size (submicron) and expected high pozzolanic activity of silica fume are thought to be responsible for this result.

Both GGBF slag and Class C flyash also provide significant reductions in concrete rapid chloride permeability. Both of these mineral admixtures provide some material that participates in the pozzolanic reaction and that is capable of hydrating to form additional cementitious phases.

Class F flyash provided the least significant reduction in rapid chloride permeability, relative to the other mineral admixtures evaluated here. This result is also not unexpected since the Class F flyash participates primarily in the pozzolanic reactions; however, it is not as reactive as the other mineral admixture in this category (silica fume). The larger mean particle size of the Class F flyash, along with its expected lower pozzolanic activity, account for the fact that its effect on rapid chloride permeability is less significant and, in fact, is not seen until the advanced curing age of 90 days.

Relative to the concretes containing no mineral admixture, the use of silica fume or Class C flyash caused increases in electrical resistivity (table 21). Concretes containing 10 percent silica fume showed the highest electrical resistivity (95,000 ohm-cm). Concretes containing the Class F flyash or the GGBF slag showed electrical resistivity values that were slightly lower than the concretes that contained no mineral admixture.

Concretes in which the total cementitious phase was 10 percent silica fume had the

highest level of compressive strength (table 21). Concretes containing no mineral admixtures showed the next highest level of compressive strength. The fact that the concrete containing no mineral admixtures has a somewhat higher compressive strength than concretes containing Class C flyash and GGBF slag is somewhat surprising. It is generally assumed that compressive strength at later curing ages will be higher when these admixtures are used. However, in this investigation, the total amount of hydrated cementitious material was held constant at 30 percent by volume. This may account for the result in this case. At both curing ages, concretes containing the Class F flyash had the lowest values of compressive strength.

Table 22 gives the mean values of corrosion rate, potential, and chloride concentration for the aggressive and moderate environments for concretes prepared with mineral admixtures of silica fume, Class C flyash, Class F flyash, GGBF slag, and no admixture. Silica fume exhibited the lowest corrosion rate for both environments. GGBF slag and Class F flyash exhibited the highest corrosion rates in both the environments. For the moderate environment, the effect of mineral admixture on corrosion potential and chloride concentration was not significant. For the aggressive environment, the mineral admixtures tended to make the corrosion potential more positive to varying degrees. All admixtures tended to decrease chloride concentration by similar amounts when compared to no admixture for the aggressive environment.

Table 22. Summary of mineral admixture data for the corrosion variables: corrosion rate, potential, and chloride concentration [1 mpy = 0.0254 mm/yr; 1 lb/yd³ = 0.6 g/m³].

Mineral Admixture	Moderate Environment			Aggressive Environment		
	Corrosion Rate (mpy)	Corrosion Potential (mV, CSE)	Chloride Concentration (lb/yd ³)	Corrosion Rate (mpy)	Corrosion Potential (mV, CSE)	Chloride Concentration (lb/yd ³)
Silica Fume	0.06	-183	1.7	0.88	-318	6.6
None	0.06	-141	2.1	3.0	-447	9.0
Class C Flyash	0.08	-160	1.4	2.1	-232	6.4
GGBF Slag	0.19	-185	2.2	5.0	-281	6.8
Class F Flyash	0.31	-148	2.3	3.6	-426	6.6

Cement

Table 23 gives the mean values of rapid chloride permeability, electrical resistivity, and compressive strength for concretes prepared with six different cements, including four Portland cements, a calcium aluminate cement, and a magnesium phosphate cement. The Portland cements include one with a low tricalcium aluminate (C3A) content, one with a high C3A content, one with a low total alkali content, and one with a high total alkali content.

Table 23. Summary of cement data for the concrete property variables: rapid chloride permeability, resistivity, and compressive strength
[1,000 psi = 6.895 MPa].

Cement	Rapid Cl Permeability		Resistivity		Compressive Strength	
	28 days (C)	90 days (C)	28 days (ohm-cm)	90 days (ohm-cm)	28 days (psi)	90 days (psi)
E - Type I Low C3A	2,358	1,109	13,000	18,000	6,920	7,684
C - Type I Low Alkali	3,692	1,813	16,000	23,000	7,351	8,015
D - Type I High C3A	5,051	2,484	12,000	22,000	7,759	8,292
A - Type I High Alkali	2,709	2,797	23,000	28,000	7,733	8,514
B - Calcium Aluminate	1,664	1,444	101,000	126,000	5,997	6,221
F - Mag Phosphate	5,891	4,227	7,000	76,000	3,613	5,045

Concretes containing the magnesium phosphate cement showed the highest values of 28- and 90-day rapid chloride permeability (table 23). For the water-cement ratios used in the task B investigation, it is expected that the porosity of the cement paste phase may be highest for the magnesium phosphate cements. This expected higher level of open porosity would contribute to an increased rapid chloride permeability. Concretes containing the calcium aluminate cement showed the lowest rapid chloride permeability at 28 days (1,664 C), and the next to lowest value at 90 days (1,444 C).

There was a surprisingly large variation in 28-day and 90-day rapid chloride permeability values as affected by the portland cement source. Concretes containing the low-C3A-content cement showed the lowest 28-day and 90-day rapid chloride permeability values (2,358 C and 1,109 C, respectively). Concretes containing the high-C3A-content cement showed the highest 28-day rapid chloride permeability value (5,051 C). Concretes containing the high alkali Portland cement had the highest value of 90-day rapid chloride permeability (2,797 C), almost three times greater than the concretes containing the low-C3A-content cement (1,109 C). The high-alkali cement showed unique behavior in that the 28-day and 90-days rapid chloride permeability values are virtually identical. The chemistry of the portland cement (as reflected in the C3A content and alkali content) had a significant effect on rapid chloride permeability.

The calcium aluminate (Lumnite) cement showed an extremely high resistivity, greater than 100,000 ohm-cm (table 23). For the Portland cements, the variability in 28-day and 90-day electrical resistivity is not large. The 28-day values ranged from around 12,000 to 24,000 ohm-cm. The 90-day values ranged from around 19,000 to 29,000 ohm-cm. Concretes containing the magnesium phosphate concrete showed somewhat anomalous electrical resistivity results. The 28-day electrical resistivity of these concretes is relatively low (around 6,000 ohm-cm), while the 90-day values are greater than 75,000 ohm-cm.

Concretes containing the magnesium phosphate cement and the Lumnite cement showed the lowest values of compressive strength (table 23). For the water-cement ratios used here — 0.3, 0.4, and 0.5 — the total water content of the magnesium phosphate concretes is moderately to significantly higher than that which would be used for these types of concretes in the field. This accounts for the fact that these concretes showed the lowest values of compressive strength in this investigation.

Table 24 gives the mean values of corrosion rate, potential, and chloride concentration for the aggressive and moderate environments for concretes prepared with cement types of Type III low C3A, Type I high C3A, Type I low alkali, Type I high alkali, calcium aluminate, and magnesium phosphate. The type of cement had significant effects on the corrosion behavior. Type I low C3A and Type I low alkali exhibited the lowest corrosion rates while Lumnite and magnesium phosphate exhibited the highest corrosion rates for both the environments. Magnesium phosphate cement exhibited a very large effect on the corrosion potential; it tended to make the corrosion potential very negative relative to the other cements. The cement type had a significant effect on the chloride concentration achieved. However, the chloride concentration and corrosion rate did not correlate well, indicating that properties of the cement were just as important as chloride in establishing corrosion behavior.

Table 24. Summary of cement data for the corrosion variables: corrosion rate, potential, and chloride concentration
[1 mpy = 0.0254 mm/yr; 1 lb/yd³ = 0.6 kg/m³].

Cement	Moderate Environment			Aggressive Environment		
	Corrosion Rate (mpy)	Corrosion Potential (mV, CSE)	Chloride Concentration (lb/yd ³)	Corrosion Rate (mpy)	Corrosion Potential (mV, CSE)	Chloride Concentration (lb/yd ³)
E - Type III Low C3A	0.02	-109	1.2	1.4	-305	6.5
C - Type I Low Alkali	0.05	-58	2.2	1.3	-320	9.1
D - Type I High C3A	0.05	-86	2.5	3.1	-296	7.9
A - Type I High Alkali	0.11	-85	1.9	1.3	-274	5.5
B - Calcium Aluminate	0.20	-165	1.4	6.6	-343	7.3
F - Mag Phosphate	0.42	-478	2.4	3.7	-508	6.1

Statistical Model

General linear main effect term models were developed to predict rapid chloride permeability, electrical resistivity, compressive strength, corrosion rate (both moderate and aggressive environment), and corrosion potential (both moderate and aggressive environments). Because of the discrete variables, the model is in a different form than that described for the previous task A work. Also, because of the large number of independent variables, only the main effect terms are included in the model and no quadratic or interaction terms are included. Details of the model parameters for all of the dependent variables (permeability, compressive strength, etc.) were provided previously in the interim report (FHWA-RD-96-207). Only the rapid permeability, compressive strength, and

corrosion rate data (moderate and aggressive environments) are discussed in this report.

Table 25 shows the intercept, the estimate for each level of each parameter (independent variable), the R-square value for the model, and the mean value for all of the data for the rapid chloride permeability model. To help clarify the magnitude of the effect of each parameter, a high and low value (range-of-effect) predicted by the model is shown for each parameter assuming that all of the other parameters are maintained at their zero estimate value. The range-of-effect data is used to show the effect that a particular parameter has on the value of a dependent variable; the absolute magnitudes are of little general interest.

To calculate the rapid chloride permeability for any combination of independent variables, the intercept is summed along with the estimate of each discrete level for the concrete mix of interest. For example, the predicted chloride permeability estimate for a mix with a water-cement ratio of 0.4 (-1,255 C), air content of 5 percent (199 C), limestone coarse aggregate (2,177 C), glacial sand fine aggregate (1,288), no mineral admixture (2,128 C), and Type I low alkali cement (-2414 C) is 5,134 C ($3,011 - 1255 + 199 + 2177 + 1288 - 2414$).

From table 25, it is seen that all of the parameters have an effect on the rapid chloride permeability, with the exception of air content. Mineral admixture and cement type can each vary the rapid chloride permeability by approximately 3,000 C depending on the particular level chosen. The R-square value of 65 percent indicates that the model presented in table 25 can explain 65 percent of the variation observed in the data. It is likely that quadratic and interaction terms, which were not part of the experimental design, represent a large portion of the variability not explained by the model.

Table 26 shows the intercept, the estimate for each level of each parameter (independent variable), the R-square value for the model, and the mean value for all of the data for the compressive strength model. Examining the range of the effects of each parameter on the magnitude of the compressive strength indicates that all parameters tested can have a large effect on the compressive strength. Water-cement ratio and cement type had the largest effect. The R-square value of 90 percent is very high and indicates that the main effect term model presented in table 26 explains the majority of the variation in the data and should provide accurate predictions of compressive strength for the range of parameters tested.

Table 25. General linear model for main effect terms for rapid chloride permeability after 90 days.

Parameter	Level	Estimate	Range of Effect (coulombs)	
			Low	High
Intercept		3,011		
Water-Cement Ratio	0.3	-1,894	1,117	3,011
	0.4	-1,255		
	0.5	0		
Air Content (%)	2	57	3,011	3,210
	5	199		
	8	0		
Coarse Aggregate	Limestone	2,177	3,011	5,188
	Quartz	0		
Fine Aggregate	Glacial Sand	1,288	3,011	4,299
	Quartz	0		
Mineral Admixture	Silica Fume	-734	2,277	5,139
	None	2,128		
	Class C Flyash	-431		
	GGBF Slag	0		
	Class F Flyash	1,279		
Cement Type	Type III Low C3A	E -3,118	-107	3,011
	Type I Low Alkali	C -2,414		
	Type I High C3A	D -1,743		
	Type I High Alkali	A -1,430		
	Calcium Aluminate	B -2,783		
	Mag Phosphate	F 0		
R-Square	65%			
Mean (C)	1,902			

Table 26. General linear model for main effect terms for compressive strength after 90 days [1,000 psi = 6.895 MPa].

Parameter	Level	Estimate	Range of Effect (psi)	
			Low	High
Intercept		3,496		
Water-Cement Ratio	0.3	3,610	3,496	7,106
	0.4	1,958		
	0.5	0		
Air Content (%)	2	1,689	3,496	5,185
	5	1,684		
	8	0		
Coarse Aggregate	Limestone	-1,700	1,796	3,496
	Quartz	0		
Fine Aggregate	Glacial Sand	-1,213	2,283	3,496
	Quartz	0		
Mineral Admixture	Silica Fume	1,306	2,421	4,802
	None	280		
	Class C Flyash	-382		
	GGBF Slag	0		
	Class F Flyash	-1,075		
Cement Type	Type III Low C3A	E 2,640	3,496	6,966
	Type I Low Alkali	C 2,970		
	Type I High C3A	D 3,247		
	Type I High Alkali	A 3,470		
	Calcium Aluminate	B 1,176		
	Mag Phosphate	F 0		
R-Square	90%			
Mean (psi)	7,647			

Table 27 shows the intercept, the estimate for each level of each parameter (independent variable), the R-square value for the model, and the mean value for all of the data for corrosion rate in the moderate environment. The parameter with the largest magnitude effect is the cement type. Coarse aggregate has minimal effect on the magnitude of corrosion rate in the moderate environment. The R-square value of 44 percent is relatively low and it indicates that the model presented in table 27 can explain only 44 percent of the variation observed in the data. It is likely that quadratic and interaction terms represent a large portion of the inability of the model to predict corrosion rates.

Table 28 shows the intercept, the estimate for each level of each parameter (independent variable), the R-square value for the model, and the mean value for all of the data for corrosion rate in the aggressive environment. Examining the range of the effect, the mineral admixtures and the cement type have the largest effect on corrosion rate. The R-square value for this model is 40 percent. As for the model for corrosion rate in the moderate environment, this is a relatively low R-square value.

Table 27. General linear model for main effect terms for corrosion rate (mpy) in the moderate environment [1 mpy = 0.0254 mm/yr].

Parameter	Level	Estimate	Range of Effect (mpy)	
			Low	High
Intercept		0.426		
Water-Cement Ratio	0.3	-0.050	0.32	0.43
	0.4	-0.107		
	0.5	0.000		
Air Content (%)	2	0.024	0.36	0.45
	5	-0.066		
	8	0.000		
Coarse Aggregate	Limestone	0.036	0.43	0.46
	Quartz	0.000		
Fine Aggregate	Glacial Sand	0.175	0.43	0.60
	Quartz	0.000		
Mineral Admixture	Silica Fume	-0.127	0.30	0.55
	None	-0.121		
	Class C Flyash	-0.108		
	GGBF Slag	0.000		
	Class F Flyash	0.123		
Cement Type	Type III Low C3A	E -0.404	0.02	0.43
	Type I Low Alkali	C -0.373		
	Type I High C3A	D -0.371		
	Type I High Alkali	A -0.314		
	Calcium Aluminate	B -0.218		
	Mag Phosphate	F 0.000		
R-Square	44%			
Mean (mpy)	0.09			

Table 28. General linear model for main effect terms for corrosion rate (mpy) in the aggressive environment.

Parameter	Level	Estimate	Range of Effect (mpy)	
			Low	High
Intercept		4.52		
Water-Cement Ratio	0.3	-1.92	2.6	4.5
	0.4	-1.07		
	0.5	0.00		
Air Content (%)	2	1.30	4.5	5.8
	5	0.11		
	8	0.00		
Coarse Aggregate	Limestone	1.32	4.5	5.8
	Quartz	0.00		
Fine Aggregate	Glacial Sand	2.19	4.5	6.7
	Quartz	0.00		
Mineral Admixture	Silica Fume	-4.11	0.41	4.5
	None	-2.04		
	Class C Flyash	-0.29		
	GGBF Slag	0.00		
	Class F Flyash	-1.44		
Cement Type	Type III Low C3A	E -2.23	2.1	7.5
	Type I Low Alkali	C -2.38		
	Type I High C3A	D -0.56		
	Type I High Alkali	A -2.39		
	Calcium Aluminate	B 2.98		
	Mag Phosphate	F 0.00		
R-Square	40%			
Mean (mpy)	2.3			

DISCUSSION: TASK B – CONCRETE CHEMICAL AND PHYSICAL PROPERTIES

The data presented in the results section provides a significant database to analyze concrete deterioration and to predict corrosion behavior for a range of concrete compositions. In the following paragraphs, specific aspects of the data are discussed.

Effects of Independent Variables

A primary focus of task B was to characterize the effects of the independent variables (water-cement ratio, air content, coarse aggregate, fine aggregate, mineral admixture, and cement type) on the measured dependent variables. These effects are summarized in table 29. Table 29 uses arrows to indicate whether there is an effect and the direction of the effect. For example, an increase in the water-cement ratio increases the rapid chloride permeability; therefore, a low water-cement ratio is desired. All of the independent variables examined had a significant effect on one or more of the dependent variables measured.

Table 29. Summary of effects for the independent variables on the measured dependent variables.

Independent Variable	Dependent Variable							Chloride at Steel Surface, Moderate	Chloride at Steel Surface, Aggressive
	Rapid Chloride Permeability	Resistivity	Compressive Strength	Corrosion Rate, Moderate	Corrosion Rate, Aggressive	Corrosion Potential, * Moderate	Corrosion Potential, * Aggressive		
Water-Cement Ratio	↑	↓	↓	↑	↑	↑	↑	↔	↑
Air Content	↔	↔	↓	↔	↓	↑	↑	↔	↔
Coarse Aggregate**	↓	↑	↑	↓	↓	↔	↑	↔	↔
Fine Aggregate**	↓	↑	↑	↓	↓	↔	↔	↔	↔
Mineral Admixture	↓↑	↓↑	↓↑	↓↑	↓↑	↔	↓↑	↓↑	↓↑
Cement Type	↓↑	↓↑	↓↑	↓↑	↓↑	↓↑	↓↑	↓↑	↓↑

- ↓ : Decrease in dependent variable with an increase in independent variable.
 ↑ : Increase in dependent variable with an increase in independent variable.
 ↔ : No trend in dependent variable with an increase in independent variable.
 ↓↑ : Significant change in dependent variable with change in independent variable.
 * : Increase in corrosion potential is an increasingly more negative potential.
 ** : Increasing aggregate refers to increasing resistance to water absorption (going from limestone to quartz or glacial sand to quartz increases resistance to water absorption).
 Moderate: Moderate environment (21 °C (70 °F) - 75% Relative Humidity, 1.8 kg/m³ (3 lb/yd³) chloride).
 Aggressive: Aggressive environment (38 °C (100 °F), 98% Relative Humidity, 6 kg/m³ (10 lb/yd³) chloride).

Correlation Among Dependent Variables

A correlation matrix was performed on the data for the dependent variables given in table 29. Correlation coefficients were calculated for all the data together and for only the portland cement data as a subset. Only a few weak correlations were observed with the exception of rapid chloride permeability and 1/resistivity. The correlations between corrosion rate and potential and between rapid chloride permeability and resistivity are discussed below.

Corrosion Rate Versus Potential

The polarization behavior of a metal in an electrolyte is characterized by plotting the logarithm of the current versus the potential. The anodic polarization curve characterizes the corrosion behavior as a function of potential, since the anodic current is a measure of the corrosion rate. Steel in concrete is characterized by an active-passive behavior: (1) at a positive potential, steel is passive and (2) at a sufficiently negative potential, steel can become active. In task B, a range of concrete compositions was tested in two different environments, and the corrosion rate and corrosion potential were measured. The following analysis included only the four portland cements used in task B. The analysis indicated only weak correlations between the logarithm of the corrosion rate and the potential (coefficients of -0.4 and 0.6 for the moderate and aggressive environments respectively). But it was interesting that the correlation coefficient for the moderate environment data was negative and that for the aggressive environment it was positive.

Figure 16 shows the data for the moderate and aggressive environments. These data represent many different concretes of varying compositions. The ranges of corrosion rates indicated in the figure correspond to those previously used for minimal, intermediate, high, and very high corrosion rates. The data for the moderate environment indicate that corrosion rates increase as the potential becomes more negative, while the metal surface goes from a passive to an active corrosion condition. This is the typical observation for steel in chloride-contaminated concrete. This is also typical of corrosion of a passive metal during the passive to active corrosion transition.

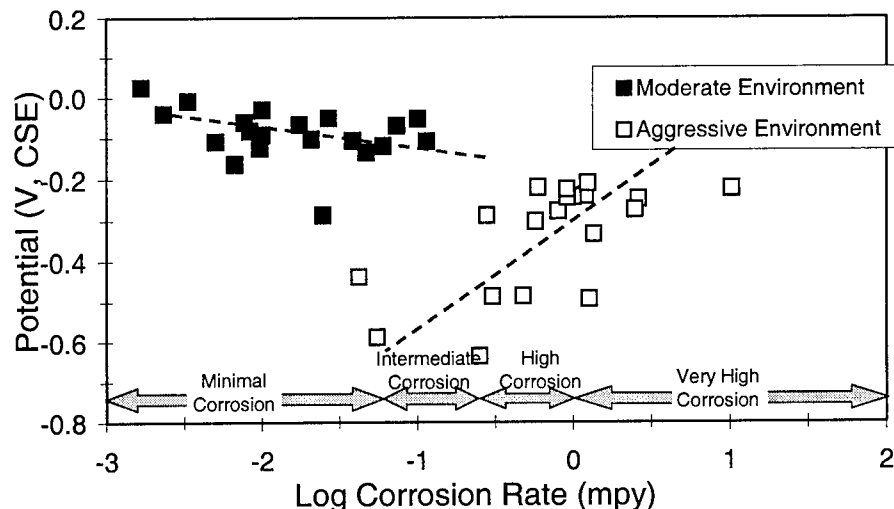


Figure 16. Logarithm of corrosion rate versus potential for the Portland Cement concretes tested in task B (averages of triplicate test specimens for each condition) [1 mpy = 0.0254 mm/yr].

For the aggressive environment, the observed relationship between corrosion rate and potential is the opposite of that described for the moderate environment and is not the normal behavior observed for steel in concrete. However, this is the typical relationship observed for active metal corrosion, i.e. the corrosion rate decreases as the potential becomes more negative. For the aggressive environment (high chlorides), the steel surface is predominantly active and the behavior in the absence of macrocells is typical for active corrosion.

Figure 17 shows a series of photographs of test specimens with a range of measured corrosion rates. Macrocell corrosion is observed on the two lower corrosion rate test specimens, while the highest corrosion rate specimen's surface is completely active.

The experimental test design for tasks A and B does not promote macrocell corrosion, although some was observed. For tests that promote macrocell corrosion by design, the more negative potential would increase the difference in the driving potential of the macrocell, and the corrosion rate would likely increase with more negative potentials.

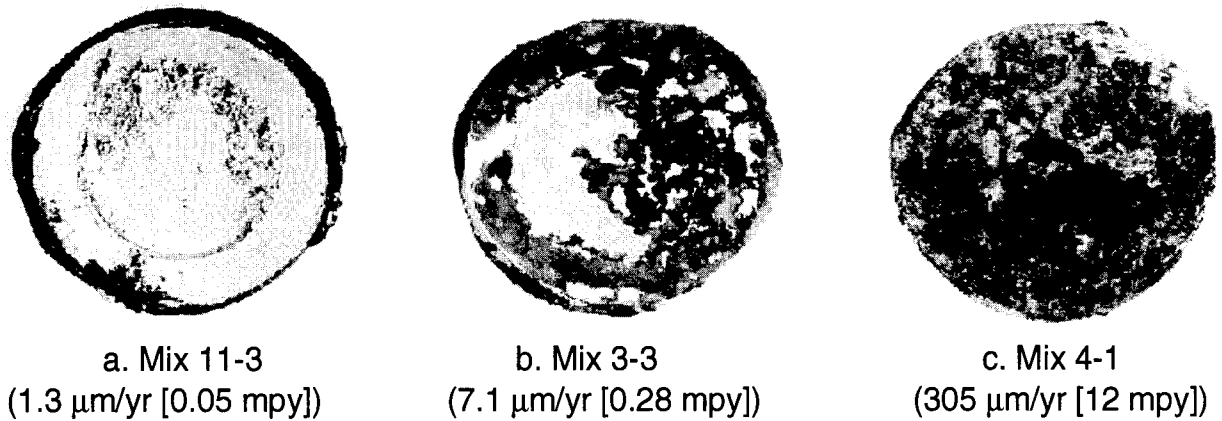


Figure 17. Photographs of typical corrosion in the aggressive environment in task B.

For this project, it is important to note the range of corrosion behavior possible for different environmental conditions and different concrete mix designs. Figure 16 provides an indication of the range of behavior observed as a function of environment (moderate versus aggressive) and for a range of concrete mix designs (range of data for a given environment).

Figure 18 shows potential versus logarithm of corrosion rate for the individual test cells for portland cement task B concretes and for the task A portland cement mortar (mortar A-2) and concrete (concrete A-5). This includes all individual test specimen data involving portland cement based materials from tasks A and B. The rate of corrosion can vary over three orders of magnitude at a given potential depending on the concrete mix components and the environment.

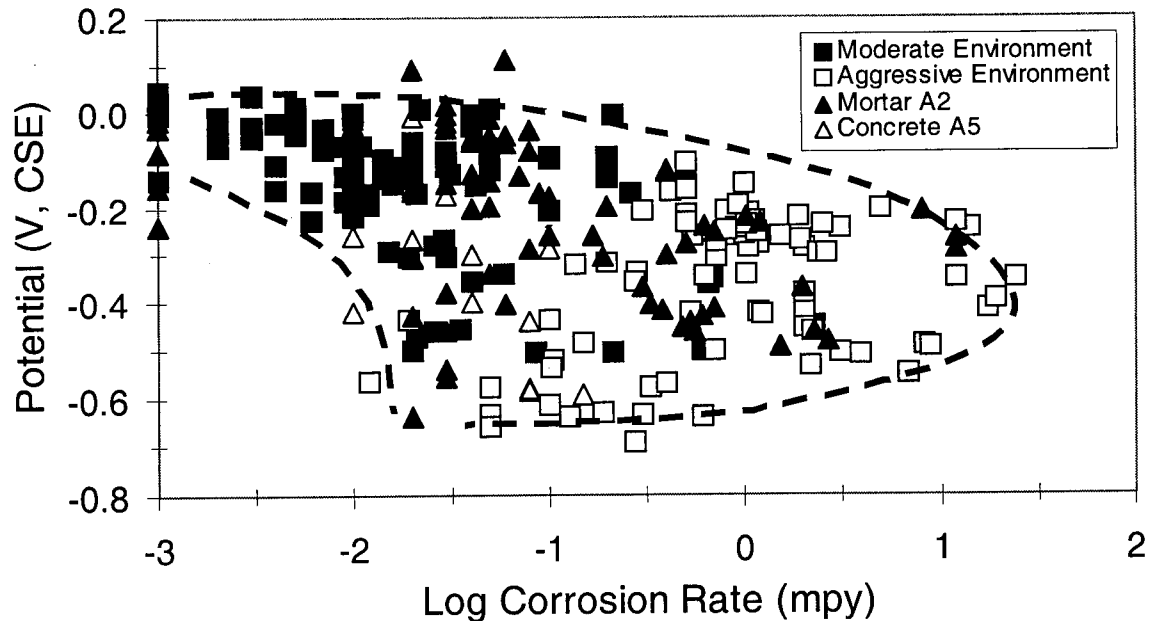


Figure 18. Logarithm of corrosion rate versus potential for the portland cement concretes tested in task A and B combined (individual test specimen data is given) [1 mpy = 0.0254 mm/yr].

Rapid Chloride Permeability Versus Resistivity

A very strong correlation was found between rapid chloride permeability and $1/\text{resistivity}$. The correlation coefficient was only 0.60 when all cement types were included. However, when only the portland cement types were analyzed as a subset, the correlation coefficient for rapid chloride permeability versus $1/\text{resistivity}$ was 0.99. Figure 19 shows rapid chloride permeability versus $1/\text{resistivity}$ for the portland cement data. The excellent agreement suggests that the resistivity test, which is easier to perform than the rapid chloride permeability test, has merit as a qualification test for concrete and there is no additional benefit for performing the rapid chloride permeability test. This is the same conclusion that was reported by Arup et al. and Feldman et al.^{2,3}

² A. Arup et al., "The Rapid Chloride Permeability Test – An Assessment." Corrosion/93, Paper No. 334, NACE, Houston, TX, 1993.

³ R.F. Feldman et al., "Investigation of the Rapid Chloride Permeability Test," *ACI Materials Journal*, May/June, 1994, p. 246.

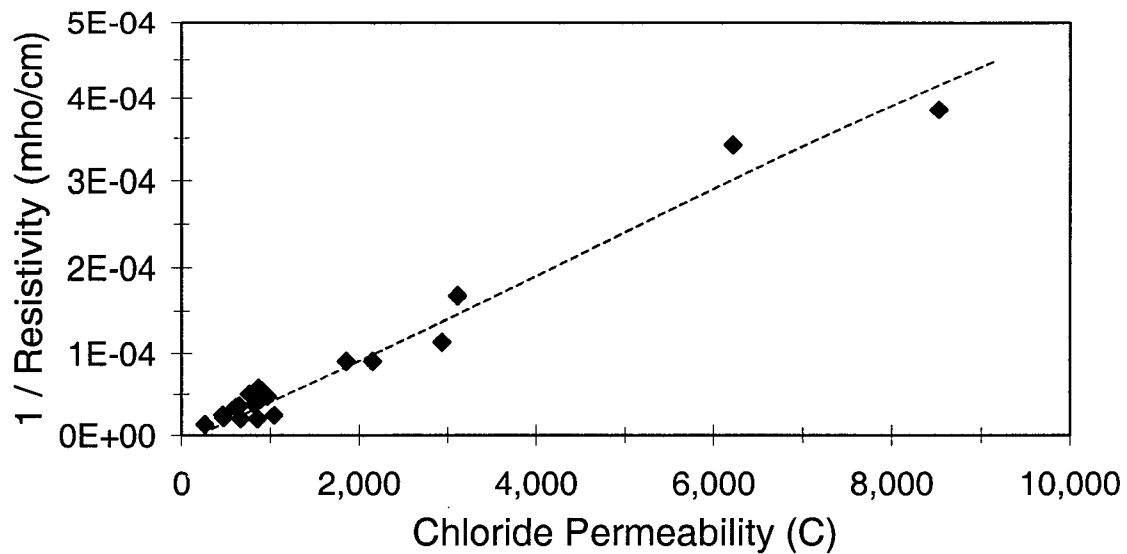


Figure 19. Rapid chloride permeability versus 1/resistivity for task B portland cement concrete.

Corrosion Rate Versus Resistivity

A relationship between corrosion rate and environment resistivity is often discussed. The expected relationship is one of greater resistivity resulting in a lower corrosion rate. In environments that are controlled by macrocell corrosion, this is especially important. Therefore, a relationship between 1/resistivity and corrosion rate is expected. The correlation coefficients utilizing all of the task B data were poor for both the moderate and aggressive environment. Some improvement in correlation for the aggressive environment was found when limiting the data to Portland cement concrete. Figures 20 and 21 show corrosion rate versus 1/resistivity for the aggressive and moderate environments respectively. The correlation coefficient for the aggressive environment data was only 0.58. There is significant scatter in the data, but the expected relationship is observed. These data indicate that resistivity is important; however, other factors also are important to explain the variations in the data. This was also clear from the statistical analysis of the task B data if rapid chloride permeability model results are substituted for 1/resistivity.

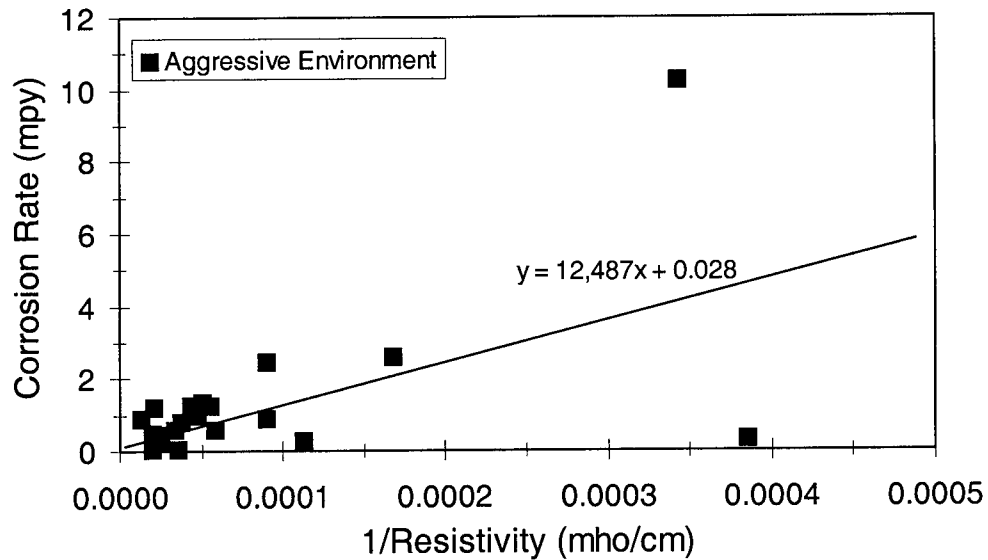


Figure 20. Corrosion rate versus 1/resistivity in the aggressive environment for task B portland cement concrete [1 mpy = 0.0254 mm/yr; 1 mho/cm =].

The correlation coefficient for the moderate environment data was less than 0.5. Figure 21 shows that no relationship can be drawn from the data. Therefore, for moderate environments, other factors are critical in establishing corrosion behavior.

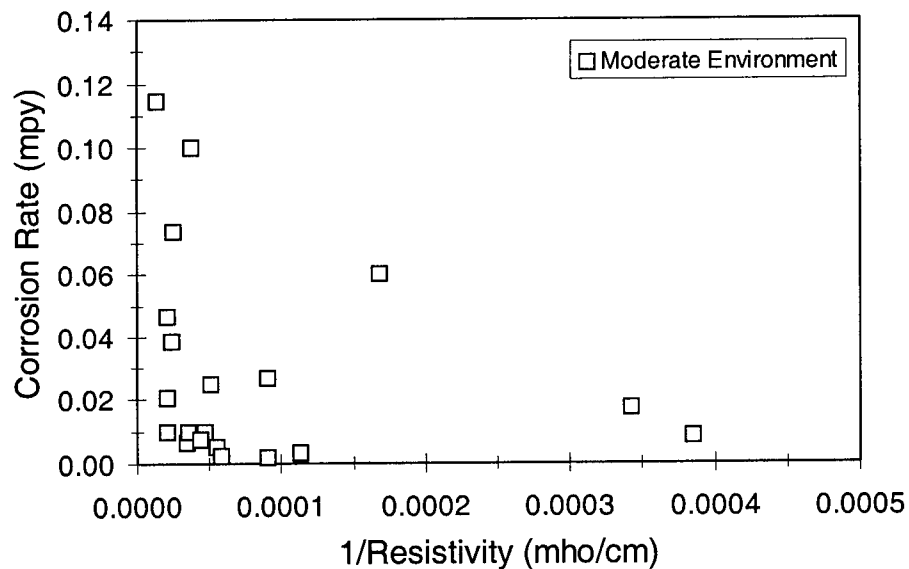


Figure 21. Corrosion rate versus 1/resistivity in the moderate environment for task B portland cement concrete [1 mpy = 0.0254 mm/yr; 1 mho/cm =].

Corrosion Rate Versus Chloride Concentration

The relationship between corrosion and chloride concentration is well established for steel in concrete. This relationship was shown in the task A results. Figure 22 shows a graph of corrosion rate versus chloride concentration for two of the concrete mixes in task B. These data represent the two environments (moderate and aggressive) used in task B. Each mix indicates the expected relationship between the increase in corrosion rate and the increase in chloride. However, temperature and relative humidity also increased in going from the moderate to the aggressive environments, therefore, chloride is not the only variable in these tests. This makes it difficult to draw significant conclusions from these data, although it is still worthwhile examining these data. Figure 23 shows all of the data for the tests involving portland cements (cements A, C, D, and E). These data indicate that the critical chloride concentration for corrosion initiation is approximately 1.2 to 1.5 kg/m³ (2 to 2.5 lb/yd³). It should be noted that this was dependent of the concrete mix and a few of the mixes indicated higher (1.8 to 2.4 kg/m³ [3 to 4 lb/yd³]) critical chloride concentration for corrosion initiation.

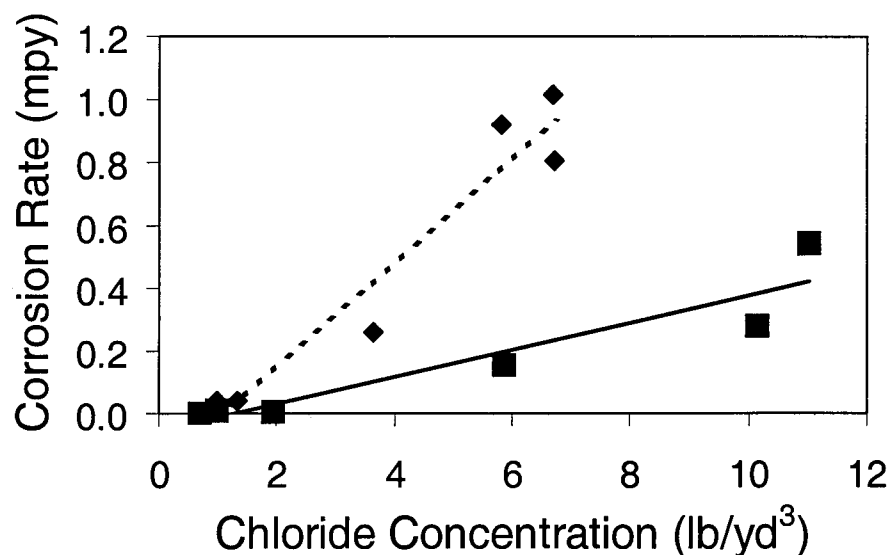


Figure 22. Corrosion rate versus chloride concentration for mix nos. 28 and 3 in task B [1 mpy = 0.0254 mm/yr; 1 lb/yd³ = 0.6 g/m³].

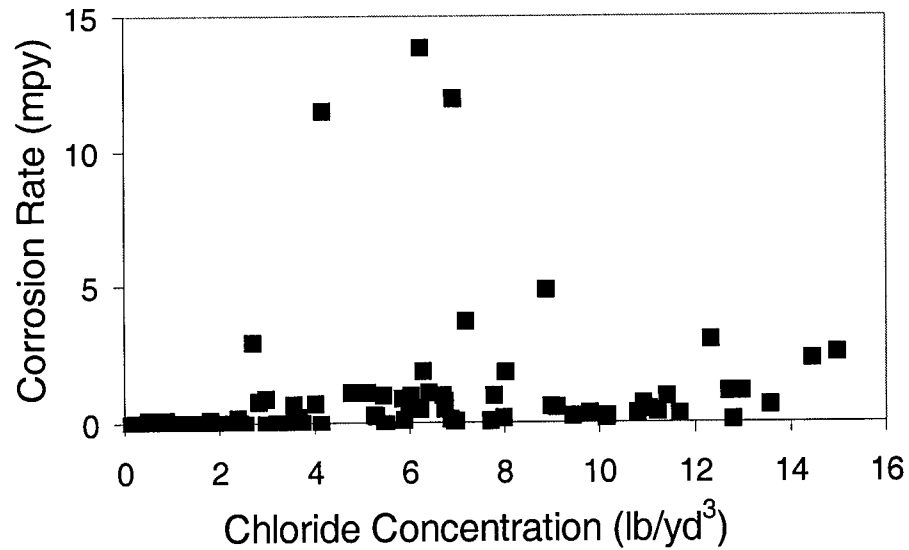


Figure 23. Corrosion rate versus chloride concentration for all Portland cements in task B [1 mpy = 0.0254 mm/yr; 1 lb/yd³ = 0.6 kg/m³].

Optimization for Corrosion Resistance

Optimizing concrete mix design for corrosion resistance is a main goal of this project. In addition to this overall goal, task B had a goal to select concretes for use in task C. Task C had a main goal to validate the findings of tasks A and B using larger scale slab specimens. In the following paragraphs, two optimization procedures are discussed: (1) predictions based on the general linear main effect models established in task B and (2) selection of optimum concrete mixes from the test matrix of concretes tested in task B.

Model Predictions

Chloride permeability was selected as the dependent variable that best describes the process of chloride diffusion. Corrosion rates in the moderate and aggressive environments were selected as the dependent variables that best describe the process of corrosion of steel. Table 30 shows the model estimates for these three dependent variables. The magnitude of the effect can be determined by adding the model estimate to the intercept value for that particular dependent variable. A negative estimate for a level indicates that the intercept value of the dependent variable would decrease by that amount and a positive estimate would increase the intercept value.

To the right of the Model Estimates, a qualitative ranking is provided, entitled Ranked by Deterioration Resistance. Within each independent variable, the levels are ranked (based on the model estimates) in order of their qualitative concrete deterioration resistance, most resistance first. Based on the magnitude of the effect, an indication is given as to whether the independent variable had a significant effect or not and whether two or more levels produced similar effects. For example, changing the levels of the independent variable “air content” had no appreciable effect on the dependent variables

“moderate environment corrosion rate” or “chloride permeability”. For “aggressive environment corrosion rate”, there was no appreciable difference in 5 or 8 percent air content, but 2 percent air content gave a higher corrosion rate.

Table 30. Levels of each independent variable ranked according to corrosion resistance for corrosion rate (moderate and aggressive environments) and rapid chloride permeability.

Independent Variable	Level	Model Estimates			Ranked by Deterioration Resistance*		
		Corrosion Rate, Moderate (mpy)	Corrosion Rate, Aggressive (mpy)	Chloride Permeability Estimate (C)	Corrosion Rate, Moderate	Corrosion Rate, Aggressive	Chloride Permeability
Intercept		0.426	4.523	3011			
Water-Cement Ratio	0.3	-0.050	-1.919	-1894	0.4	0.3	0.3
	0.4	-0.107	-1.067	-1255	0.3	0.4	0.4
	0.5	0.000	0.000	0	0.5	0.5	0.5
Air Content (%)	2	0.024	1.304	57		8	
	5	-0.066	0.114	199		5	
	8	0.000	0.000	0		2	
Coarse Aggregate	Limestone	0.036	1.322	2177		Quartz	Quartz
	Quartz	0.000	0.000	0		Limestone	Limestone
Fine Aggregate	Glacial Sand	0.175	2.186	1288	Quartz	Quartz	Quartz
	Quartz	0.000	0.000	0	Glacial Sand	Glacial Sand	Glacial Sand
Mineral Admixture	Silica Fume	-0.127	-4.109	-734	Silica	Silica	Silica
	None	-0.121	-2.035	2128	none	none	Class C FA
	Class C Flyash	-0.108	-0.292	-431	Class C FA	Class F FA	Slag
	GGBF Slag	0.000	0.000	0	Slag	Class C FA	Class F FA
	Class F Flyash	0.123	-1.444	1279	Class F FA	Slag	none
Cement Type	Type III Low C3A	E	-0.404	-3118	E	A	E
	Type I Low Alkali	C	-0.373	-2378	C	C	B
	Type I High C3A	D	-0.371	-1743	D	E	C
	Type I High Alkali	A	-0.314	-1430	A	D	D
	Lumnite	B	-0.218	-2783	B	F	A
	Mag Phosphate	F	0.000	0	F	B	F

↑ : No significant difference in magnitude of effect.
 ↔ : Independent variable does not affect dependent variable.

Note : 1.0 mpy = 0.0254 mm/year.

* : The levels in each independent variable are ranked from highest corrosion- induced deterioration resistance to least resistance.

For the “moderate environment corrosion rate” dependent variable, cement types E, C, and D have similar effects on the value of the corrosion rate; cements A and B are next, with cement F producing the highest corrosion rate. Cement F is also near the worst corrosion rate based on the “aggressive environment corrosion rate” variable and the worst rapid chloride permeability. Therefore, the model would predict that cement F would provide the highest concrete deterioration of the cements tested when exposed to a chloride environment. Cement E is one of the best performers based on the three dependent variables given in table 30. Likewise, silica fume was the best performer of the mineral admixtures based on all three dependent variables. Quartz aggregate was the best performer for both coarse and fine aggregates in improving concrete deterioration resistance.

The overall concrete deterioration resistance of cement A is somewhat more difficult to determine since it is the most corrosion resistant in the aggressive environment but has one of the highest chloride permeabilities. The good corrosion resistance might be explained by the high alkali content of cement A, but the overall performance of the concrete might be compromised by the higher conductivity (which suggests a higher

chloride permeability). The same difficulty in evaluating the overall performance of “no (none) mineral admixture” is true. The condition of “no mineral admixture” was good for lowering corrosion rate (both environments), but produced the highest rapid chloride permeability. Based on the model predictions, concretes can be designed that have a range of corrosion and chloride permeability behaviors.

Task B Test Matrix Optimization

In the above analysis, it was shown how concretes could be selected based on the model predictions of the statistical models. In this section, experimental data are used to rank the performance of the individual concretes tested in task B.

An optimization equation to predict the concrete deterioration resistance can be based on any number of variables. In this analysis, three variables were selected: (1) chloride permeability, (2) corrosion rate - moderate environment, and (3) corrosion rate - aggressive environment (the same as used above to rank concretes based on the statistical model). The critical component to this type of prediction model is how much weight is placed on each variable. The first step in optimizing for concrete deterioration resistance was to normalize the data using the following equation:

$$\text{Normalized Value} = (\text{Value} - \text{Minimum})/(\text{Maximum} - \text{Minimum}) \quad (2)$$

This type of normalization is required to permit the handling of variables of different types, and it sets the range of each variable between 1 (maximum value) and 0 (minimum value). For example, the normalized values for concrete mix no. 25 are calculated as follows:

$$\begin{aligned} \text{Moderate Corrosion Rate} &= (0.03-0.00)/(1.18-0.00) = 0.02 \\ \text{Aggressive Corrosion Rate} &= (1.86-0.06)/16.01-0.06) = 0.11 \\ \text{Rapid Cl - Permeability} &= (1,059-230)/12,332-230) = 0.07 \end{aligned}$$

Once normalized, equations can be used to weigh the importance of the dependent variables and a ranking of concrete deterioration resistance can be calculated simply by summing the normalized values times the weighting factor. The simple concrete deterioration resistance (CDR) equation used in this analysis was to give each of the three variables equal weighting. Both the resistance to chloride penetration prior to corrosion initiation and the rate of corrosion following initiation are critical to establishing the concrete deterioration resistance. See the equation below:

$$\text{CDR} = (0.33 \times \text{Moderate CR}) + (0.33 \times \text{Aggressive CR}) + (0.33 \times \text{Permeability}) \quad (3)$$

Other equations could be developed that give permeability greater weight, but it was felt that the equal weightings given above would provide a good first estimate for ranking the task B concretes. The calculation for CDR for concrete mix no. 25 is given below:

$$\text{CDR} = (0.33 \times 0.02) + (0.33 \times 0.11) + (0.33 \times 0.07) = 0.069$$

Table 31 gives the average and normalized values for the following dependent variables: corrosion rate - moderate environment, corrosion rate - aggressive environment,

and chloride permeability. Table 31 also gives the results of the above equation used to rank the corrosion deterioration resistance. The data in table 31 was sorted based on the ranking, from best corrosion deterioration resistance to worst.

Table 31. Optimizing concrete deterioration resistance based on the concretes tested in task B.[1 mpy = 0.0254 mm/yr].

Concrete Mix	Average Values			Normalized Values			CDR Ranking* 0.33 x Mod CR** Plus 0.33 x Agg CR*** Plus 0.33 x Perm****
	Mod CR (mpy)	Agg CR (mpy)	Rapid CI Perm (C)	Mod CR (mpy)	Agg CR (mpy)	Rapid CI Perm (C)	
11	0.01	0.04	645	0.01	0.00	0.03	0.014
18	0.03	0.67	230	0.03	0.04	0.00	0.022
30	0.02	0.06	850	0.02	0.00	0.05	0.023
3	0.01	0.59	605	0.00	0.03	0.03	0.023
24	0.00	0.57	863	0.00	0.03	0.05	0.029
10	0.02	1.15	299	0.01	0.07	0.01	0.030
5R	0.01	1.20	472	0.01	0.07	0.02	0.033
15R	0.05	0.48	663	0.04	0.03	0.04	0.034
1	0.07	0.47	460	0.06	0.03	0.02	0.036
23	0.04	0.28	1,037	0.03	0.01	0.07	0.038
9	0.01	1.00	965	0.01	0.06	0.06	0.043
6	0.01	1.26	893	0.00	0.08	0.05	0.045
26	0.01	1.24	888	0.01	0.08	0.05	0.045
12	0.02	1.35	759	0.02	0.08	0.04	0.048
16	0.01	2.09	438	0.01	0.13	0.02	0.050
28	0.11	0.91	260	0.10	0.05	0.00	0.051
2	0.10	0.80	815	0.08	0.05	0.05	0.060
25	0.03	1.86	1,059	0.02	0.11	0.07	0.069
8	0.13	0.07	1,486	0.11	0.00	0.10	0.071
27	0.00	0.91	2,149	0.00	0.05	0.16	0.071
13	0.00	0.25	2,933	0.00	0.01	0.22	0.079
7	0.03	0.22	2,854	0.02	0.01	0.22	0.083
19	0.03	2.48	1,854	0.02	0.15	0.13	0.103
17	0.06	2.61	3,111	0.05	0.16	0.24	0.149
29	0.01	0.30	8,520	0.01	0.02	0.69	0.235
21	0.30	6.46	981	0.25	0.40	0.06	0.239
22	0.02	10.26	6,218	0.01	0.64	0.49	0.382
4	0.25	16.01	539	0.21	1.00	0.03	0.413
20	1.18	10.93	12,332	1.00	0.68	1.00	0.893

*CDR : Corrosion deterioration resistance.

**CR-Mod : Corrosion rate - moderate environment.

***CR-Agg : Corrosion rate - aggressive environment.

****Perm : Chloride permeability.

SUMMARY: TASK B – CONCRETE AND PHYSICAL PROPERTIES

Statistical data analysis showed that corrosion resistance of concrete was

dependent on several concrete mix variables (table 29), including:

- Air content.
- Water-cement ratio.
- Aggregate type.
- Cement chemistry.
- Mineral admixture.

Statistical data analysis showed that chloride permeability of concrete (as measured by the rapid chloride permeability method) was dependent on the above mix variables with the exception of air content.

Statistical models to predict the effects of concrete mix variables on the following dependent variables were developed:

- Corrosion rate of reinforcing steel in concrete exposed to an aggressive environment (high relative humidity [98 percent], high temperature [38 °C], and 6-kg/m³ chloride concentration).
- Corrosion rate of reinforcing steel in concrete exposed to a moderate environment (moderate relative humidity [75 percent], moderate temperature [21 °C], and 1.8-kg/m³ chloride concentration).
- Chloride permeability (as measured by the rapid chloride permeability test).
- Compressive strength.

These models were used to optimize concrete deterioration resistance based on corrosion resistance and chloride permeability. In addition, these predictive models are required for the life prediction and concrete optimization analyses performed in task D.

The models developed and the test results were used to select different concrete mix designs for testing in task C large-scale slab tests.

CHAPTER 5. TASK C – LONG-TERM PERFORMANCE STUDIES

The primary goal of task C was to validate the findings and model predictions made in task B through long-term exposure of larger slab specimens that more closely simulate an actual concrete exposure. The following also was examined:

1. Mechanical aspect of the concrete deterioration resistance.
2. Optimization models for estimating concrete deterioration resistance.
3. Effect of macrocell couples on the corrosion rate predictions made in task B.

EXPERIMENTAL APPROACH: TASK C – LONG-TERM PERFORMANCE STUDIES

Selection of Task C Concretes

Table 32 gives the eight concretes selected for testing in task C: six concretes predicted to provide good concrete deterioration resistance (nos. 31, 11, 15R, 1, 3, and 24) and two concretes predicted to provide poor concrete deterioration resistance (nos. 22 and 29). Concrete no. 31 is the optimum concrete based on the statistical model results for maximizing concrete deterioration resistance. All of the other concretes were task B concretes selected to provide a range of performance characteristics.

Table 32. Concretes selected for task C [1 mpy = 0.0254 mm/yr].

Independent Variable	Level	Model Predictions	Optimization of Task B Mix Designs						
		Maximize CDR Mix Design 31	Maximize CDR Mix Design 11	Maximize CDR Mix Design 15R	Maximize CDR Mix Design 1	Maximize CDR Mix Design 3	Maximize CDR Mix Design 24	Minimize CDR Mix Design 22	Minimize CDR Mix Design 29
Water-Cement Ratio	0.3 0.4 0.5	0.3		0.5		0.3	0.3	0.3	0.4 0.5
Coarse Aggregate	Limestone Quartz	Quartz	Quartz	Quartz	Quartz	Quartz	Limestone	Limestone	Limestone
Fine Aggregate	Glacial Sand Quartz	Quartz	Quartz	Glacial Sand	Quartz	Glacial Sand	Quartz	Glacial Sand	Quartz
Mineral Admixture	Silica Fume None Class C Flyash GGBF Slag Class F Flyash	Silica		Silica		Class C FA Class C FA	Slag	None	None
Cement Type	Type III Low C3A Type I Low Alkali Type I High C3A Type I High Alkali Lumnite Mag Phosphate	E C D A B F	E	C		A	C	E D	A
Corrosion Rate - Moderate Prediction (mpy) :		-0.15	0.15	0.10	-0.05	0.07	0.01	0.04	0.027
Corrosion Rate - Aggressive Prediction (mpy) :		-3.74	0.85	0.22	-0.07	2.12	1.69	4.36	1.425
Chloride Permeability Prediction (C) :		-2735	1172	1151	-744	-440	176	5606	5886

CR-Mod : Corrosion rate - moderate environment.
CR-Agg : Corrosion rate - aggressive environment.
Perm : Chloride permeability.

Table 32 also gives the model predictions for each mix design. For some of the concretes, the model prediction values came out to be negative. This makes no physical

sense, but provides a relative performance prediction. Concrete mix no. 31 had the lowest corrosion rates (both moderate and aggressive environment) and the lowest chloride permeability. Recall that concrete no. 31 was designed, based on the model, to provide optimum concrete deterioration resistance performance. Of the task B concretes, concrete no. 1 stands out as having the next lowest value. Concrete nos. 22 and 29 have, by far, the highest chloride permeability values, as well as high corrosion rates. The predictions of the remaining concretes depend on the relative importance of corrosion rate performance versus chloride permeability.

Table 33 gives the ranking of concretes selected for task C testing according to: (1) the normalized moderate corrosion rate, aggressive corrosion rate, and chloride permeability data (table 31) and (2) statistical predictions (table 32). Based on these rankings different concretes provide different performance characteristics depending on the concrete deterioration resistance parameter selected and the optimization method. The only significant anomaly that stands out is: Task B data optimization ranked concrete no. 1 worst in the moderate environment corrosion rate, while it was one of the best in the statistical model prediction. These rankings will be referred to again in the task C analysis.

Table 33. Ranking of concretes selected for task C.

Ranking	Task B Measured Data (Table 31)			Statistical Model Predictions (Table 32)		
	Mod CR (Mix No.)	Agg CR (Mix No.)	Rapid CI Perm (Mix No.)	Mod CR (Mix No.)	Agg CR (Mix No.)	Rapid CI Perm (Mix No.)
1	24	11	1	1	1	1
2	3	29	3	24	15R	3
3	29	1	11	29	11	24
4	11	15R	15R	22	29	15R
5	22	24	24	3	24	11
6	15R	3	22	15R	3	22
7	1	22	29	11	22	29

TEST SPECIMEN DESIGN

Two types of specimens were used in the task C work. The standard specimen was used to evaluate the long-term corrosion performance of reinforcing steel in concrete. The repair/patch specimen was used to evaluate the corrosion performance of adjacent reinforcing steel in the repair/patch material and the concrete containing chloride.

Standard Specimen

The standard specimen used in the task C work for evaluating concrete materials is shown in figure 24. The sides of the specimen were coated with an epoxy. The concrete

surface above the reinforcing steel bars right and center was ponded with a 15 percent NaCl solution. The concrete surface above the reinforcing steel bar the left was ponded with deionized water. Chloride ingress into the concrete containing the right and center reinforcing steel bars produced a corrosion couple between the center and left reinforcing steel bars when electrically connected. The significance of the couple depended on the amount of chloride in the concrete and the corrosion resistance of the concrete. This slab specimen simulates reinforcing steel couples that have chloride gradients in the concrete.

The cover of the concrete to the top of the reinforcing steel bar was 19 mm (0.75 in). This provided for a cover that was twice the maximum diameter of the large aggregate. By maintaining a minimum cover, chloride ingress down to the reinforcing steel level was maximized.

The ends of the reinforcing steel bars were coated with a coal tar epoxy coating to insulate the transition of the steel into the concrete specimen. This coating extended into the concrete by 25.4 mm (1.0 in). This provided an uncoated steel specimen length of 254 mm (10 in) or an exposed surface area of 7,597 mm² (11.78 in²) for a bar diameter of 0.95 cm (0.375 in, no. 3 bar). The bottom of the concrete specimen was left open to the atmosphere (no coating). This promoted drying of the concrete from the bottom, creating a moisture gradient from the top of the concrete specimen (ponded) to the bottom, enhancing chloride diffusion into the concrete.

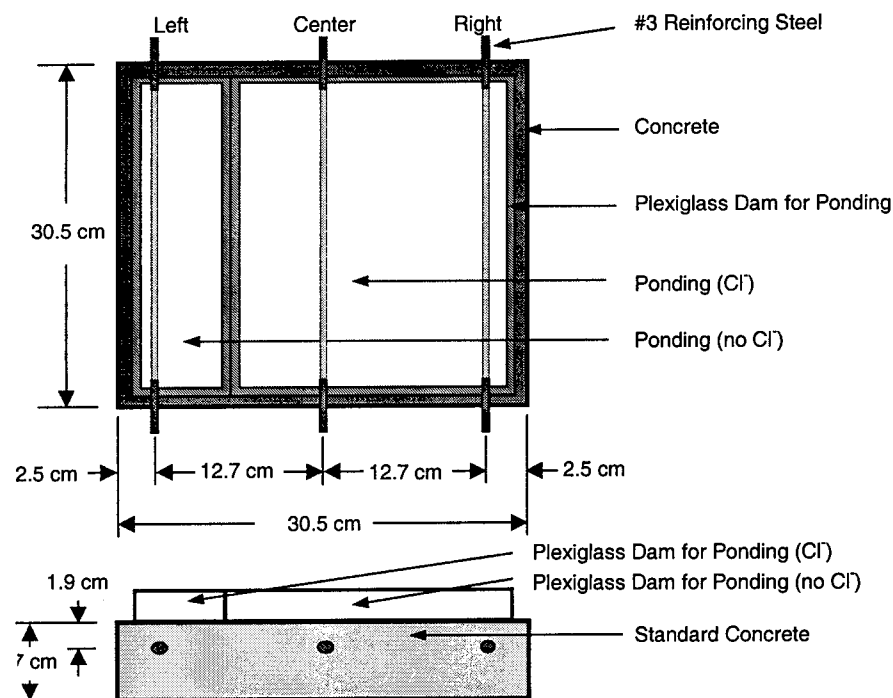


Figure 24. Schematic of task C standard slab specimen
[2.54 cm = 1 in].

Repair/Patch Specimens

The repair/patch specimens were similar to the standard specimens with the following exceptions. Chlorides were mixed into the standard concrete to pre-contaminate the concrete with 6.0-kg/m^3 (10-lb/yd^3) chlorides. This created a corrosive environment for the reinforcing steel from the start of the test. A temporary partition was placed in the mold so the standard concrete could be cast separate from the repair/patch concrete. The standard concrete was poured first and allowed to set. The partition was removed and the repair/patch concrete was cast (see figure 25). The primary measurement was between the right and center reinforcing steel bars (repair/patch concrete and standard concrete containing chloride). The pond above these two reinforcing steel bars was filled with 15 percent NaCl solution and the pond above the left steel bar in the contaminated concrete was filled with deionized water.

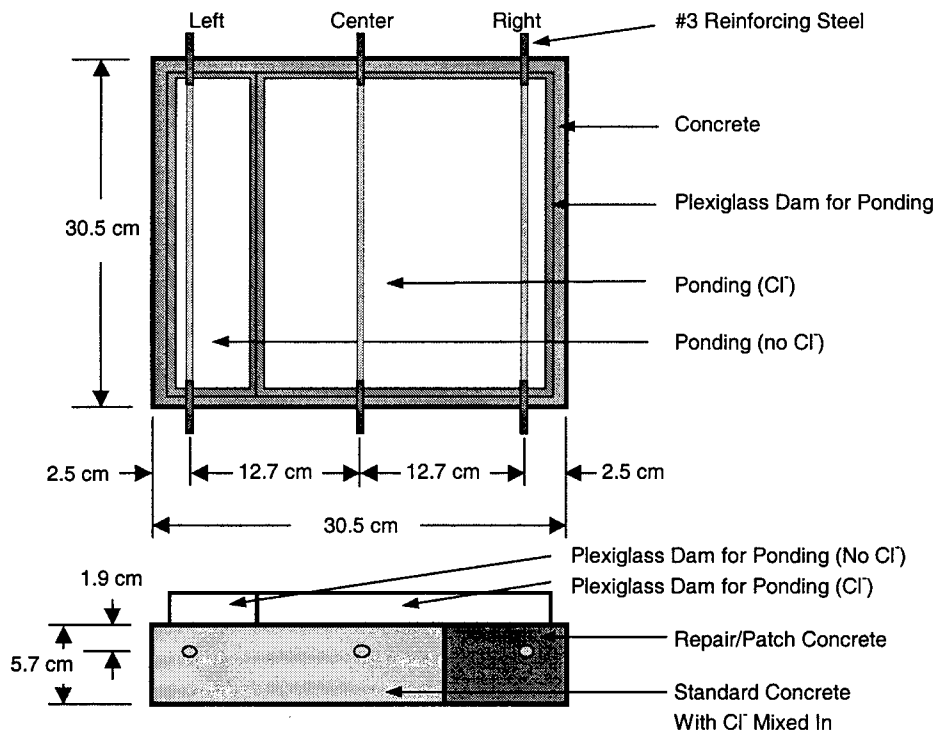


Figure 25. Schematic of task C repair/patch slab specimen
[2.54 cm = 1 in].

Standard Concretes

Ten concretes were examined in task C using the standard specimens (figure 24). Four repair/patch materials were selected (figure 25). Eight different concrete mixes were identified based on the task B work (nos. 1, 3, 11, 15R, 22, 24, 29, and 31). The mix components for these concretes are shown in table 34. Concrete no. 31 was not tested in task B, but is based on the results of the statistical model predictions. Concrete no. 31 was selected to give the combination of lowest corrosion rates and chloride permeability.

Concrete nos. 1, 3, 11, 15R, and 24 were selected to have good concrete deterioration resistance. Concrete nos. 22 and 29 were selected to have poorer concrete deterioration resistance. The selections were based on optimization of the actual measured values.

In all 29 of the concretes tested in task B, the cement paste (total cementitious phases plus water) was maintained at 30 percent by volume. The effect of variations in the cement paste content was evaluated in task C. To accomplish this, concrete no. 1 (table 34) was prepared at a cement paste content of 25 percent by volume (concrete no. 37) and 40 percent by volume (concrete no. 38). To achieve the desired cement paste content, the coarse and fine aggregates were varied in equal proportions. Table 35 gives the mix designs for these concretes.

Table 34. Concrete mix designs selected for task C concretes.

Mix Design	Independent Variables						
	W-C Ratio	Air Content (%)	Coarse Aggregate	Fine Aggregate	Mineral Admixture	Cement Type*	Cement Paste % Vol
1	0.3	2	Quartz	Quartz	Class C FA	A	30
3	0.3	8	Quartz	Glacial Sand	Class C FA	C	30
11	0.5	2	Quartz	Quartz	Class F FA	E	30
15R	0.5	8	Quartz	Glacial Sand	Silica	C	30
22	0.4	2	Limestone	Glacial Sand	None	D	30
24	0.3	8	Limestone	Quartz	Slag	E	30
29	0.5	8	Limestone	Quartz	None	A	30
31	0.3	5	Quartz	Quartz	Silica	E	30
37	0.3	2	Quartz	Quartz	Class C FA	A	25
38	0.3	2	Quartz	Quartz	Class C FA	A	40

* A: Type I High Alkali

C: Type I Low Alkali

D: Type I High C3A

E: Type III Low C3A

Repair/Patch Concretes

Four repair/patch concretes were examined using the specimen design shown in figure 25. These four concrete chemistries are shown in table 36 along with the standard concrete that has the 6.0-kg/m³ (10-lb/yd³) chloride mixed in (concrete no. 13 from task B). One of the repair/patch concretes (concrete no. 40) is a commercially available repair material (magnesium phosphate cement - Master Builders Set-45). Repair concrete 41 is a typical repair/patch concrete using a calcium aluminate cement. Repair concrete nos. 42 and 43 were selected based on the task B testing and analysis. These were concretes nos. 1 and 31 and represent the concretes expected to have the best resistance to corrosion deterioration based on task B data. These mixes have the desired properties of a

repair/patch material—low permeability and low corrosion rates. The low permeability (high resistivity) will minimize any macrocell couple effect.

The standard concrete pre-contaminated with chlorides and used in the specimens for evaluating the repair/patch concretes was mix no. 13 from task B. Mix no. 13 had intermediate values for corrosion rate and chloride permeability.

In addition to the repair/patch specimens (figure 25), standard specimens (figure 24) were also prepared for the repair/patch concretes. The standard specimens provided a baseline for comparing the results of the repair/patch specimens.

Table 35. Example of mix designs for concrete nos. 31, 37, and 38.

Concrete No. 31 (Task C)						
Concrete Constituents	Batch Weights		Density		Volume Ratio Component to Concrete	
	kg/m ³	lb/yd ³	kg/m ³	lb/ft ³	m ³ /m ³	ft ³ /yd ³
Cement E	429	723	3,152	196.6	0.136	3.68
Silica Fume	47	80	2,300	143.5	0.021	0.56
Quartz Sand	861	1,452	2,651	165.4	0.325	8.78
Quartz Aggregate	851	1,434	2,621	163.5	0.325	8.77
Water	143	241	1,000	62.4	0.143	3.86
Air					0.050	1.35
Totals	2,331	3,930			0.999	27.00

Theoretical cement paste (cement + mineral admixture + water) content = 30% vol

Theoretical unit weight = 2334 kg/m³ (145.6 lb/yd³)

Water-cementitious material ratio = 0.3

Air content = 5% vol

Concrete No. 37 (Task C)						
Concrete Constituents	Batch Weights		Density		Volume Ratio Component to Concrete	
	kg/m ³	lb/yd ³	kg/m ³	lb/ft ³	m ³ /m ³	ft ³ /yd ³
Cement A	298	503	3,152	196.6	0.095	2.56
Class C Flyash	99	167	2,770	172.8	0.036	0.97
Quartz Sand	968	1,631	2,651	165.4	0.365	9.86
Quartz Aggregate	957	1,613	2,621	163.5	0.365	9.87
Water	119	201	1,000	62.4	0.119	3.22
Air					0.020	0.53
Totals	2,441	4,115			0.999	27.00

Theoretical cement paste (cement + mineral admixture + water) content = 25% vol

Theoretical unit weight = 2,442 kg/m³ (152.3 lb/yd³)

Water-cementitious material ratio = 0.3

Air content = 2% vol

Concrete No. 38 (Task C)						
Concrete Constituents	Batch Weights		Density		Volume Ratio Component to Concrete	
	kg/m ³	lb/yd ³	kg/m ³	lb/ft ³	m ³ /m ³	ft ³ /yd ³
Cement A	477	804	3,152	196.6	0.151	4.09
Class C Flyash	159	268	2,770	172.8	0.057	1.55
Quartz Sand	768	1,295	2,651	165.4	0.290	7.83
Quartz Aggregate	759	1,280	2,621	163.5	0.290	7.83
Water	191	322	1,000	62.4	0.191	5.16
Air					0.020	0.54
Totals	2,354	3,969			0.999	27.00

Theoretical cement paste (cement + mineral admixture + water) content = 40% vol

Theoretical unit weight = 2357 kg/m³ (147.0 lb/yd³)

Water-cementitious material ratio = 0.3

Air content = 2% vol

Table 36. Repair/patch concrete mix designs selected for task C.

Mix Design	Independent Variables						
	W-C Ratio	Air Content (%)	Coarse Aggregate	Fine Aggregate	Mineral Admixture	Cement Type*	Cement Paste % Vol
13	0.4	5	Quartz	Quartz	none	C	30
40	(*)	2	Quartz	p	p	Set-45	p
41	0.35	5	Quartz	Quartz	none	B	30
42	0.3	2	Quartz	Quartz	Class C FA	A	30
43	0.3	5	Quartz	Quartz	Silica	E	30

p: Proprietary

(*): 7.3% water based on dry Set-45

A: Type I High Alkali

B: Calcium Aluminate Cement

C: Type I Low Alkali

E: Type III Low C3A

Environment

For tasks A and B, chlorides were diffused into the concrete prior to exposure to the desired environment. Temperature and relative humidity (external) were controlled to selected values during the exposures. For task C, a more conventional means of introducing chlorides into the concrete (i.e., ponding with a 15 percent NaCl solution, either cyclic or constant ponding) was utilized. Ponding with chlorides makes external humidity control less important. For the task C tests, the conditions selected were 38 °C (100 °F) and 50 percent external relative humidity. The high temperature enhanced both the corrosion rate of the reinforcing steel and the ingress of chlorides into the concrete. The 50 percent relative humidity promoted drying of the exposed concrete that was not ponded or coated. When the concrete specimens were ponded, drying of the bottom of the concrete enhanced ingress of the chlorides into the concrete by establishing a moisture gradient in the 57-mm (2.25-inch) thickness of the concrete cover below the steel bar. When the specimens were not ponded, the low relative humidity promoted drying of the concrete that enhanced chloride ingress into the concrete during the ponding cycle.

Exposure

Eight concrete specimens were cast for each standard concrete and repair/patch concrete to be examined in task C. After fabrication, these specimens were cured for a minimum of 28 days in a 100 percent humidity room before ponding. Four each of these specimens were tested under two exposure conditions: (1) continuous ponding and (2) cyclic ponding. The continuous ponding exposure consisted of continuous ponding with a 15 percent NaCl solution within a 38 °C (100 °F) room maintained at a maximum of 50 percent relative humidity.

In this exposure, the concrete was dried from the bottom setting up a moisture gradient that enhances the ingress of chlorides into the concrete. The total exposure period was 600 to 700 days, depending on the particular specimen.

The cyclic ponding exposure consisted of the following:

1. Dried specimens at 38 °C (100 °F), 50 percent maximum relative humidity until 40 to 50 percent of the total free water was removed from the concrete (weighed specimens).
2. Ponded with 15 percent NaCl solution for 14 days.
3. Removed ponding solution and allowed to dry for 7 days.
4. Repeated ponding-drying cycle steps 2 and 3 for the duration of the exposure (600 to 700 days).

The initial drying period was designed to remove a significant amount of the free water in the concrete to accelerate chloride ingress once the initial ponding with the 15 percent NaCl solution was performed. Figure 26 shows the percentage of water loss (based on theoretical free water) versus drying time. A wide range of drying behavior was observed.

The length of the wet-dry cycle was selected to permit monitoring of the corrosion activity during this cyclic exposure. Also, the length of the cycle and the low relative humidity (maximum 50 percent) of the external environment permitted drying of the concrete to greater depths, which enhances chloride ingress into the concrete.

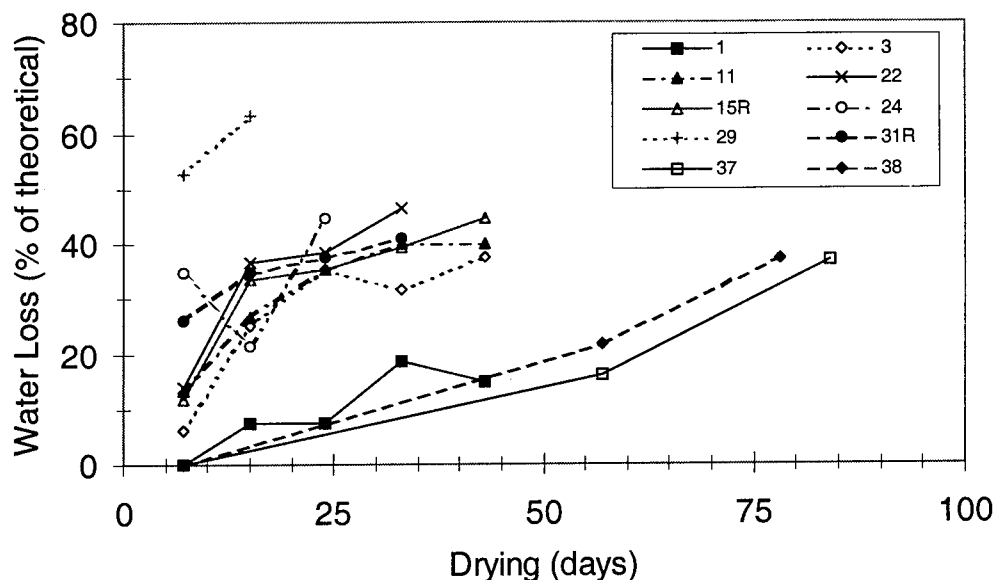


Figure 26. Percentage of water loss during initial drying exposure for task C concretes.

Measurements

Measurements were divided into the following three categories: (1) rate of chloride ingress, (2) rate of corrosion, and (3) rate of corrosion-induced damage.

Rate of Chloride Ingress

Acid soluble chloride at the reinforcing steel depth was measured at the completion of the exposure period. Figure 27 shows the locations at which chloride analyses were performed for each of the concrete slabs (standard and repair).

Resistivity of the concrete was measured following 1, 7, and 28 days, and 3, 6, 12, 18, and 24 months of exposure at 100 percent humidity. These measurements were performed on small cup samples specially designed for a two-pin resistivity measurement. For portland cement concretes, this resistivity measurement was shown to be inversely proportional to the rapid chloride permeability measurement.

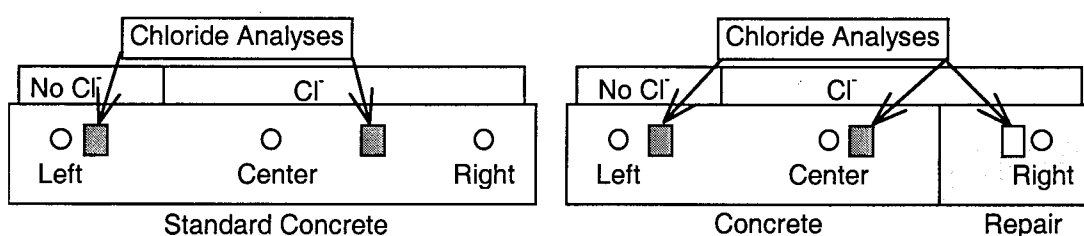


Figure 27. Schematic showing chloride analysis locations.

Rate of Corrosion

The following measurements were made:

1. Coupled current measurements were made between the left and center steel bars for the standard concrete slab (figure 28) or the center and right steel bars for the repair/patch slab (figure 28). Coupled currents were measured periodically during the exposure period. For the cyclic exposures, coupled current measurements were made immediately following the wet exposure.
2. Linear polarization resistance (LPR) measurements were made for all three steel bars (uncoupled) for both slab types (standard and repair/patch). The reference electrode is placed over the steel bar being measured and an adjacent steel bar is used as the counter electrode for the measurement (figure 29). Solution resistance correction was made and measurements were performed periodically based on the results of the coupled current measurements.
3. Potential measurements were made with respect to a Cu/CuSO_4 (CCS) reference electrode performed in conjunction with the LPR measurements.

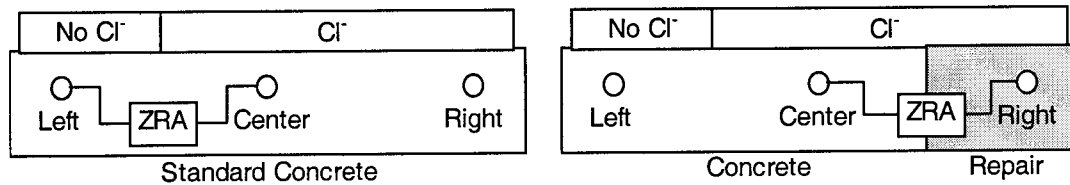


Figure 28. Coupled current measurement using zero resistance ammeter (ZRA).

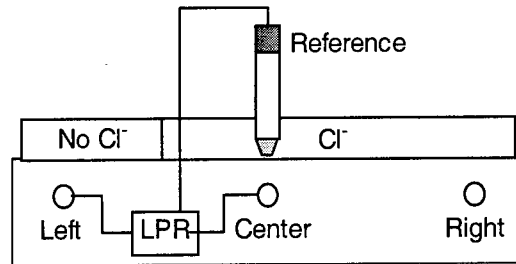


Figure 29. LPR corrosion rate measurement for the center steel bar.

Rate of Corrosion-Induced Damage

The following measurements were made to characterize the mechanical properties of the concretes (which may in turn be related to the ability to resist damage).

1. Compressive strength was measured on 4- x 8-in (102- x 203-mm) cylinders following 28-day, 6-, 12-, and 24-month exposures at 100 percent humidity.
2. Modulus of elasticity was measured on 4- x 8-in (102- x 203-mm) cylinders following 28-day, 6-, 12-, and 24-month exposures at 100 percent humidity.
3. Flexural strength was measured on 4- x 4- x 14-in (102- x 102- x 356-mm) beams following 28-day, 6-, 12-, and 24-month exposures at 100 percent humidity.

An ultrasonic pulse velocity measurement technique was performed on the exposed concrete slabs to assess the onset and extent of damage in the concrete. This technique did not prove to be accurate for the specimen configuration used. Damage was assessed by noting the time to first visible cracking.

Concrete Chemistry

Efforts were made to correlate chloride ingress, corrosion rate, and damage rate with chemical and mineralogical properties of the concretes. To accomplish this, the following measurements were made:

1. pH of the concrete specimens as a function of depth on representative specimens selected for post-test examination.
2. Petrographic analysis (ASTM C856) on selected specimens following exposure.

RESULTS: TASK C – LONG-TERM PERFORMANCE STUDIES

Concrete Property Data

Concrete property data collected on the task C concretes included compressive strength, flexural strength, modulus of elasticity, and electrical resistivity.

Compressive Strength

Table 37 shows compressive strength as a function of curing time. Compressive strength continued to increase as a function of curing time during the first year of exposure. The only exception to this was repair concrete no. 41, which is calcium aluminate cement. The 28-day compressive strength for the concretes ranged from 29.6 to 64.8 MPa (4,300 to 9,400 psi).

Table 37. Compressive strength data for task C concretes
[1,000 psi = 6.895 MPa].

Mix Design	Compressive Strength (psi)			
	28 Day	6 Month	1 Year	2 Year
1	8,180	9,340	10,910	10,740
3	6,540	8,490	9,140	9,280
11	4,665	6,855	7,610	7,615
15R	5,265	5,505	5,942	5,780
22	7,165	8,025	8,335	8,325
24	7,650	8,040	8,540	8,335
29	4,270	4,730	4,970	4,600
31	9,400	10,565	11,180	10,595
37	7,850	9,495	10,250	10,460
38	9,345	10,595	11,320	11,417
40	7,170	9,410	9,170	8,410
41	6,375	8,620	4,550	3,370
13	6,050	8,420	8,490	8,810

Flexural Strength

Table 38 shows the flexural strength for the task C concretes as a function of curing time. The strength developed after 28 days, in general, does not significantly change with curing time (some decrease slightly and some increase). For the concretes tested, the 28-day flexural strength ranged from 4.83 to 10.7 MPa (700 to 1,550 psi).

Table 38. Flexural strength data for the task C concretes
[1,000 psi = 6.895 MPa].

Mix Design	Flexural Strength (psi)			
	28 Day	6 Month	1 Year	2 Year
1	1,450	1,515	1,455	1,130
3	1,025	1,080	975	1,040
11	800	1,015	1,020	1,135
15R	790	850	850	835
22	875	980	900	955
24	925	1,040	985	1,025
29	655	735	700	670
31	1,340	1,535	1,430	1,330
37	1,440	1,410	1,155	1,255
38	1,240	1,565	1,555	1,575
40	645	630	740	860
41	1,005	1,025	665	320
13	940	845	775	860

Modulus of Elasticity

Table 39 shows the modulus of elasticity for the task C concretes as a function of curing time. The modulus developed after 28 days, in general, does not significantly change with curing time (some decrease slightly and some increase). For the concretes tested, the modulus ranges from 2.3×10^4 to 4.6×10^4 MPa (3.3×10^6 to 6.7×10^6 psi).

Resistivity

Table 40 shows resistivity of the task C concretes as a function of curing time. In general, resistivity continued to increase over the first year of exposure. The 28-day resistivity values ranged from 2,700 to 167,000 ohm-cm. This is a very significant range in resistivity for the different concretes.

Table 39. Modulus of elasticity for the task C concretes
[1,000 psi = 6.895 MPa].

Mix Design	Modulus of Elasticity (psi x 10 ⁶)			
	28 Day	6 Month	1 Year	2 Year
1	6.71	6.72	6.58	6.67
3	4.05	4.80	4.94	5.11
11	5.08	5.89	5.92	5.97
15R	3.72	3.83	4.31	4.01
22	3.31	3.65	3.88	4.02
24	3.71	4.43	4.39	4.50
29	2.91	3.13	3.18	2.77
31	5.92	6.47	6.41	6.56
37	6.12	6.64	6.59	6.98
38	5.93	5.98	6.03	6.19
40	6.00	6.82	6.48	6.76
41	4.38	4.61	3.77	3.19
13	5.79	5.77	5.78	5.45

Table 40. Resistivity of the task C concretes.

Mix Design	Resistivity (ohm-cm)							
	1 Day	7 Day	28 Day	3 Month	6 Month	1 Year	1.5 Year	2 Year
1	695	12,275	19,065	33,335	43,280	48,900	46,640	41,700
3	1,750	6,380	12,140	26,545	45,265	69,960	89,505	90,535
11	1,785	4,155	7,270	20,025	41,565	71,330	82,990	89,165
15R	1,850	4,525	25,510	42,385	41,565	43,280	44,995	43,210
22	1,510	2,810	3,210	3,785	4,730	9,670	6,925	7,615
24	1,850	9,330	24,000	29,495	34,155	44,785	45,130	46,435
29	795	2,085	2,705	3,005	3,925	5,075	5,660	5,350
31	1,646	22,495	167,350	240,055	231,825	187,930	211,935	155,695
37	NA	17,695	30,180	28,670	40,945	46,640	45,265	45,955
38	NA	8,520	12,220	20,440	24,620	26,200	23,935	22,015
40	9,330	18,450	41,150	97,390	877,920	>900,000	>900,000	>900,000
41	19,205	36,900	71,330	113,170	175,100	70,505	20,025	7,615
13	1,440	4,525	4,730	5,965	5,695	6,653	5,965	7,700

Corrosion Behavior – Standard Concretes

Coupled Current Measurements

Coupled currents were measured between two reinforcing steel bars, one ponded with NaCl solution and the other ponded with deionized water. The coupled current provides a good indication of the time of corrosion initiation and relative corrosion activity. Concrete nos. 1, 3, 31, 37, and 38 have exhibited no signs of initiation of corrosion on the reinforcing steel as exhibited by the negligible coupled currents after approximately 24 months of exposure to either the

continuous ponded or the cyclic wet-dry exposures. The average coupled current for the four replicate specimens is shown in Appendix B.

A corrosion rate of 0.0025 mm/yr (0.1 mpy), which is considered a lower limit for significant corrosion, is produced by a coupled current of 16.5 μA (assuming a surface area of 7,600 mm² (11.78 in²). It is important to note that the corrosion rate based on the coupled current is only a fraction of the actual corrosion rate. The measured coupled current is only that current that flows between the corroding steel bar (chloride-contaminated concrete) and the non-corroding, passive steel bar (concrete with no chloride). Additional corrosion current flows between the active sites on the corroding steel bar and the passive sites on the same steel bar, which is not part of the measured couple current. The fraction of corrosion accounted for in the coupled current measurement is difficult to estimate and probably varies depending on the concrete characteristics (resistivity, porosity, micro-cracks, etc.) for the different concretes being tested and could also vary from specimen to specimen of the same concrete. Therefore, it is difficult to relate coupled current directly to corrosion rate. In a later analysis (table 43), it was shown that the corrosion rate calculated from coupled current measurements was 5 to 10 times less than the corrosion rate measured by linear polarization resistance (LPR) methods. Therefore, it is assumed for the purposes of this study that 2 to 5 μA represents measurable corrosion activity.

Coupled current versus time for concrete no. 24 is shown in figure 30. A small amount of activity has been noted for the coupled current data for the wet condition, but these currents have remained relatively small. The data plotted in figure 30 is the average current for the four replicate slab specimens. Concrete no. 24 specimens are somewhat unusual in that there was some activity early in the exposure followed by negligible currents over the last half of the exposure. Figures 31 and 32 show the individual currents for the cycled and continuously wet exposures, respectively. All of the slabs exhibited this behavior and only one (slab E) has continued to exhibit some possible corrosion activity.

Coupled current versus time for concrete no. 15R is shown in figure 33. The coupled currents for concrete no. 15R have remained low throughout the exposure. The coupled current for the reinforcing steel in the cyclic exposure conditions was greater than the current for the continuously wet conditions. This was typical for all concretes with the exception noted above for concrete no. 24.

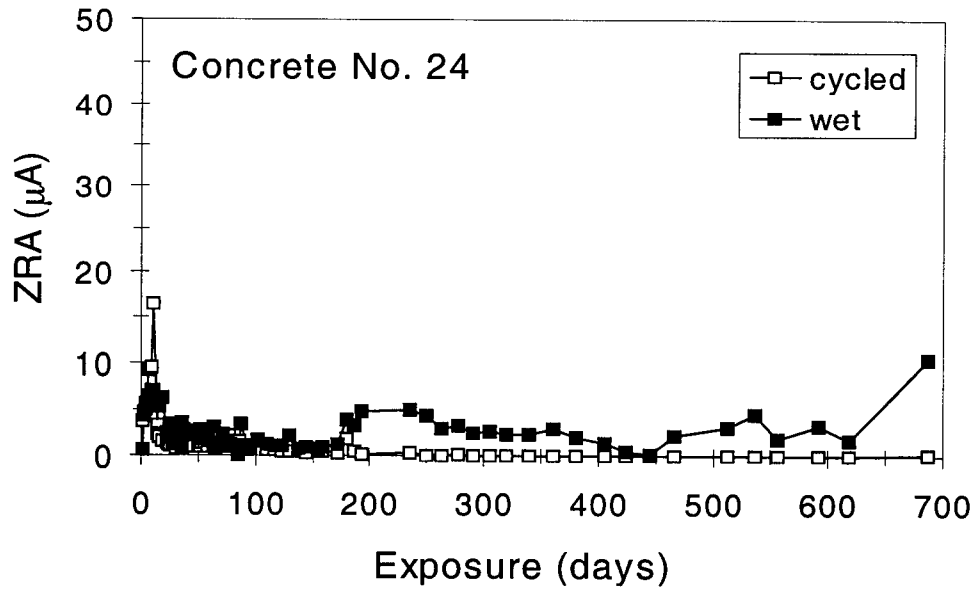


Figure 30. Averaged coupled current versus time for concrete no. 24.

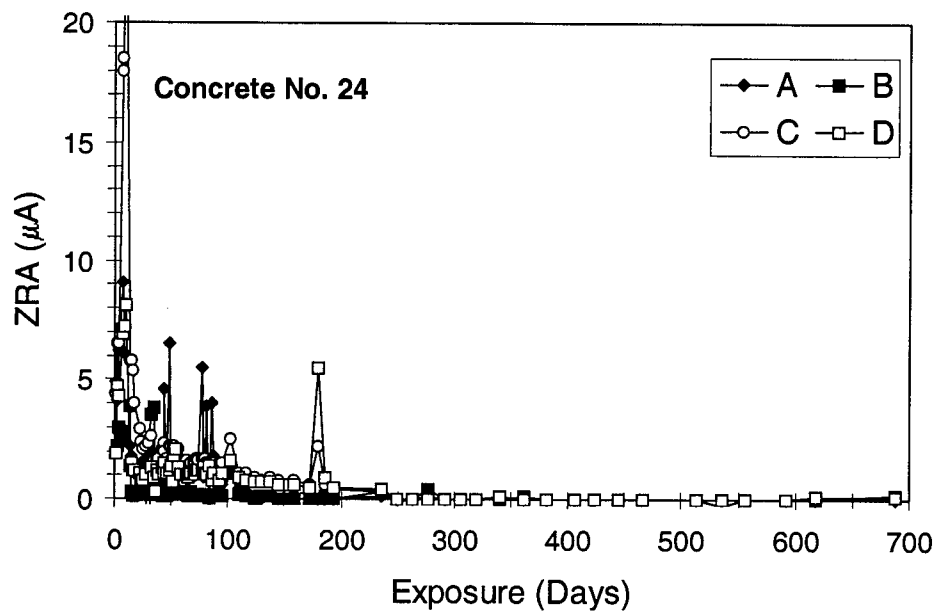


Figure 31. Coupled current versus time for individual cycled exposure specimens for concrete no. 24.

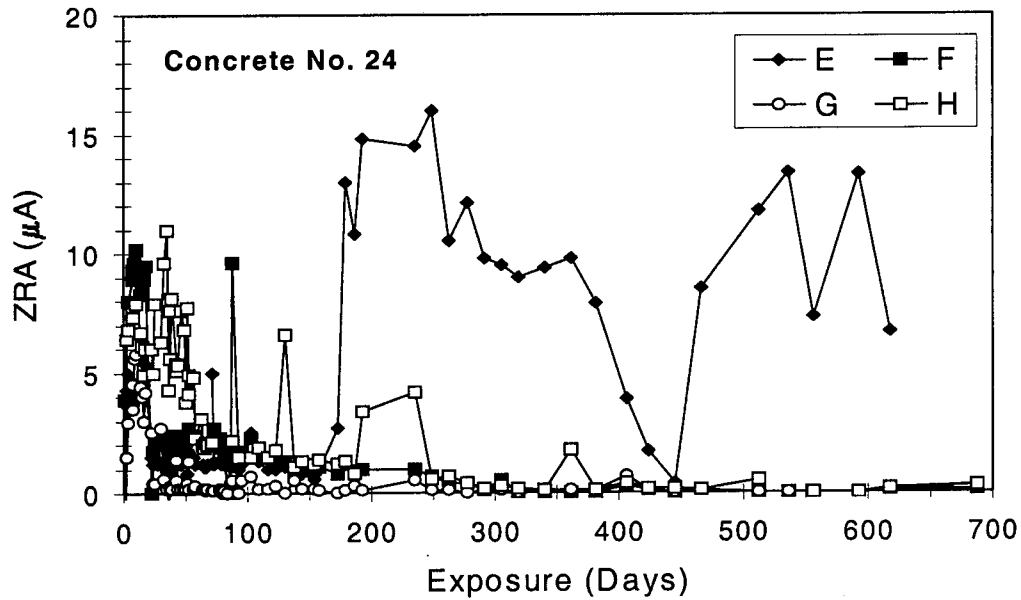


Figure 32. Coupled current versus time for individual continuously wet exposure specimens for concrete no. 24.

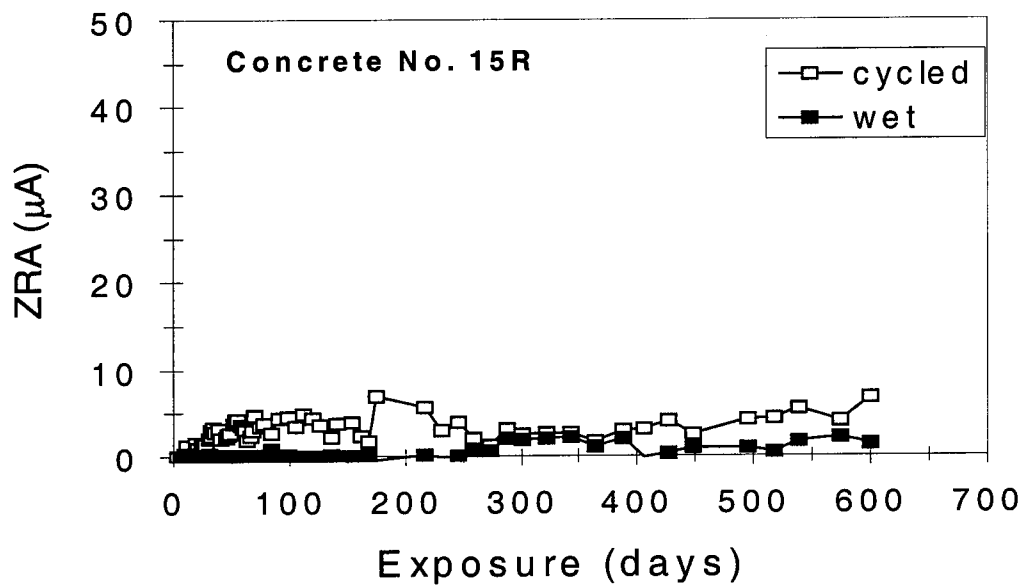


Figure 33. Averaged coupled current versus time for concrete no. 15R.

Coupled current versus time for concrete no. 11 is shown in figure 34. The coupled current for the reinforcing steel in concrete no. 11 was much greater for the wet-dry cyclic exposure than for the continuously wet exposure. The coupled current remained quite low for the continuously wet exposure.

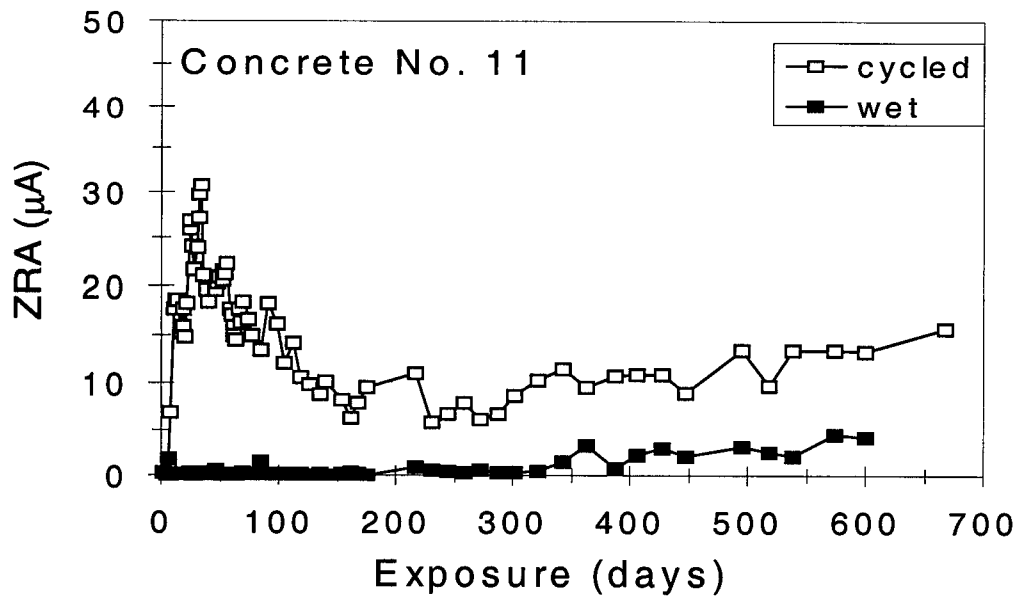


Figure 34. Averaged coupled current versus time for concrete no. 11.

Coupled current versus time for concrete nos. 29 and 22 is shown in figures 35 and 36, respectively. The reinforcing steel in concrete nos. 29 and 22 exhibited the highest measured coupled currents of the concretes tested. The decrease in coupled currents for concrete no. 22 is likely due to corrosion-induced cracking of the concrete between the two reinforcing steel bars (discussed in more detail later).

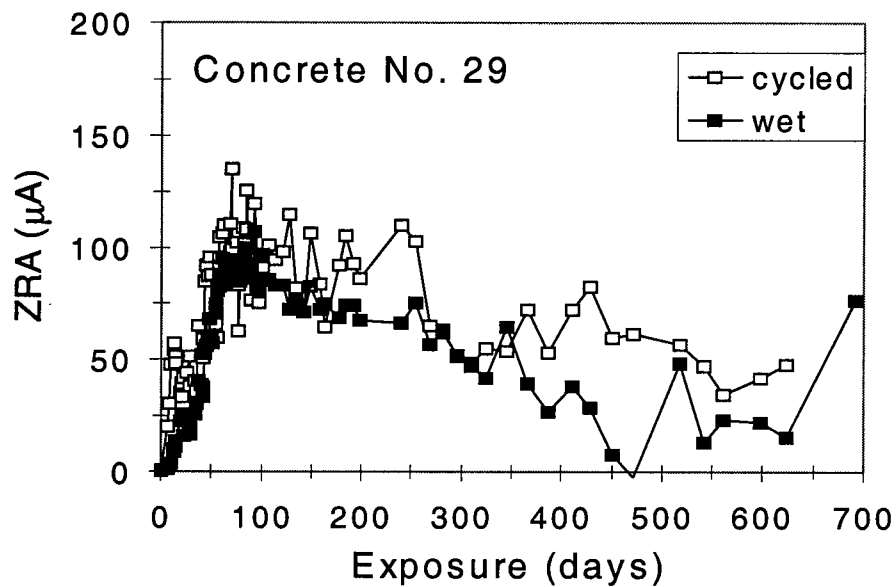


Figure 35. Averaged coupled current versus time for concrete no. 29.

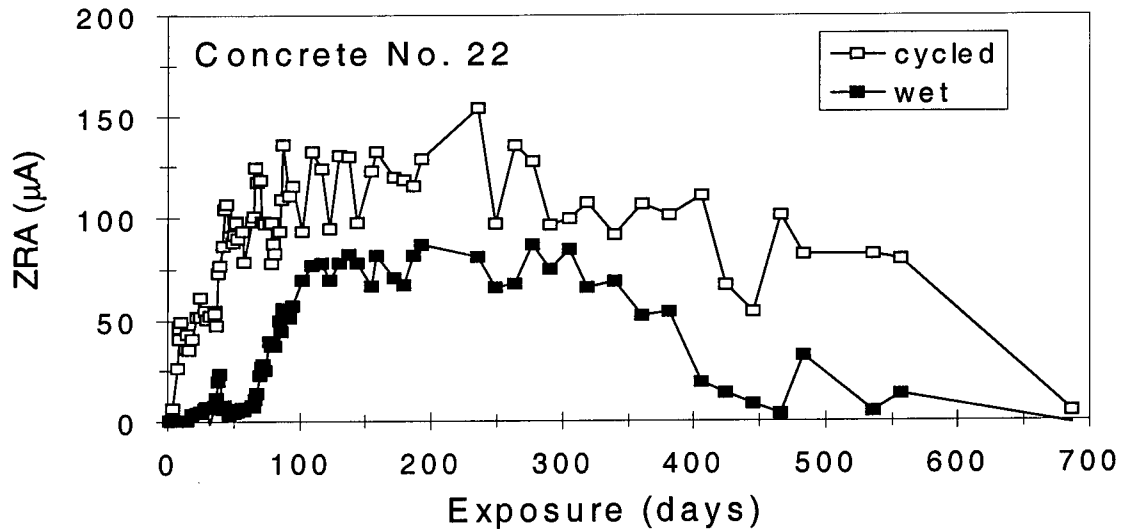


Figure 36. Averaged coupled current versus time for concrete no. 22.

Slab 11-D (concrete no. 11) was used to examine the coupled current as a function of time during a wet-dry cycle. Figure 37 shows that the coupled current varies significantly during the wet-dry cycle. Figures 38 and 39 show the corresponding humidity and temperature during the cycle. The relative humidity was measured in a well drilled into the slab down to the reinforcing steel level and sealed-off from the ponded NaCl solution. The temperature remained relatively constant (the spikes correspond to the door to the room being periodically opened). The relative humidity cycles from 90 percent during the ponded (wet) portion of the cycle to 60 percent during drying. The coupled current correlates quite well with the humidity change. It is not clear whether the humidity affects the electrochemical reaction rates by varying the moisture present at the steel surface or whether the resistance changes during drying are responsible for the change in coupled current.

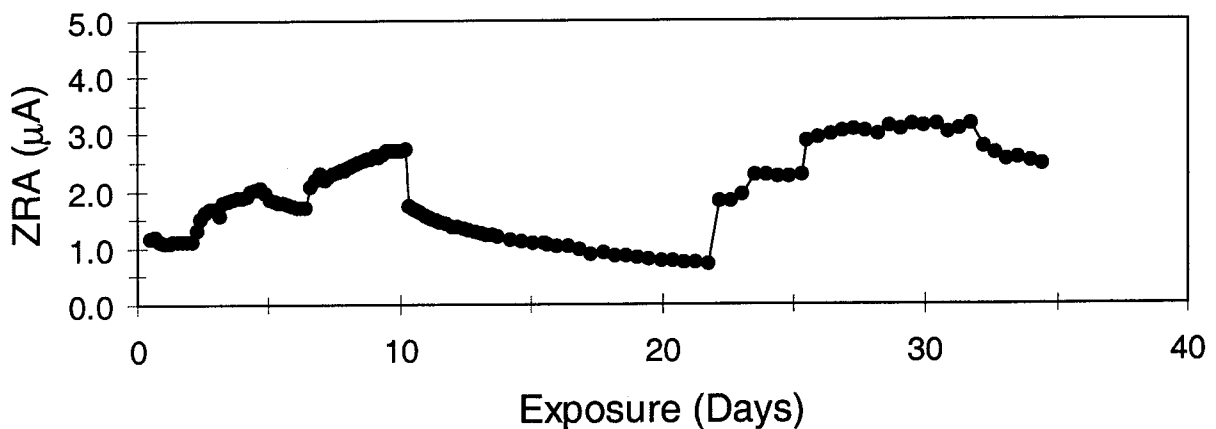


Figure 37. Coupled currents for concrete no. 11 (slab 11-D) during a wet-dry cycle.

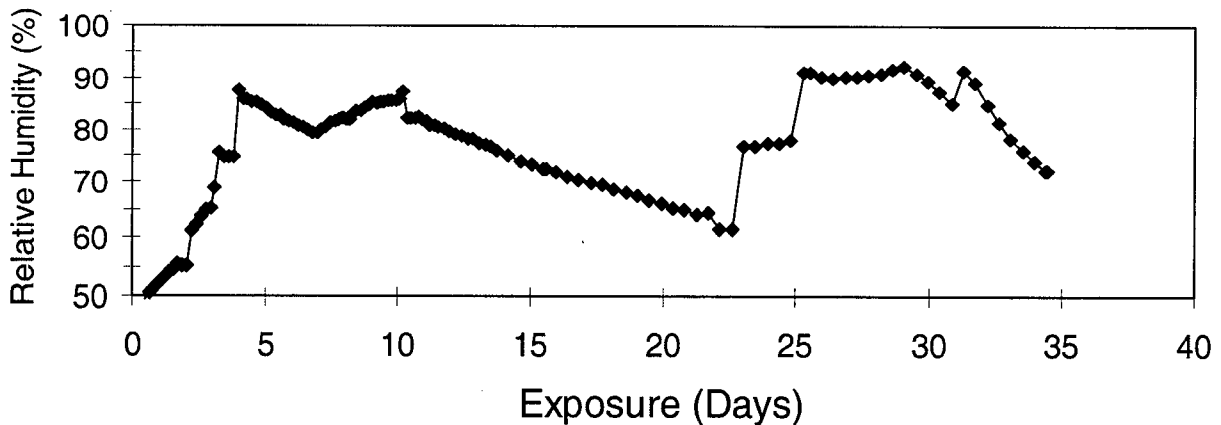


Figure 38. Humidity for concrete no. 11 (slab 11-D) during a wet-dry cycle.

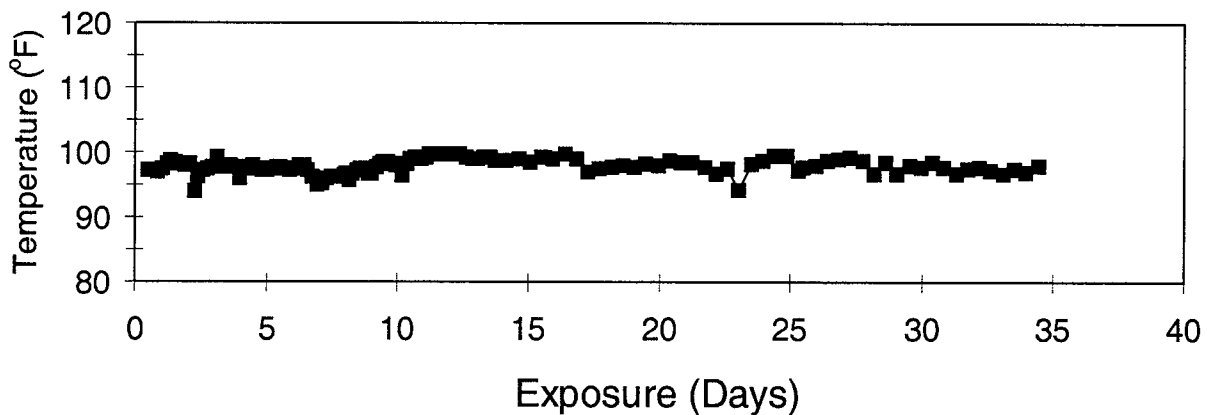


Figure 39. Temperature for concrete no. 11 (Slab 11-D) during a wet-dry cycle.

LPR Corrosion Rate and Potential

Linear polarization resistance (LPR) measurements (with solution resistance correction) were performed periodically during the exposure period. The values for corrosion rate and potentials presented in this section represent the final values measured prior to termination. It is important to measure the LPR corrosion rate and not depend on the coupled current to quantitatively express corrosion rate. The coupled current represents only a portion of the total corrosion occurring on the reinforcing steel surface. The relationship between the coupled current and the total corrosion rate is dependent on: (1) the size and distribution of local corrosion sites on the steel surface, (2) the potential difference between the two coupled steel bars, and (3) the resistance between the two coupled steel bars. Also, the LPR measurement is made with the bars uncoupled and the LPR corrosion rate does not include any acceleration of the corrosion due to the couple.

The average LPR corrosion rates and corrosion potentials for the coupled (center) bar are given in table 41. A complete set of data for LPR and potential measurements are given in Appendix C. The slab specimens for concrete nos. 1, 3, 31, 37, and 38 have a negligible corrosion rate and the potentials are representative of passive steel in concrete (more positive than -150 mV). The corrosion rates correlate very well with the coupled current data. Concrete no. 22 exhibited the highest corrosion rate and highest coupled current. Concrete no. 29 exhibited the second highest values in both tests. Concrete no. 24 exhibited low average corrosion rate and coupled current for the continuously wet condition only and no corrosion activity for the cycled condition. Close examination of the concrete no. 24 wet exposures showed that one slab specimen (slab E) had measurable corrosion and the remaining three replicates had negligible corrosion. This corresponds well with the coupled current data. In addition, LPR corrosion rate measurements indicated that, during the initial exposures, low corrosion rates were measured, but at longer exposure times (290 days), corrosion was negligible for all slabs except slab E.

Table 41. Average corrosion rates and potentials for the coupled bar (center) in task C [1 mpy = 0.0254 mm/yr].

Concrete Mix	Exposure	Potential (mV, CSE)	Corrosion Rate (mpy)
1	Cycled	-102	0.01
1	Wet	-87	0.01
3	Cycled	-131	0.01
3	Wet	-61	0.01
11	Cycled	-313	0.77
11	Wet	-377	0.36
15R	Cycled	-330	0.67
15R	Wet	-153	0.09
22	Cycled	-462	4.3
22	Wet	-449	3.6
24	Cycled	-129	0.01
24	Wet	-186	0.06
29	Cycled	-406	3.9
29	Wet	-213	2.9
31	Cycled	-60	<0.01
31	Wet	-45	<0.01
37	Cycled	-87	0.01
37	Wet	-76	0.02
38	Cycled	-149	<0.01
38	Wet	-85	0.02

Corrosion rates were measured on all three steel bars in the slabs (see figure 29 for the measurement schematic). Table 42 shows the average corrosion rate data for the four replicate specimens for each concrete mix in which corrosion had initiated. The left bar in each slab was ponded with deionized water. This bar typically had negligible corrosion rates

except for concrete no. 29. In this concrete the chloride diffusion was sufficient to diffuse over from the NaCl pond (see chloride concentration results). Both the center and right steel bars were below the chloride pond, with the only difference being that the center bar was normally coupled to the left steel bar (recall that the LPR corrosion rate measurements were performed with the bars uncoupled). For some slabs, the center bar had the higher corrosion rate, and for others, the left bar had the higher rate. In general, the chloride concentration would be expected to be similar for the center and the right bars. It is possible that the center bar (nearer to the water pond) would have a lower chloride concentration. This may offset the more aggressive corrosive condition of the normally coupled center bar.

Table 42. Average corrosion rate and potential data for the three steel bars in each of the slabs where corrosion had initiated [1 mpy = 0.0254 mm/yr].

Concrete Mix	Exposure	Steel Location	Potential (mV, CSE)	Corrosion Rate (mpy)
11	Cycled	Left	-194	0.02
		Center	-313	0.77
		Right	-424	1.3
11	Wet	Left	-71	0.01
		Center	-377	0.36
		Right	-388	1.2
15R	Cycled	Left	4	0.01
		Center	-330	0.67
		Right	-275	0.02
15R	Wet	Left	-172	0.03
		Center	-153	0.09
		Right	-393	0.40
22	Cycled	Left	-276	0.04
		Center	-462	4.3
		Right	-499	3.0
22	Wet	Left	-207	0.05
		Center	-449	3.6
		Right	-490	0.92
29	Cycled	Left	-440	1.5
		Center	-406	3.9
		Right	-484	8.2
29	Wet	Left	-132	0.01
		Center	-213	2.9
		Right	-277	3.9

Table 43 shows a comparison of LPR corrosion rates and corrosion rates calculated by coupled currents. The values shown are averaged values over the exposure and a direct comparison is difficult to make. These data provide a relative assessment of the magnitude of coupled currents compared to corrosion rates. The ratio of LPR corrosion rate to coupled current corrosion rate is typically between 10 and 20 for concrete nos. 11, 15R, 29, and 22. These data indicate that the coupled current is a relatively small portion of the total corrosion

rate. This is due to the local nature of the macro-corrosion cells. A significant amount of the macrocell current is between anodic and cathodic areas on the same bar and only a relatively small portion of the total corrosion current is between the corroding bar (chloride contaminated) and the non-corroding, passive steel bar (no-chloride concrete). It is only the coupled current between the separate steel bars that can be measured.

Table 43. Comparison of LPR and coupled current corrosion rates for task C concretes [2 mpy=0.0254 mm/yr].

Concrete Mix	Exposure	Coupled Current			LPR Corrosion Rate (mpy)	Ratio LPR to Coupled Current Corrosion Rate
		Current (μA)	Current Density ($\mu\text{A}/\text{cm}^2$)	Corrosion Rate (mpy)		
11	Cycled	12	0.158	0.07	0.77	11
	Wet	3	0.039	0.018	0.36	20
15R	Cycled	5	0.066	0.03	0.67	22
	Wet	1.5	0.020	0.009	0.09	10
29	Cycled	64	0.842	0.39	3.94	10
	Wet	55	0.724	0.33	2.93	9
22	Cycled	107	1.408	0.65	4.33	7
	Wet	69	0.908	0.42	3.57	9

Corrosion Initiation and Damage

Table 44 shows the time to corrosion initiation for the task C concretes based on coupled current data. LPR data was not collected until later in the exposure. In each case, the time to initiation was longer for the continuously wet conditions compared to the wet-dry cycled conditions. This was the most significant for concrete no. 11. Recall that the “cycled” exposure included an initial severe drying stage that results in early initiation times (a few days) for concrete nos. 11, 22, and 29. Concrete nos. 1, 3, 31, 37, and 38 did not initiate corrosion during the nearly 2-year exposure. Concrete no. 24 only initiated corrosion for one of the eight slab specimens tested (verified by LPR data, see table 71).

Table 44. Time to corrosion initiation for the task C concretes.

Exposure	Slab	Corrosion Initiation (Days)				
		Concrete No.				
		11	15R	22	24	29
Cycled	A	6	12	1	*	7
	B	7	19	3	*	9
	C	10	84	8	*	7
	D	7	32	4	*	7
Wet	E	217	259	64	160	12
	F	518	273	66	*	12
	G	231	259	14	*	7
	H	343	287	37	*	7

* No initiation.

Table 45 shows the time to cracking for the task C concretes. The time to cracking was defined as the time at which a surface crack became visible, and was typically noted during the transition from the wet to the dry cycles. The continuously wet slabs were periodically dried and examined. Figure 40 shows the type of cracking observed in these tests. Concrete slab 22-F had cracking associated with both steel bars beneath the NaCl pond. The center steel bar was coupled to the left steel bar (no chloride) and the crack runs directly above the center steel bar. For this slab (and others) a crack formed on the side of the slab and was associated with the right steel bar. Although not coupled, the right bar experienced high corrosion rates also (table 42). Figure 41 shows cracking over the right steel bar and none over the center steel bar for concrete slab 11-C.

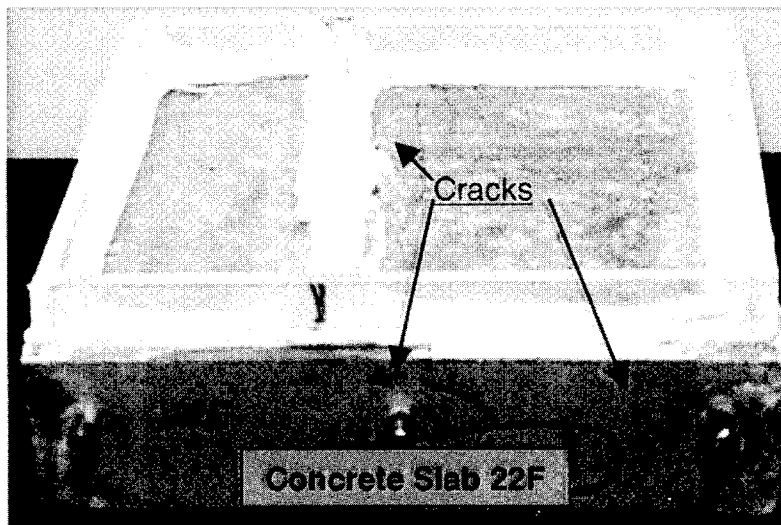
Table 45. Time to cracking for the task C concretes [1 mpy = 0.0254 mm/yr, 1 mil = 0.254mm].

Concrete Mix	Exposure	Slab	Time to Corrosion Initiation After Ponding (days)	Time to Cracking After Ponding (days)	LPR Rate (mpy)	Cumulative Corrosion Prior to Cracking (mil)
11	Cycled	A	6	360	1.57	1.5
11	Cycled	C	10	360*	3.76	3.7
11	Cycled	D	7	360	0.27	0.3
Average for Concrete No. 11						1.8
22	Cycled	A	7	424	0.14	0.2
22	Cycled	B	4	556	2.48	3.8
22	Cycled	C	8	340	5.26	4.8
22	Cycled	D	7	556	9.43	14
Average for Concrete No. 22 - Cycled						5.7
22	Wet	E	64	556	1.11	1.5
22	Wet	F	66	556	1.65	2.2
22	Wet	G	14	466	9.70	12
22	Wet	H	37	556	1.81	2.6
Average for Concrete No. 22 - Wet						4.6
29	Cycled	A	7	715*	6.04	11.7
29	Cycled	B	9	715*	5.89	11.4
29	Cycled	C	7	715*	1.15	2.2
29	Cycled	D	7	715*	2.69	5.2
Average for Concrete No. 29 - Cycled						7.6
29	Wet	E	12	744	1.51	3.0
29	Wet	F	12	744	4.86	9.7
29	Wet	G	7	744	1.44	2.9
29	Wet	H	7	561	3.89	5.9
Average for Concrete No. 29 - Wet						5.4
Average for All Data						5.2

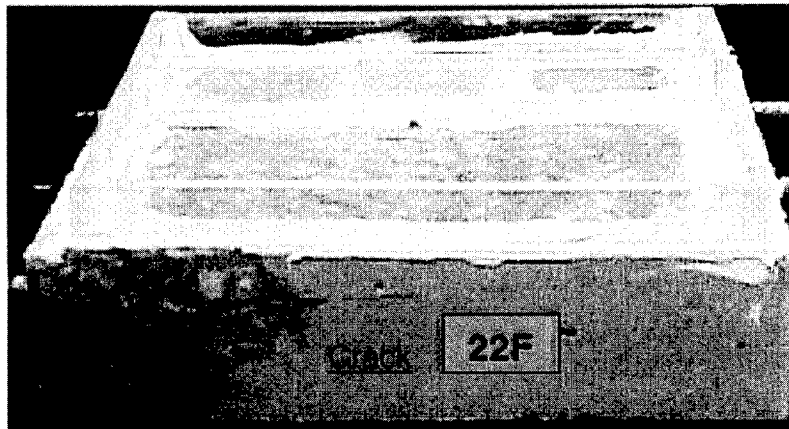
*Cracking observed over the right steel bar.

Also shown in table 45 are estimates for the cumulative corrosion prior to the appearance of visible surface cracks. The value for cumulative corrosion was calculated using the difference in "time to corrosion initiation" and "time to cracking" as the time of corrosion. Coupled currents are not necessarily a good quantitative measure of corrosion. Furthermore, the relationship between the coupled current and corrosion rate will probably change as corrosion progresses and the distribution of corrosion sites changes. Therefore, the best information on corrosion rate is the LPR measurement. This measurement was performed only a few times during the exposure period. A primary assumption made in table 43 calculations was that the corrosion rate was constant during the period following corrosion initiation and prior to cracking. Also, the most consistent set of corrosion rate data was collected following cracking for concrete slab nos. 22 and 29. It is likely that the corrosion rates are higher following cracking than prior to cracking. Note that coupled currents often decrease upon cracking in a laboratory

slab specimen (the crack introduces a high-resistance path between coupled specimens); corrosion rates (LPR) on an individual bar specimens do not necessarily decrease. Therefore, the cumulative corrosion prediction may be higher than the actual corrosion prior to cracking for concrete nos. 22 and 29. Concrete no. 11 is the only concrete for which a complete set of corrosion rate data was available prior to cracking. The average cumulative corrosion prior to cracking for concrete no. 11 was 1.8 mil (0.05 mm). This was less cumulative corrosion than for concrete nos. 22 and 29, whose average cumulative corrosion prior to cracking ranged from 4.6 to 7.6 mil (0.11 to 0.19 mm). The average for all of the cracked concrete slabs was 5.2 mil (0.13 mm).



a. Front view.



b. Side view.

Figure 40. Photograph of concrete slab 22-F showing cracking over center steel bar and cracking of side (right steel bar).

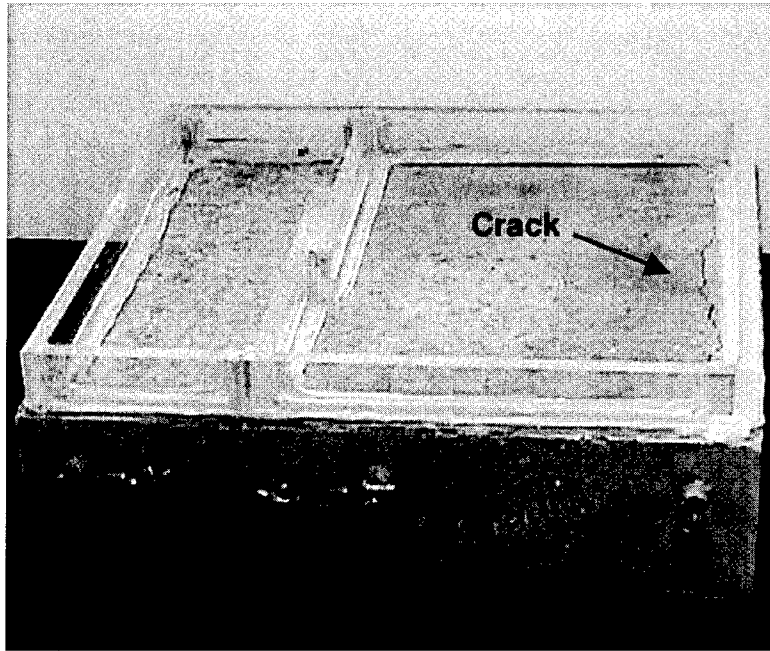


Figure 41. Photograph of concrete slab 11-C showing cracking over right steel bar and none over the center steel bar.

Chloride Concentrations

Chloride analyses were performed on one of the four replicates for each test condition (figure 27). The values given in table 46 represent the chloride concentration in the concrete at the steel bar level. Chloride concentrations are given for both the NaCl-ponded and the water-ponded section of the concrete slabs. As is expected, in every case, the water ponded concrete had significantly less chloride concentration than the NaCl ponded concrete. In most cases, concentrations over the water-ponded concrete were negligible. In the few conditions where this concentration was significant (no. 22 cycled, no. 22 wet, and no. 29 cycled), the chlorides diffused through the concrete from the chloride-ponded concrete.

Recall that negligible corrosion activity was observed for concrete nos. 1, 3, 31, 37, and 38. For these concretes, only no. 3 cycled (0.061 percent) and no. 31 wet (0.047 percent) had chloride concentrations greater than 0.025 percent ($\sim 1 \text{ lb/yd}^3$ [0.6 kg/m^3]) chloride.

Concrete no. 24 exhibited negligible corrosion in the latter part of exposure (figure 30 and table 41) following an initial period of activity indicated by coupled currents (figures 30 through 32). The chloride concentration for this concrete was 0.084 percent (3.3 lb/yd^3 [2 kg/m^3]) in the cycled condition and 0.11 percent (4.0 lb/yd^3 [2.4 kg/m^3]) in the wet condition. Therefore, these concentrations are insufficient to sustain corrosion in concrete no. 24.

The two concretes with the highest corrosion rates (nos. 22 and 29) for steel bars also had the highest chloride concentrations (greater than 0.5 percent, 20 lb/yd^3 [12 kg/m^3]). Steel in

concrete nos. 11 and 15R exhibited higher corrosion rates in the cycled than in the wet conditions. In particular, steel in concrete no. 15R wet, slab H (Appendix C) exhibited a low, but measurable, corrosion rate of 0.0038 mm/yr (0.15 mpy). This relatively low corrosion rate for steel in concrete no. 15R corresponds to a relatively high chloride concentration of 0.51 percent (19 lb/yd³ [11.4 kg/m³]). For comparison, concrete no. 29 wet, slab H had a chloride concentration of 0.58 percent (21 lb/yd³ [12.6 kg/m³]) and steel in this slab had a corrosion rate (Appendix C) of 0.099 mm/yr (3.9 mpy). Therefore, the concrete mix design can have a significant effect on corrosion behavior at similar chloride concentrations.

Table 46. Final chloride concentrations for task C concretes
[1 lb/yd³ = 0.6 kg/m³].

Concrete Mix	Sample Location	Exposure	Slab	Chloride (%)	Chloride (lb/yd ³)
No. 1	NaCl	Cycled	D	<0.003	<0.1
	Water			<0.003	<0.1
	NaCl	Wet	H	<0.003	<0.1
	Water			<0.003	<0.1
No. 3	NaCl	Cycled	D	0.061	2.4
	Water			<0.003	<0.1
	NaCl	Wet	H	<0.003	<0.1
	Water			<0.003	<0.1
No. 11	NaCl	Cycled	D	0.45	18
	Water			0.006	0.3
	NaCl	Wet	H	0.23	9.1
	Water			<0.003	<0.1
No. 15R	NaCl	Cycled	D	0.25	9.1
	Water			<0.003	<0.1
	NaCl	Wet	H	0.51	19
	Water			0.003	0.1
No. 22	NaCl	Cycled	D	0.63	24
	Water			0.20	7.8
	NaCl	Wet	H	0.62	24
	Water			0.14	5.5
No. 24	NaCl	Cycled	D	0.084	3.3
	Water			<0.003	<0.1
	NaCl	Wet	H	0.11	4.0
	Water			0.016	0.6
No. 29	NaCl	Cycled	D	0.76	27
	Water			0.31	11
	NaCl	Wet	H	0.58	21
	Water			0.005	0.2
No. 31	NaCl	Cycled	D	0.008	0.3
	Water			<0.003	<0.1
	NaCl	Wet	H	0.047	1.8
	Water			<0.003	<0.1
No. 37	NaCl	Cycled	D	<0.003	<0.1
	Water			<0.003	<0.1
	NaCl	Wet	H	0.004	0.2
	Water			<0.003	<0.1
No. 38	NaCl	Cycled	D	<0.003	<0.1
	Water			<0.003	<0.1
	NaCl	Wet	H	0.019	0.7
	Water			<0.003	<0.1

Post-Test Analysis

Visual Examination

Following exposure, a majority of the slabs were broken to reveal the steel bar condition. See Appendix D for detailed information on each slab. In general, excellent agreement was found between the measured corrosion rates and the observed corrosion condition of the bar. Figure 42 shows the results of the concrete no. 15R slab A. The following is data from table 69 (Appendix C).

Left bar	90 mV	0.00 mm/yr (0.00 mpy)
Center bar	-334 mV	0.015 mm/yr (0.60 mpy)
Right bar	-302 mV	0.0002 mm/yr (0.01 mpy)

It is seen that the photograph in figure 42 corresponds to the corrosion rate measured (center bar has relatively high corrosion rate and right and left bars have no or insignificant corrosion). It is not fully understood why for concrete no. 15R, the center steel bar initiated corrosion and the right bar (also under the NaCl pond, but not coupled) did not initiate corrosion. However, the post-test examination of the steel bar surface confirmed the measured corrosion rate results. It may be simply that the corrosion resistance for the conditions present was marginal and the enhanced driving force of the coupled was sufficient to initiate corrosion.

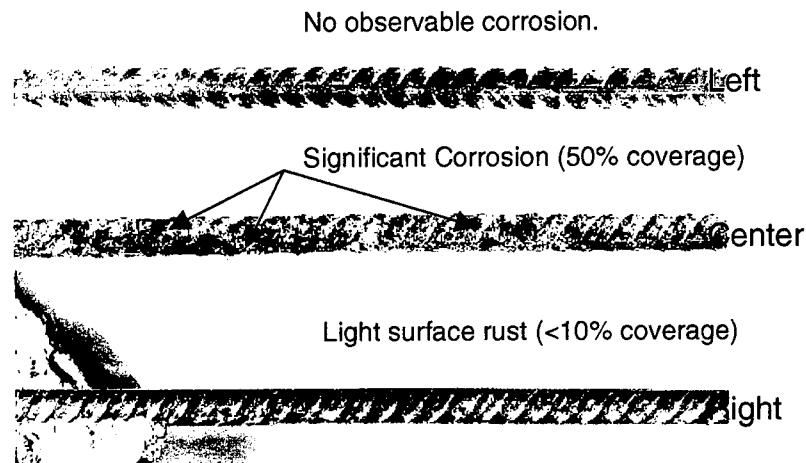


Figure 42. Photograph of steel bars from concrete no. 15R, slab A.

Table 47 gives a summary of data for the task C concrete slabs (coupled currents, LPR corrosion rates, corrosion potentials, and chloride concentrations) compared to the visual examination of the steel bar condition. Excellent agreement was found between the measured properties of corrosion and the observed conditions of the steel bars. That is, high chloride concentration correlate to high coupled currents which correlates to high LPR

corrosion rates which correlate to high negative corrosion potentials, which correlate to high surface coverage of corrosion. There are a few conditions that do not fit the typical “rule-of-thumb” for corrosion in concrete. One example was given above in figure 42. Another example is for concrete no. 24. Recall that it did not exhibit ordinary behavior for coupled currents in that the currents were high during the early stages of exposure and decreased to negligible values after some time. Concrete no. 24 in table 48 had measured chloride concentrations of 1.8 to 2.4 kg/m³ (3 to 4 lb/yd³), but exhibited negligible corrosion rates (along with negligible coupled currents after the short initial period. The visual inspection of the steel bar confirmed negligible corrosion on the steel bar. The typical rule-of-thumb would say that 1.8 to 2.4 kg/m³ (3 to 4 lb/yd³), of chloride is sufficient to initiate corrosion. For this particular concrete, the threshold for corrosion initiation must be greater than this level. It is likely that the concrete mix components affect the chloride threshold for initiation in a similar manner as the corrosion rate properties measured in task B.

Appendix D gives the surface conditions of the concrete slabs following exposure. All concretes were in good condition except concrete nos. 22 and 29. Concrete no. 29 exhibited the most deterioration. The surface was rough and powdery. The surface of concrete no. 22 that had been exposed to the chloride pond was chalky and slightly rough. Little difference was observed between the continuous ponded and cycled conditions.

Table 47. Summary of measured corrosion variables compared to post-test visual examination [1 mpy = 0.0254 mm/yr; 1 lb/yd³ = 0.6 kg/m³].

Concrete Mix	Exposure	Chloride (lb/yd ³)		Coupled Current Macrocell (μA)	Corrosion Rate LPR (mpy)	Potential (mV)	Post-Test Analysis (Average) Percent Corrosion Coverage		
		NaCl Ponded	Water Ponded				Center Bar ^a (%)	Right Bar ^b (%)	Left Bar ^c (%)
1	cycled	<0.1	<0.1	0	0.01	-102	0	0	0
1	wet	<0.1	<0.1	0	0.01	-87	-	-	-
3	cycled	2.4	<0.1	0	0.01	-131	0	0	0
3	wet	<0.1	<0.1	0	0.01	-61	-	-	-
11	cycled	18	0.3	12	0.77	-313	62	75	0
11	wet	9.1	<0.1	3	0.36	-377	31	56	<10
15R	cycled	9.1	<0.1	5	0.67	-330	50	10	<10
15R	wet	19	<0.1	1.5	0.09	-153	17	17	11
22	cycled	24	7.8	107	4.3	-462	100	100	<10
22	wet	24	5.5	69	3.6	-449	88	94	<10
24	cycled	3.3	<0.1	0	0.01	-129	<10	<10	<10
24	wet	4.0	0.6	5	0.06	-186	<10	<10	<10
29	cycled	27	11	64	3.9	-406	67	92	23
29	wet	21	0.2	55	2.9	-213	100	94	<10
31	cycled	0.3	<0.1	0	<0.01	-60	0	0	0
31	wet	1.8	<0.1	0	<0.01	-45	-	-	-
37	cycled	<0.1	<0.1	0	0.01	-67	0	<10	<10
37	wet	0.2	<0.1	0	0.02	-76	-	-	-
38	cycled	<0.1	<0.1	0	<0.01	-149	0	0	0
38	wet	0.7	<0.1	0	0.02	-85	0	<10	0

a: Center bar beneath NaCl pond and coupled to "left bar."

b: Right bar beneath NaCl pond (not coupled).

c: Left bar beneath water pond and coupled to "center bar."

-: Slab not examined.

0% - No visible sign of corrosion.

<10% - Possible very light corrosion, but difficult to determine (negligible).

Petrographic Analysis

A number of the reinforced concrete slabs were examined petrographically to provide additional insight into the distress mechanisms associated with the corrosion of embedded reinforcing steel.

Six of the reinforced concrete slabs were used in this investigation (representing five different portland cement concrete compositions). The constituents of these concretes are identified in table 48.

The corrosion behavior and activity exhibited by these concretes during the course of the task C study is summarized in table 49. The concretes examined here were selected on the basis of wide variability in: (1) time to initiation of corrosion, (2) time to initiation of cracking, and (3) rate and severity of corrosion-related distress. One of the concretes examined here (concrete no. 31) showed no corrosion activity or distress over the 2.5-year exposure.

Table 48. Constituents of concretes evaluated in the petrographic examination.

Concrete Number	Portland Cement	Coarse Aggregate	Fine Aggregate	Mineral Admixture	Air Content (%)	Water-to-Cement Ratio
11	Lone Star Zero C3A (Cement E)	Quartz	Quartz	Type F Flyash	2	0.5
15R	Holnam Holly Hill Type I Low Alkali (Cement C)	Quartz	Glacial Sand	Microsilica	8	0.5
22	Holnam Artesia Type I High C3A (Cement D)	Limestone	Glacial Sand	None	2	0.4
29	Medusa Type I High Alkali (Cement A)	Limestone	Quartz	None	8	0.5
31	Lone Star Zero C3A (Cement E)	Quartz	Quartz	Microsilica	5	0.3

Table 49. Corrosion activity of reinforced concrete slabs in task C study.

Concrete Slab Number	Corrosion Rate (Task C)	Time to Initiation of Corrosion (days)	Time to Crack Initiation (days) ^(a)
11 (A)	Moderate	6	360
15R (B)	Moderate	10	No Cracking ^(b)
22 (B)	High	3	550
20 (A)	High	1	700
31 (A)	Low	No Corrosion Activity	No Cracking

^(a) Pertains to cracking that is observed on exterior exposed surfaces of the slabs.

^(b) Cracking did occur in this slab but did not reach the exposed surfaces.

The slab specimens contain three no. 3 deformed reinforcing steel bars. The spacing between the bars is 127 mm (5 in). The depth of cover of the bars is 19 mm (0.75in).

The condition of the slabs following their use in the task C work was assessed regarding the number of corrosion-related cracks and the orientation, severity, and extent of the cracks.

Four sawcuts were made in each slab (diamond saw), parallel to the long dimension of the reinforcing bar. This sawcutting step yielded concrete prisms measuring approximately 63 mm (2.5 in) by 76 mm (3 in) by 305 mm (12in), three of which contained the reinforcing steel bar. Following sawcutting, the sawcut surfaces were sprayed with indicating solutions (phenolphthalein and rainbow indicator) to provide information on the carbonation and pH of the concretes.

Following this step, additional sawcuts were made perpendicular to the reinforcing steel bars, yielding 25-mm (1-in) by 63-mm (2.5-in) by 76-mm (3-in) specimens for more detailed microscopic examinations. Petrographic examinations of these concrete samples were made following the guidelines outlined in ASTM C 856-95, "The Standard Practice for Petrographic Examination of Hardened Concrete." Information gained in these examinations is described below.

Slab 31-A. Slab A for concrete no. 31 (slab 31-A) showed no corrosion activity and no visible distress on the exposed slab surfaces over the duration of the task C study. A section view of this concrete (perpendicular to the slab wearing surface and the reinforcing steel is not carbonated and has a pH in the normal range for portland cement concrete (12.5 to 13.5).

There is no cracking or spalling distress in this concrete slab. Concrete surrounding the reinforcing steel shows a tight and uninterrupted bond with the concrete. There is no physical evidence of any corrosion activity. An oxide layer on the steel bar surface is attributed to original mill scale and is about 0.025 mm (0.001 in) thick.

Slab 15R-B. Slab B for concrete no. 15R showed a moderate rate of corrosion, but no cracks were observed on the exterior slab surfaces at the completion of the task C work. Section views of the middle steel bar in Slab 15R-B are shown in figures 43 and 44. Although no cracking was observed on the exterior slab surfaces, corrosion-related cracking had, in fact, occurred in this slab (figure 43). The corrosion on the bar is concentrated on the top portion of the steel bar. The thickness of the steel corrosion product on the bar at this location varies from 0.25 to 0.9 mm (0.01 to 0.035 in). Cracking in the concrete originates at this region of maximum corrosion product build-up.

There has been a significant amount of diffusion of steel corrosion product into the cement paste adjacent to the steel bar, into air voids at the steel/cement interface, and along the crack plane surfaces (see figure 45). There has also been some diffusion of steel corrosion product into fractures in the quartz coarse aggregate particles.

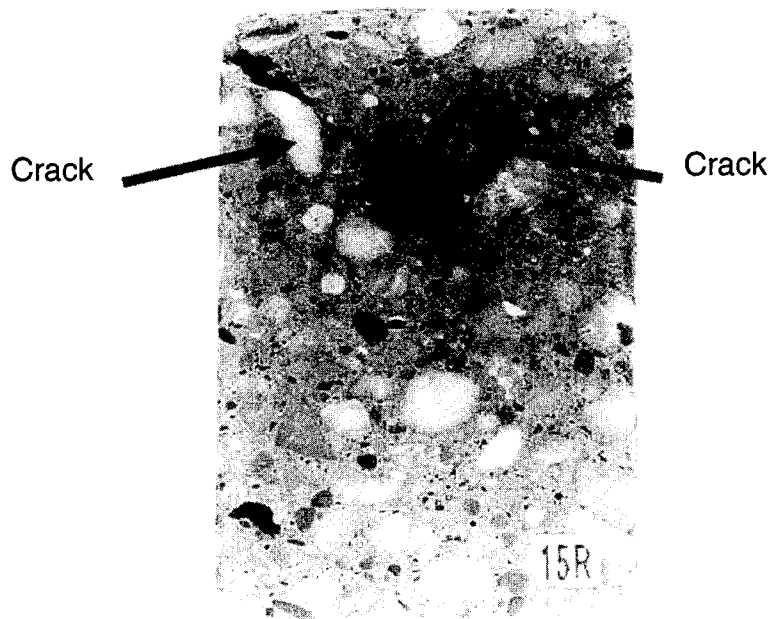


Figure 43. Cross-sectional view of steel bar in slab 15R-B showing cracking in the concrete matrix, but not extending to the slab surface.

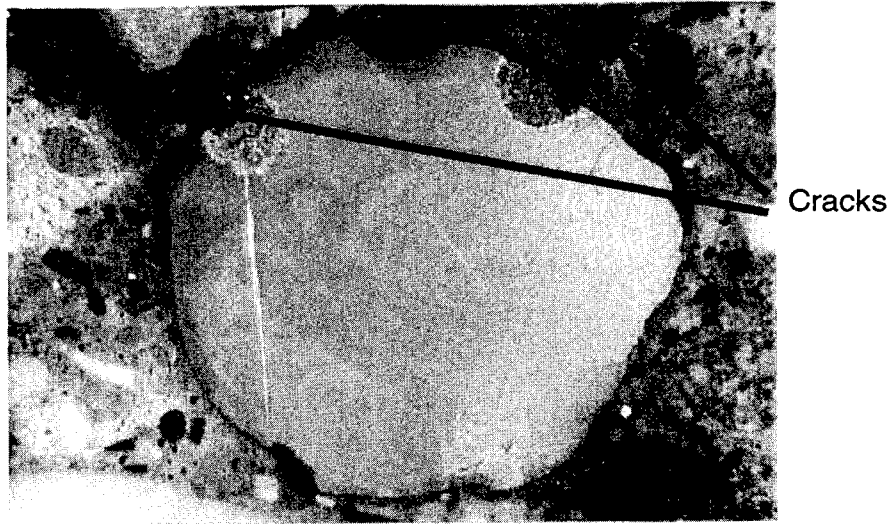


Figure 44. Close-up of cross-section shown in figure 43.

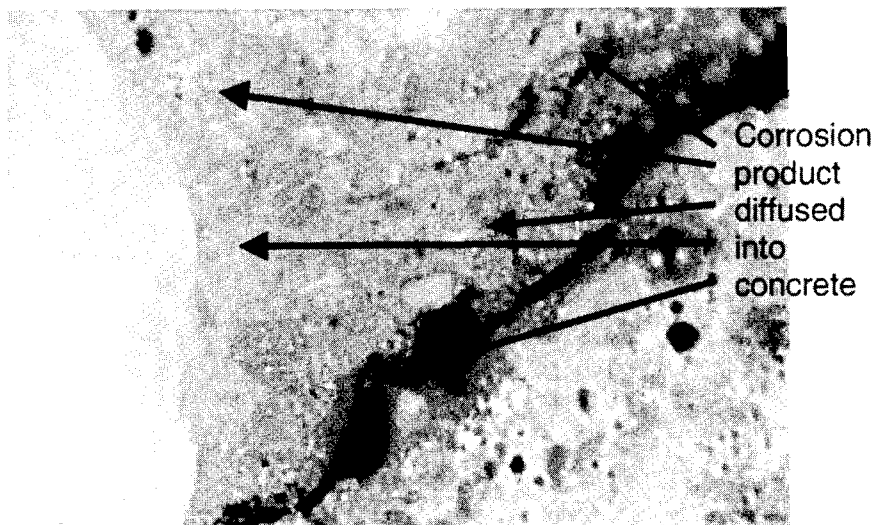


Figure 45. Cross-sectional view for slab 15R-B shows diffusion of corrosion product into concrete matrix.

Slab 22-B. Slab B for concrete no. 22 exhibited a high corrosion rate and cracking on exterior surfaces was first observed at 550 days. In this concrete, virtually the entire surface of the steel bar shows corrosion product, with the reaction layer varying in thickness from 0.13 to 0.56 mm (0.005 to 0.022 in). The average corrosion product layer thickness is 0.36 mm (0.014 in).

With the corrosion product encompassing a large portion of the surface area of the bar, multiple cracks were initiated around the steel bar circumference (see figure 46). Because all but one crack are hard to see without close examination, the cracks were outlined with a

marker. The diffusion of corrosion product into the cement paste contacting the steel bar is minimal. However, there is a significant diffusion of steel corrosion product into the porous limestone coarse aggregate particles and, to a more limited extent, along the fracture plane surfaces (see figures 47 and 48).

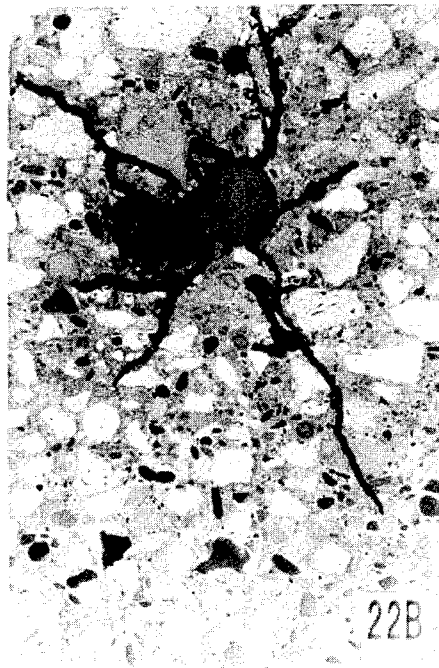


Figure 46. Cross-sectional view of steel bar in slab 22-B with cracks highlighted (the top crack extends to the slab surface)

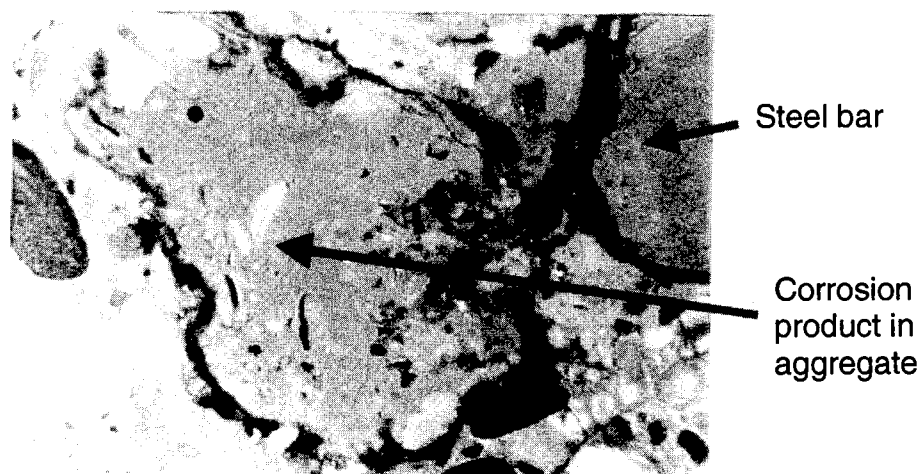


Figure 47. Close-up of cross-section from figure 46 showing diffusion of steel corrosion product into the porous coarse aggregate.

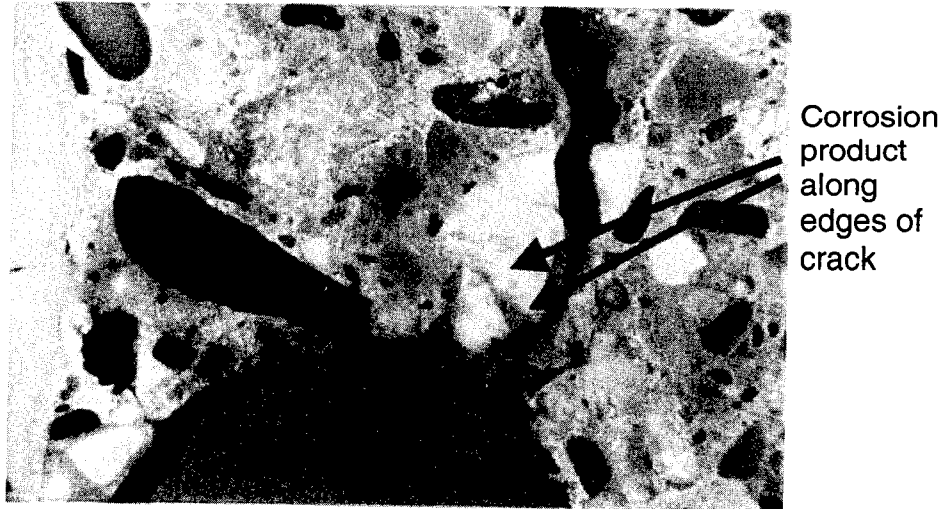


Figure 48. Close-up of cross-section from figure 46 showing limited diffusion of steel corrosion product along the fracture plane surfaces.

Slab 29-A. Slab A from concrete no. 29 exhibited a high corrosion rate, although cracking on exterior surfaces was not observed until 700 days. Corrosion product is evident over the entire surface of the bar with the corrosion layer thickness ranging from 0.08 to 0.56 mm (0.003 to 0.022 in). The average thickness of the corrosion product layer is 0.25 mm (0.01 in).

Corrosion-related cracking is present in all quadrants of concrete surrounding the reinforcing steel. There has been diffusion of corrosion products into both the cement paste and the limestone coarse aggregate particles, as well as along the crack fracture planes.

Slabs 11-A and 11-C. Slab A from concrete no. 11 exhibited cracking associated with both bars in the chloride-ponded area at 360 days. Slab 11-C also exhibited cracking at 360 days, but only over the steel bar at the outside edge of the slab (not over the center steel bar) in the ponded portion of the slab. The interior bar showed no cracking in slab 11-C over the duration of the task C study.

For slab 11-A, corrosion product was observed over the entire surface of the bar. The thickness of the corrosion product layer is reasonably uniform at 0.12 mm (0.005 in). Steel corrosion products have diffused into the cement paste phase of the concrete in contact with the reinforcing steel. Steel corrosion products are also deposited in the fracture planes adjacent to the steel bar. For slab 11-C, corrosion activity was observed on 60 percent to 70 percent of the surface of the bar, although the corrosion product layers are only about 0.002-in (0.05 mm) thick. Diffusion of corrosion product into the cementitious phase has occurred in concrete adjacent to corroding steel surfaces.

Corrosion Behavior – Repair/Patch Concretes

Coupled Currents – Standard Slab Specimens

Recall that the standard slab specimens (figure 24) have no chloride mixed in and are a homogeneous specimen fabricated from the repair concrete. Four repair materials have been examined. They are designated as repair material nos. 40, 41, 42, and 43. Concrete slabs identical to the standard test slabs were tested for each of these materials. Repair material nos. 42 and 43 are the same as concrete nos. 1 and 31, respectively. The coupled currents for the standard slab specimens for repair material no. 42 (concrete no. 1) and repair material no. 43 (concrete no. 31) were given in Appendix B. The coupled currents for these materials remained zero throughout the exposure and showed no signs of corrosion. Figures 49 and 50 show the standard slab specimens for repair material nos. 40 and 41. Both materials initiated corrosion relatively quickly following exposure. The coupled current for repair material no. 40 was not very large and decreased with time. The coupled current for repair material no. 41 was much greater and the decrease with time for this material is likely due to the cracking observed (see discussion of cracking damage); no cracking was observed for repair material no. 40.

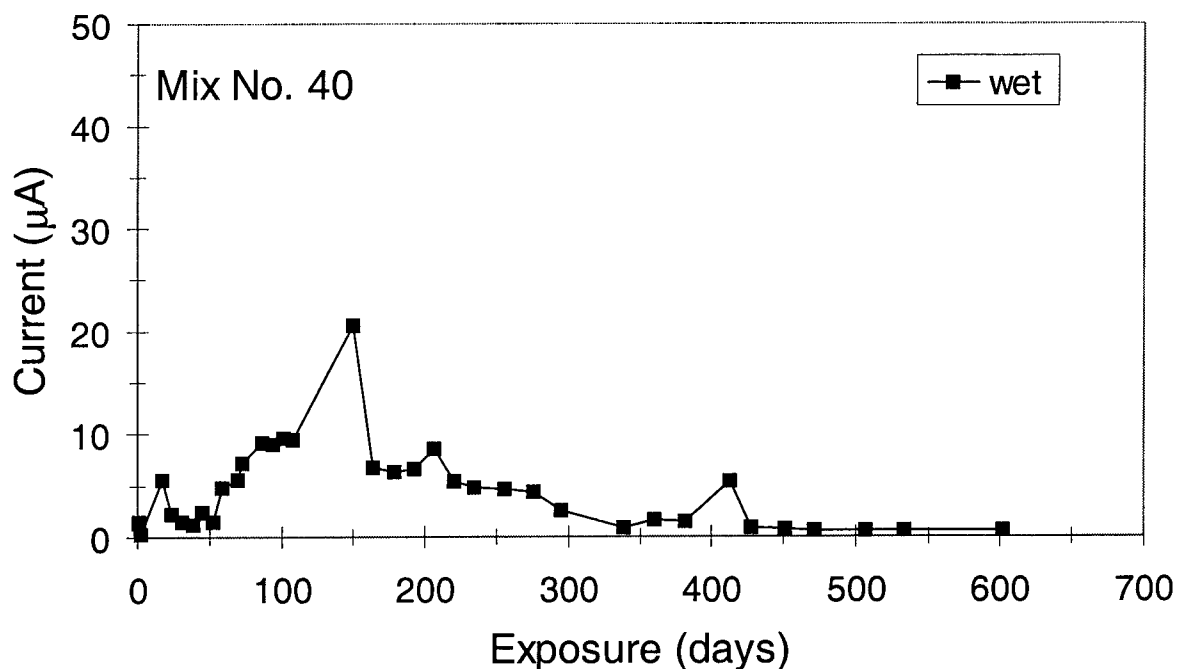


Figure 49. Averaged coupled current versus time for standard slab repair material no. 40.

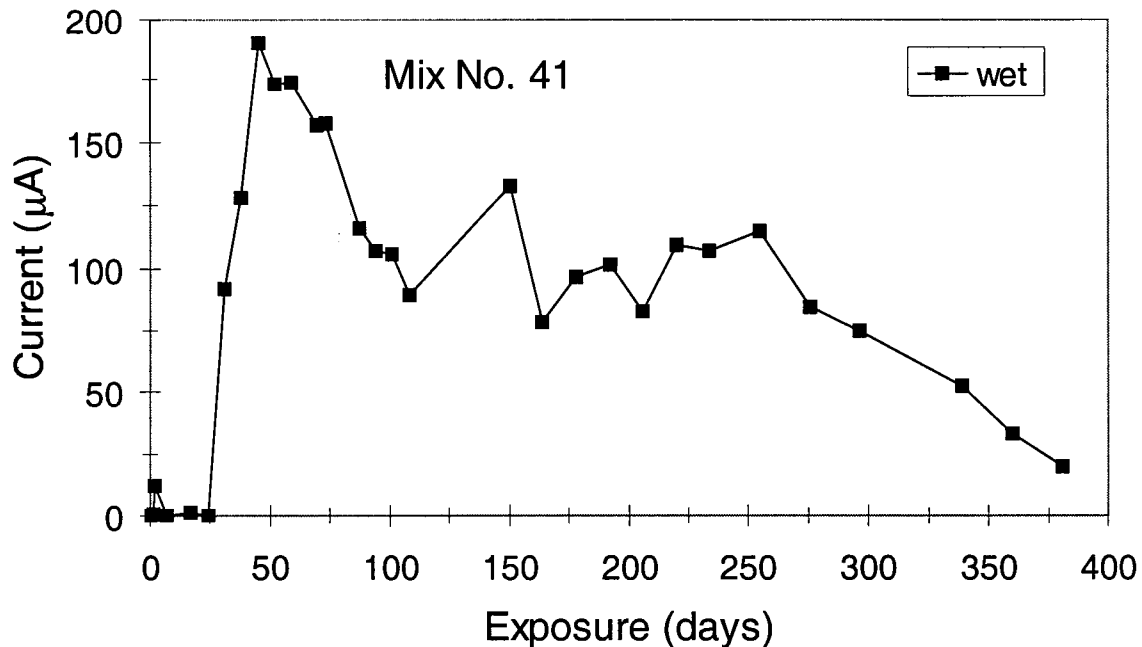


Figure 50. Averaged coupled current versus time for standard slab repair material no. 41.

Coupled Currents – Repair Slab Specimens

Figures 51 through 54 show the averaged coupled currents for the four replicate repair slabs (figures 25 and 28). Recall that the repair material is cast into the slab next to concrete that had chloride mixed into the concrete to simulate aged concrete. The coupled current is between the reinforcing steel bar in the repair material and the steel bar in the concrete. Figure 51 shows that for repair material no. 40, the current initially was a positive value, containing chloride indicating corrosion of the steel bar in the concrete containing chloride. However, after only a few days, the coupled current reversed (negative values), indicating corrosion of the steel bar in the repair material. The direction of current was supported by the potential measurements over the individual steel bars. The potentials are dependent on both the chloride concentration and the concrete chemistry (for example, pH). The lower pH of repair concrete no. 40. (and no. 41) is an important factor in the observed behavior.

Similar behavior was observed for repair material no. 41, as discussed above for no. 40. The currents for repair material no. 41 were very high and the decrease in current probably is due to cracking of the concrete. For both repair material nos. 40 and 41, the coupled current indicates that after a brief period, the macrocell couple tends to accelerate the corrosion of the steel in the repair material.

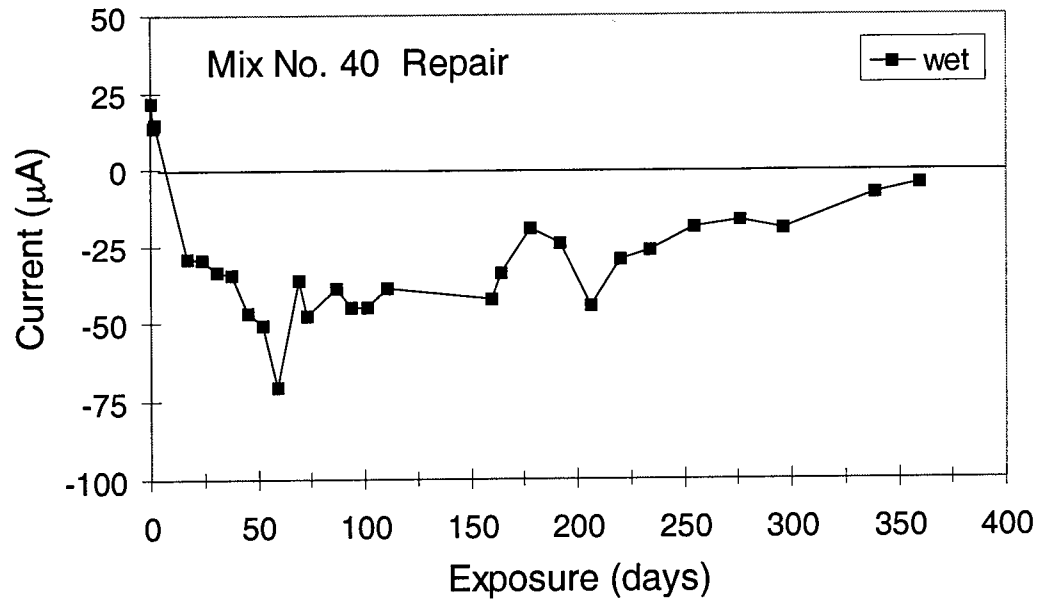


Figure 51. Averaged coupled current versus time for repair slab material no. 40.

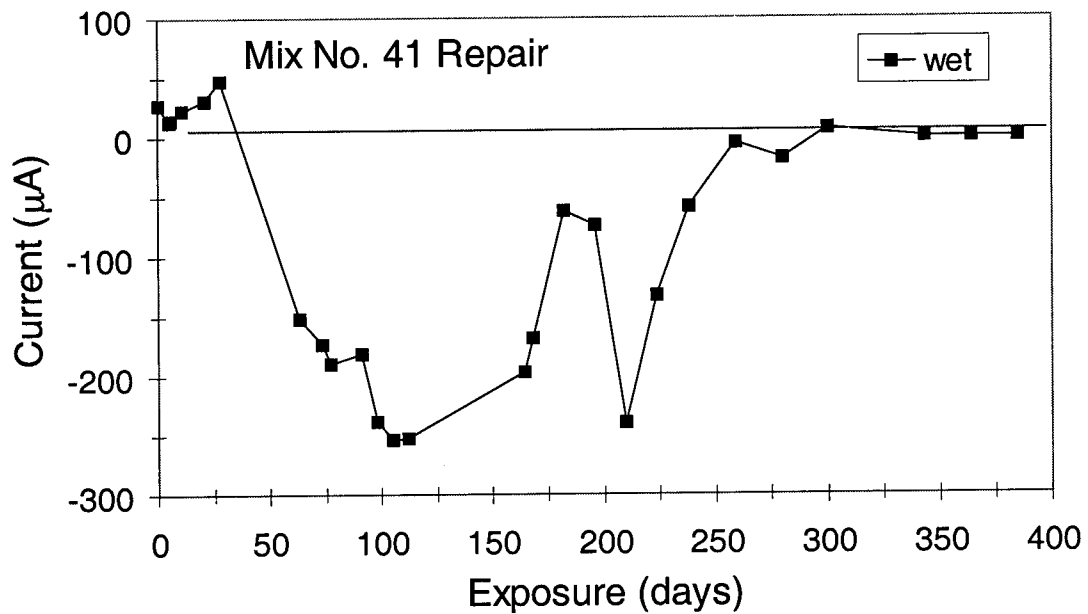


Figure 52. Averaged coupled current versus time for repair slab material no. 41.

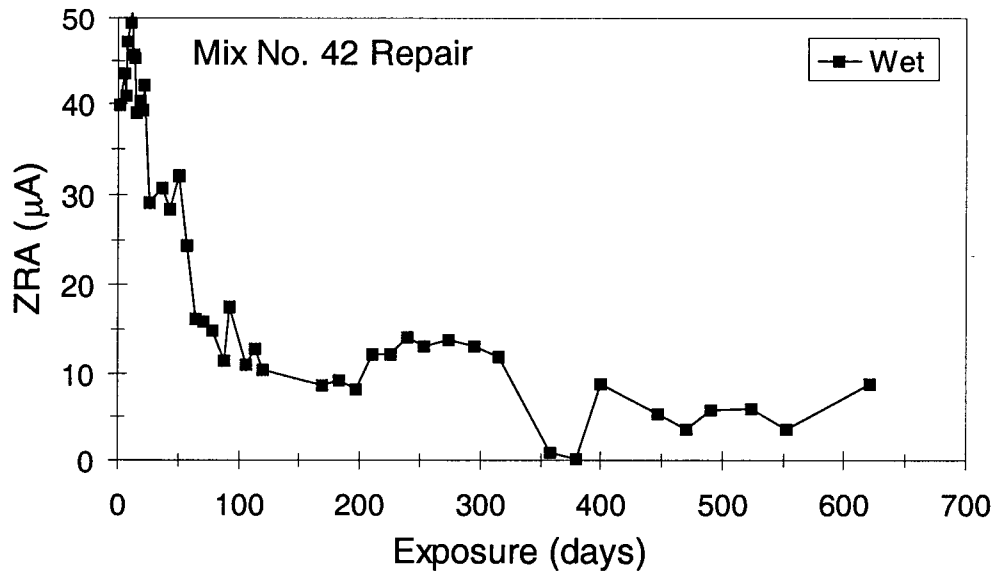


Figure 53. Averaged coupled current versus time for repair slab material no. 42.

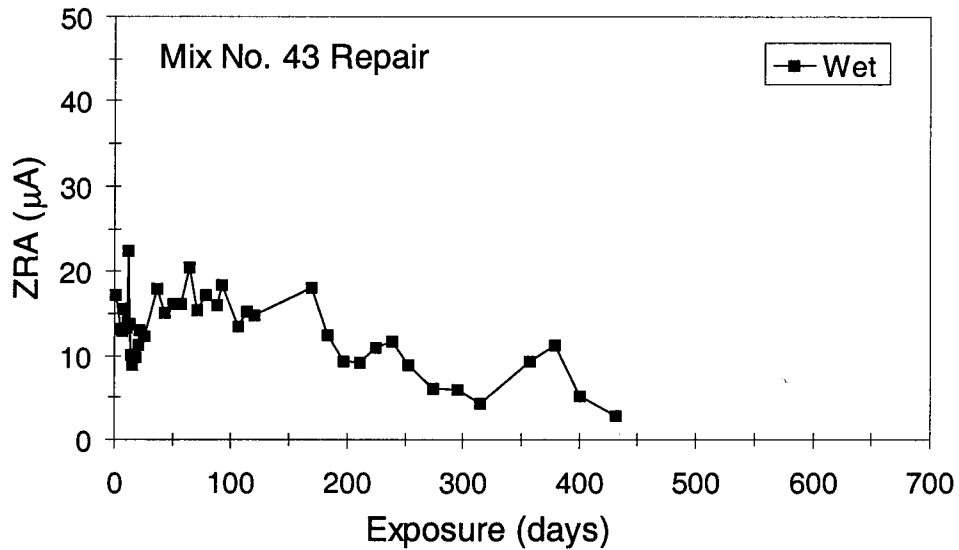


Figure 54. Averaged coupled current versus time for repair slab material no. 43.

The repair material nos. 42 and 43 (figures 53 and 54, respectively) show different behavior from repair material nos. 40 and 41. For repair material nos. 42 and 43, the coupled current remains positive, indicating enhanced corrosion of the steel bar in the concrete containing chloride while the steel in the repair material remained the cathodic member of the

macrocell couple. Also, the coupled current was relatively low, indicating that the magnitude of macrocell driven corrosion was relatively low.

The repair slabs had a problem with separation between the repair material and the contaminated concrete. This could be attributed to differences in thermal expansion and/or drying shrinkage strain. This, in part, explains the decrease in coupled current over time for repair slab nos. 40, 41, and 43.

LPR Corrosion Rate and Potential

Corrosion rate and potential data for each individual slab for both the standard and the repair slabs are given in Appendix E. Average corrosion rates for the standard slab (figure 24) tests for the repair materials are shown in table 50. Repair material no. 41 exhibited the highest corrosion rate, followed by repair material no. 40. Repair material nos. 42 and 43 had negligible corrosion in the standard slab specimens.

Table 50. Corrosion rate and potential for standard slab repair materials
[1 mpy = 0.0254 mm/yr].

Repair Material	Exposure	Potential (mV, CSE)	Corrosion Rate (mpy)
40	Wet	-274	0.11
41	Wet	-254	1.2
42	Wet	-87	0.01
43	Wet	-45	<0.01

Corrosion rates and potentials measured for the repair slabs (figure 25) are shown in table 51. Corrosion rates were measured for both the steel bar in the contaminated (chlorides) concrete and in the repair material. During normal operation, these two steel bars were coupled together. For LPR corrosion rate measurements, the bars had to be disconnected. Table 51 shows that the steel in the contaminated concrete had very high corrosion rates. This is expected since the concrete had chlorides mixed in at the time of casting. Also, cracks had formed over these areas on many of the slabs, permitting the extremely high rates. The corrosion rates in the repair areas for repair material nos. 40 and 41 were relatively high. The corrosion rates in the repair area for repair material nos. 42 and 43 were negligible.

Corrosion Initiation and Damage

For the repair slabs, cracking occurred over the steel bars in most of the contaminated concrete slabs. No cracking was observed over the steel bars in any of the repair materials. Figure 55 shows repair slab no. 43-D, which was typical of the cracking observed for the

repair slabs. Recall that chlorides were pre-mixed into the concrete in the repair slabs. Because the pre-mixed chlorides permits corrosion initiation over the entire bar, higher corrosion rates than normally experienced were measured. Therefore, calculation of the cumulative corrosion prior to cracking was not applicable for these slabs.

Table 51. Corrosion rates and potentials for the steel bars in the repair slabs
[1 mpy = 0.0254 mm/yr].

Concrete	Exposure	Steel Location	Potential (mV, CSE)	Corrosion Rate (mpy)
No. 40 Repair	Wet	Center - Contaminated Concrete	-430	29
No. 40 Repair	Wet	Right - Repair Material	-495	0.73
No. 41 Repair	Wet	Center - Contaminated Concrete	-390	18
No. 41 Repair	Wet	Right - Repair Material	-315	5.6
No. 42 Repair	Wet	Center - Contaminated Concrete	-464	13
No. 42 Repair	Wet	Right - Repair Material	-200	<0.01
No. 43 Repair	Wet	Center - Contaminated Concrete	-225	1.2*
No. 43 Repair	Wet	Right - Repair Material	-175	<0.01

*:Average of three slabs. Fourth slab with very high corrosion rate was not measured.

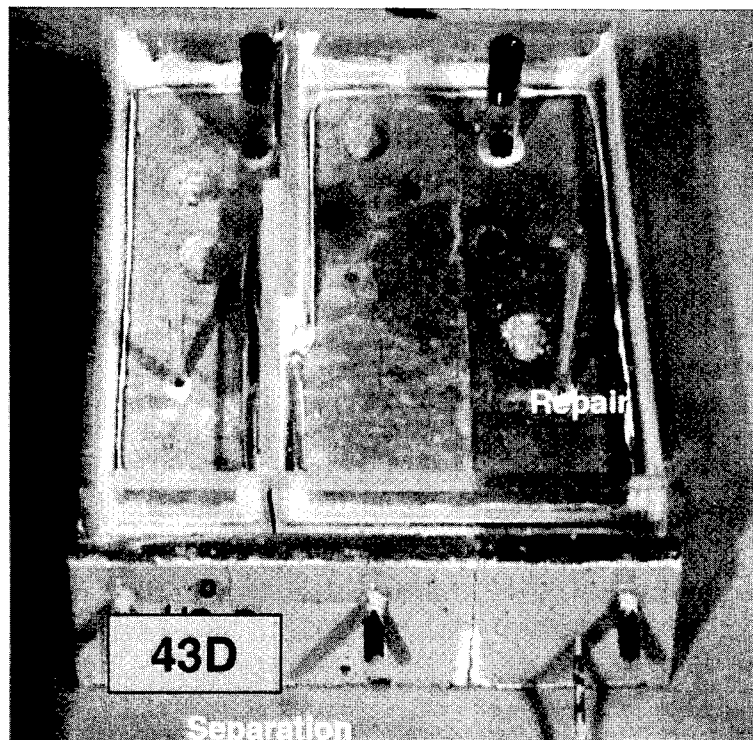


Figure 55. Photograph of repair slab 43-D showing typical cracking.

Chloride Concentrations

Table 52 shows the chloride concentrations from the standard slabs (figures 24 and 27) for the repair materials (recall that repair material no. 42 is concrete no. 1 and repair material no. 43 is concrete no. 31). Repair material no. 42 exhibited the lowest chloride concentration in the standard slabs, followed by repair material no. 40 and no. 43. Repair material no. 41 had significantly greater chloride concentration and also had a significantly greater corrosion rate (table 50). Although the chloride concentration for repair material no. 40 was relatively low (0.018 percent, 0.41 kg/m^3 [0.68 lb/yd^3]), the corrosion rate (Appendix E, slab D) was measurable (0.0027 mm/yr [0.11 mpy]). This can be compared to repair material no. 43 that had a chloride concentration of 0.047 mm/yr (1.8 mpy) and negligible corrosion ($<0.0003 \text{ mm/yr}$ [0.01 mpy]).

Table 53 shows chloride concentrations for the repair slabs (figures 25 and 27). The center concrete (contaminated concrete) was the same for all repair slabs. Table 53 gives the chloride concentrations for this concrete ponded with NaCl as 0.39, 0.51, 0.36, and 0.45 percent (9, 11.4, 8.4, and 10.2 kg/m^3 [$15, 19, 14$ and 17 lb/yd^3]) for slabs nos. 40-Repair, 41-Repair, 42-Repair, and 43-Repair, respectively. These values are in reasonable agreement, indicating consistency in the tests. The data collected in the contaminated concrete ponded with water is less consistent. This could be due, in part, to the combined action of: (1) the water pond tending to remove chlorides (concentration gradient), (2) water migration into the concrete and drying from the bottom tending to concentrate chlorides toward the bottom of the slab, or (3) permeability of the concrete. The targeted chlorides in the contaminated concrete was 0.27 percent (6 kg/m^3 [10 lb/yd^3]).

For the repair slabs, repair material no. 40 exhibited the lowest chloride concentration (0.093 percent, 2.1 kg/m^3 [3.5 lb/yd^3]) followed by repair material nos. 43 and 42. Repair material no. 41 exhibited significantly higher chloride concentration (0.71 percent, 16.2 kg/m^3 [27 lb/yd^3]) and had the highest corrosion rate for steel in a repair material (table 51 and table 78, Appendix E). Although repair material nos. 42 and 43 had chloride concentrations of 0.30 percent 6.6 kg/m^3 [11 lb/yd^3] and 0.21 percent (4.7 kg/m^3 [7.9 lb/yd^3]) respectively, the corrosion rates for steel in both repair materials was negligible ($<0.0003 \text{ mm/yr}$ [$<0.01 \text{ mpy}$]). The corrosion rate (Appendix E) for repair material no. 40, slab D was relatively low, but measurable (0.0015 mm/yr [0.06 mpy]). The average corrosion rate (table 51) for repair material no. 40 (0.018 mm/yr [0.73 mpy]) was greater than the slab D rate, indicating that the remaining slabs for repair material no. 40 sustained greater corrosion rates.

Table 52. Chloride concentrations for standard slab repair materials
[1 lb/yd³ = 0.6 kg/m³].

Repair Mix	Sample Location	Exposure	Slab	Chloride (lb/yd ³)
No. 40	NaCl Water	Wet	D	0.68 <0.1
No. 41	NaCl Water	Wet	D	18 5.0
No. 42	NaCl Water	Wet	H	<0.1 <0.1
No. 43	NaCl Water	Wet	H	1.8 <0.1

Table 53. Chloride concentrations for the repair slabs [1 lb/yd³ = 0.6 kg/m³].

Concrete Mix	Sample Location	Exposure	Slab	Chloride (lb/yd ³)
No. 40 Repair	Left (Concrete) - Water	Wet	D	10
	Center (Concrete) - NaCl			15
	Right (Repair Mat.) - NaCl			3.5
No. 41 Repair	Left (Concrete) - Water	Wet	D	5.0
	Center (Concrete) - NaCl			19
	Right (Repair Mat.) - NaCl			27
No. 42 Repair	Left (Concrete) - Water	Wet	D	2.9
	Center (Concrete) - NaCl			14
	Right (Repair Mat.) - NaCl			11
No. 43 Repair	Left (Concrete) - Water	Wet	D	6.6
	Center (Concrete) - NaCl			17
	Right (Repair Mat.) - NaCl			7.9

Post-Test Analysis

Post-test analysis for the repair slabs was limited to comparison of the measured corrosion behavior with LPR to the corrosion observed on the steel bars. In all cases, the relative amount of corrosion observed on the steel bars was agreed with the corrosion rates measured.

DISCUSSION: TASK C – LONG-TERM PERFORMANCE STUDIES

Comparison to Task B Model Predictions

One of the primary goals of task C was to validate the model predictions of the task B statistical models. Recall that the task A and task B tests used small test cells and task C used larger slab specimens. Chloride permeability is the best data available for comparing task B and task C data. The corrosion rate predictions will also be compared, but the amount of chloride at the steel surface varied dramatically in these two tests.

Chloride Concentration

To compare chloride permeability, rapid chloride permeability data based on the task B model predictions (table 32) is compared to the amount of chloride measured at the steel surface following task C exposures (table 46). Two comparisons were performed: normalized data and correlation analysis. The data was normalized as described previously in task B (equation is repeated below):

$$\text{Normalized Value} = (\text{Value} - \text{Minimum})/(\text{Maximum} - \text{Minimum}) \quad (2)$$

This type of normalization is required to permit the handling of variables of different types, and it sets the range of each variable between 1 (maximum value) and 0 (minimum value). The results of task B (model predictions) and task C (chloride permeability) gave similar results (table 54), indicating good ability of the task B model to predict behavior in the larger scale chloride-ponding task C tests. Sample calculations for concrete mix no. 11 are given below (average values of measured chloride for cycled and wet conditions were used):

$$\begin{aligned} \text{Normalized Cl Permeability Model (table 32)} &= [(1172) - (-2735)]/[5886 - (-2735)] = 0.45 \\ \text{Normalized Cl Measured (table 46)} &= (13.6 - 0.1)/(24 - 0.1) = 0.56 \end{aligned}$$

Table 54. Comparison of normalized data for rapid chloride permeability model predictions (table 32) and chloride concentration at the steel surface from task C (table 46).

Concrete Mix	Normalized Chloride Measured Task C	Normalized Cl Permeability Model Prediction
1	0.00	0.23
31	0.04	0.00
3	0.05	0.27
24	0.15	0.34
11	0.56	0.45
15R	0.58	0.45
29	0.99	1.00
22	1.00	0.97

In direct comparison of the values of rapid chloride permeability model predictions and chloride concentration in the concrete at the steel level, a correlation coefficient of 0.94 was calculated. Figure 56 shows a plot of the rapid chloride permeability model predictions (task B) versus chloride concentration in the concrete at the steel level for the task C concrete.

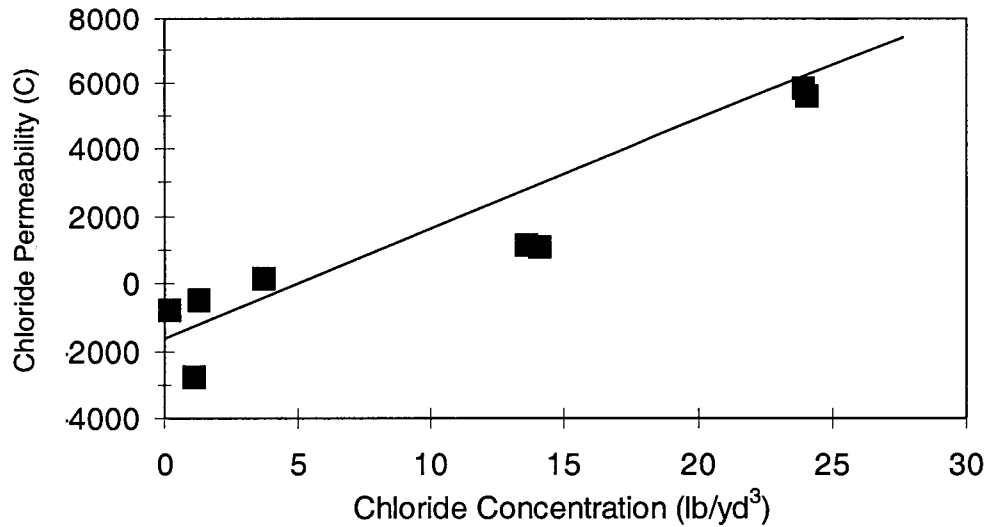


Figure 56. Plot of chloride permeability (task B) versus chloride concentration (task C) [$1 \text{ lb/yd}^3 = 0.6 \text{ kg/m}^3$].

Corrosion Rate

The problem with comparing the corrosion rate model predictions from task B with the corrosion rate measurements from task C is that the chloride levels were quite different. In the task B tests, the chloride levels were targeted at one of two levels: moderate (1.8 kg/m^3 [3 lb/yd^3]) or aggressive (6 kg/m^3 [10 lb/yd^3]). For task C, the chloride concentrations ranged from 0.06 to 14 kg/m^3 (0.1 to 24 lb/yd^3), depending on the concrete. The following data analysis was performed to account for the differences in chloride concentrations.

A value of 3 kg/m^3 (5 lb/yd^3) for chloride concentration was selected as a cut-off for using moderate versus aggressive environment data for comparison with task C data. In task C tests, concrete nos. 1, 3, 24, and 31 had less than 3 kg/m^3 (5 lb/yd^3) chloride concentration. The task B moderate environment model predictions were used for these concretes. In task C tests, concrete nos. 11, 15R, 22, and 29 had greater than 3 kg/m^3 (5 lb/yd^3) chloride concentration. The task B aggressive environment model predictions were used for these concretes. Table 55 compares corrosion rates for the task B model predictions with the average (cycle and continuously wet) task C data. Also, given in table 55 are the normalized values for the task B predictions and the task C data. There is excellent agreement between the task B model predictions and the large-scale slab tests in task C.

Table 55. Comparison of corrosion rate from task B model predictions to task C data [1 mpy = 0.0254 mm/yr].

Concrete Mix	Task B Model Prediction Corrosion Rate (mpy)	Average Task C Corrosion Rate (mpy)	Normalized Task B Model Prediction Corrosion Rate (mpy)	Normalized Average Task C Corrosion Rate (mpy)
3	0.07*	0.01	0.06	0.00
31	-0.15*	0.01	0.00	0.00
1	-0.05*	0.01	0.03	0.00
24	0.01*	0.04	0.04	0.01
15R	0.22**	0.38	0.10	0.09
11	0.85**	0.59	0.27	0.14
29	1.4**	3.4	0.42	0.85
22	3.6**	4.0	1.00	0.99

*: Moderate Environment

**: Aggressive Environment

Figure 53 shows a plot of the corrosion rate for the task B model predictions versus task C concrete slab data. The correlation coefficient for these two data sets was 0.91. As for the chloride concentration data, very good agreement was observed between the model predictions and the large-scale slab tests.

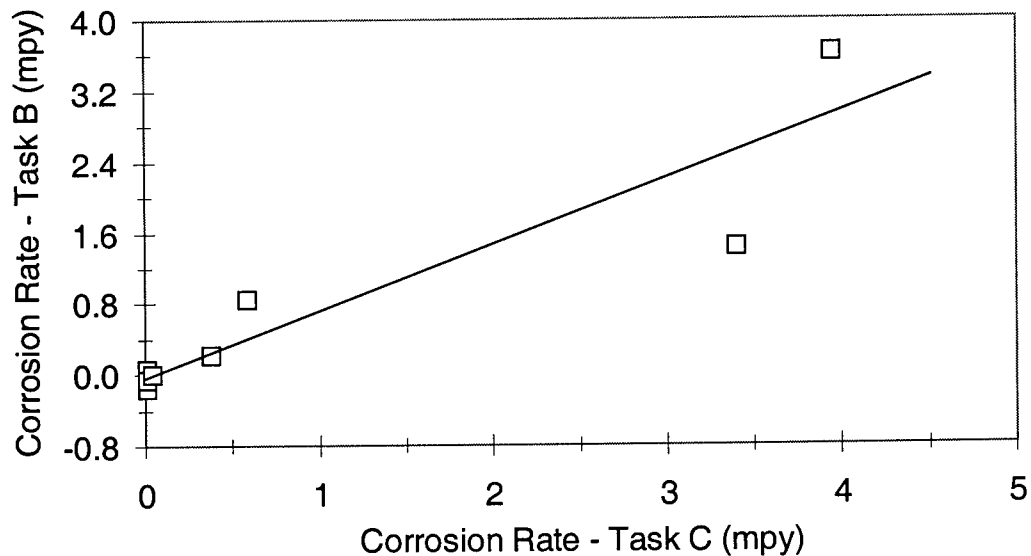


Figure 57. Plot of corrosion rate for task B model predictions versus task C data [1 mpy = 0.0254 mm/yr].

Concrete Damage

As expected, there is a correlation between the onset and severity of cracking and the thickness of the corrosion product reaction layer. There is further correlation between this variable and the number of cracks occurring in concrete adjacent to the corroding bar.

The extent of diffusion of steel corrosion product into the cementitious phase of the concrete is dependent upon water-cement ratio within the range 0.3 to 0.5. As the water-cement ratio is increased, the porosity of the cementitious phase is increased, which provides an increase in the rate of diffusion of corrosion products into the cementitious phase.

Diffusion of steel corrosion products also takes place in aggregate particles adjacent to the corroding bars. The extent of this diffusion is influenced by the porosity of the coarse aggregate. In the present concretes, aggregates representing extremes in accessible porosity were used, including a limestone aggregate with a water absorption of 9.8 percent and a quartz aggregate with a water absorption of 0.6 percent. Some limestone aggregate particles adjacent to corroding steel bars were totally invaded by steel corrosion products. In contrast, diffusion of steel corrosion products into the quartz aggregate only occurred along fracture planes in these particles.

The effect of the diffusion of accumulating steel corrosion products into the various constituents of the concrete is to alleviate stresses that might otherwise develop in the absence of this event. This appears to delay, for some period of time, the onset of cracking in concrete that is undergoing active corrosion. Concrete slab 29-A, for example, although showing high corrosion rates, required 700 days to exhibit cracking. This concrete had a water-cement ratio of 0.5 and contained the porous limestone coarse aggregate.

Table 56 compares cumulative corrosion prior to visible cracking to the mechanical properties tested in this task. The cumulative corrosion prior to cracking is for the cycled corrosion exposures because this was the only condition with data for all three concrete mix designs. The 1 year mechanical property data was used for comparison because some of the mechanical properties continued to change for up to 6 months to 1 year. Correlation coefficients also are given in table 56. The best correlation was observed between "cumulative corrosion to cracking" and "modulus of elasticity". More cumulative corrosion to cracking occurs for concretes with lower modulus of elasticity. Therefore, everything else being equal, a lower modulus concrete that permits more cumulative corrosion prior to cracking is beneficial to extending the life of a concrete structure. For the range of conditions tested in this project, the cumulative corrosion prior to cracking can be estimated by the modulus of elasticity. For this project, no predictive model was developed for estimating the modulus of elasticity as a function of concrete mix design (the mechanical model developed was for compressive strength).

It should be noted that the properties in concrete that would permit more cumulative corrosion prior to cracking (porosity in the cement paste and aggregate phases) would probably be detrimental to chloride permeability, corrosion behavior, and strength. Therefore,

designing concrete based on improved cracking resistance (low modulus) is probably an unacceptable trade-off for increasing chloride permeability.

Table 56. Comparison of cumulative corrosion prior to cracking with mechanical properties [1 psi = 6.895 kPa]

Mix Design	Cumulative Corrosion to Cracking (cycled) (mil [mm])	Modulus of Elasticity (1 year) (psi x 10 ⁶)	Flexural Strength (1 year) (psi)	Compressive Strength (1 year) (psi)
11	1.8 [0.046]	5.9	1,020	7,600
22	5.7 [0.145]	3.9	900	8,300
29	7.6 [0.193]	3.2	700	5,000
Correlation Coefficient Between Corrosion to Cracking and Strength		-0.997	-0.943	-0.604

SUMMARY: TASK C – LONG-TERM PERFORMANCE STUDIES

Significant differences were observed in the concrete deterioration resistance for the concrete mix designs tested in task C. These differences in behavior were attributed to both chloride permeability into the concrete and corrosion resistance of the concrete. Differences were also reported in the damage behavior (cracking at a given cumulative corrosion) as a function of the concrete mix design. All of these factors are important in establishing the concrete deterioration resistance of a particular concrete mix design.

In general, the properties of deterioration-resistant concrete are the same properties desired in a repair/patch concrete:

- Low chloride permeability.
- Corrosion resistance (higher chloride threshold for corrosion and low corrosion rate following initiation).
- Greater cumulative corrosion prior to cracking.
- Higher resistivity to minimize macrocell corrosion.

Predictions of the statistical models developed in task B were compared to the results of the larger concrete slab specimens tested in task C:

- The predictions of the task B Rapid Chloride Permeability Model provided excellent agreement with the chloride measured in the concrete at the steel bar level.
- The predictions of the task B corrosion rate models provided excellent agreement in ranking the concrete mix designs as to their corrosion resistance as measured in task C.

Although a predictive model relating a damage function (amount of damage as a function of cumulative corrosion) to a concrete mix design was not developed, information on cumulative corrosion prior to visible cracking was determined. It was shown that the concrete matrix could absorb steel corrosion products to different degrees, depending on the accessible porosity of the cementitious phase and the aggregate phases, thereby affecting the relationship between damage and cumulative corrosion. Furthermore, it was shown that a good correlation exists between modulus of elasticity and cumulative corrosion prior to cracking.

Having validated the usefulness of the task B model predictions through large-scale slab testing in task C, the prediction models were used in the final optimization model developed in task D.

CHAPTER 6. TASK D — IMPLEMENTATION

The purpose of task D was to develop a life prediction/optimization model for concrete structures that would permit selection of application-specific concrete mix designs. This task consolidated the results of tasks A, B, and C. The model was designed to provide the bridge engineer with a tool that would require site-specific data (e.g., climatic conditions and average number of salt applications) and permit both life prediction and optimization for a selected concrete mix design. The purpose of the life prediction is primarily to compare concrete mix design selections.

The model developed considers only concrete corrosion and chloride permeation resistance properties and not other field conditions that may ultimately limit the structure's life. Also, the model was developed based on averaged laboratory-measured properties. Therefore, for the cases in which an unusually long life is predicted, the model is indicating that average concrete properties of corrosion resistance and chloride permeability resistance are sufficient to extend the life, and other processes not included in the model will probably limit actual life achieved. Under realistic field conditions, the in-place concrete will have inhomogeneous density, variable concrete cover over reinforcement, and susceptibility to cracking during curing and under traffic loads. These field conditions may significantly limit the life of any given structure to much lower values than those based on the model presented below.

Figure 58 shows the flow diagram for the concrete optimization process. This six-step process permits life prediction and economic analysis of new concrete.

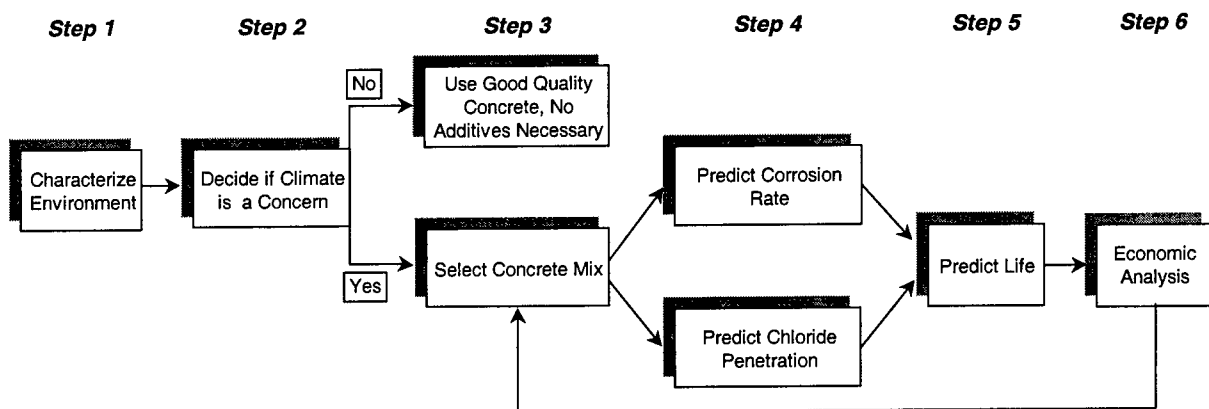


Figure 58. Flow diagram for concrete optimization.

STEP 1 – DETERMINE AVERAGE CLIMATIC CONDITIONS

In step 1, the average environment is characterized. There are many ways of accomplishing this. The ultimate goal is to establish whether or not the climatic conditions exist to support corrosion of reinforcing steel in concrete as defined in figure 15.

It is assumed that calculations are performed for those areas where chloride either naturally occurs (marine) or where deicing salts are routinely used. Therefore, chlorides are present and the chloride permeability of the concrete is a critical parameter. Furthermore, it is assumed that chlorides will eventually permeate the concrete and the high chloride map from figure 15 is used for this analysis. Figure 59 shows the high chloride map and a three-dimensional surface plot for temperature-humidity-corrosion rate. For areas of low humidity (<50 percent), corrosion is not a problem. Also at low temperatures corrosion is observed at relatively low levels for intermediate humidity only. The surface plot shows that corrosion is greatly accelerated at high temperature and high humidity combinations.

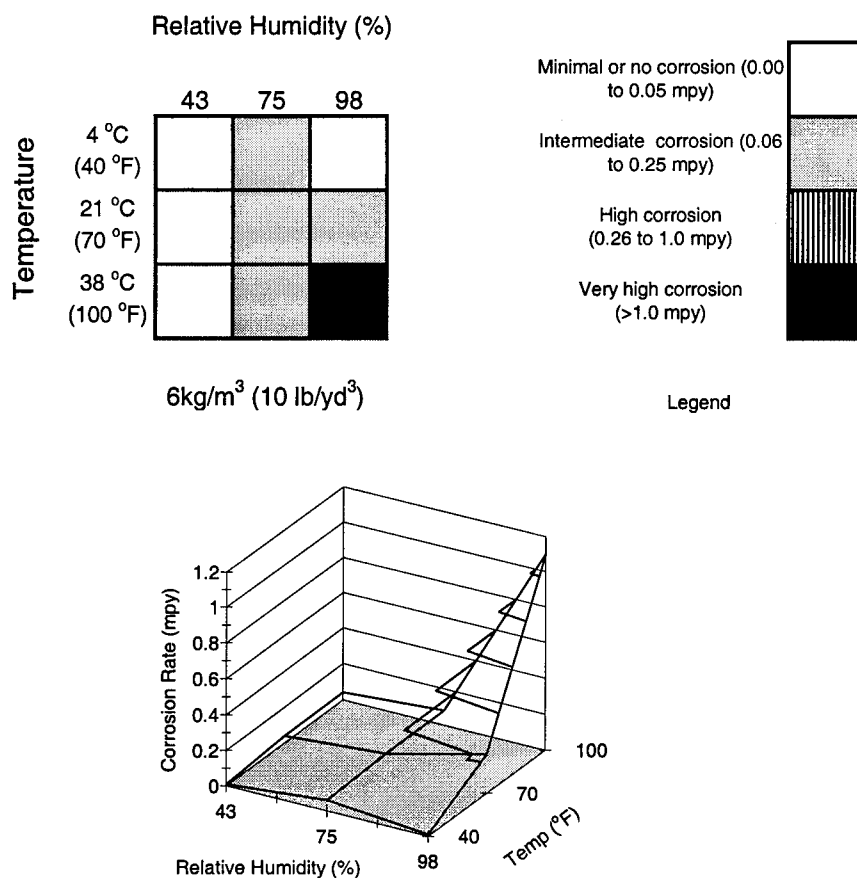


Figure 59. Environmental map for corrosion as a function of temperature and relative humidity [1 mpy = 0.025 mm/yr].

Based on this data, figure 60 was developed to divide the temperature-humidity plot into four classes based on corrosion:

- Class I – Conditions cannot sustain corrosion (corrosion negligible).
- Class II – Conditions can sustain light corrosion ($0.05 < \text{CR [mpy]} < 0.15$).
- Class III – Conditions can sustain significant corrosion ($0.15 < \text{CR [mpy]} < 0.5$).
- Class IV – Conditions can sustain very high corrosion rates ($\text{CR [mpy]} > 0.5$).

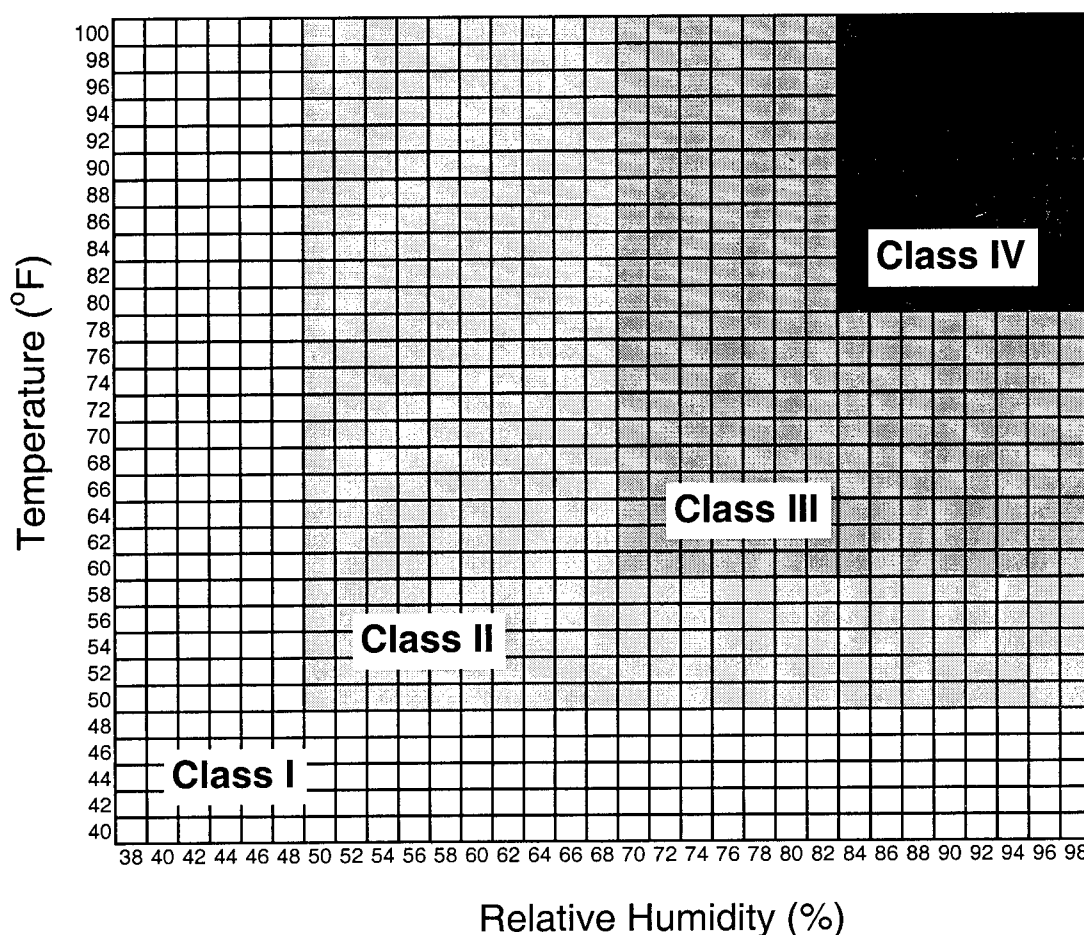


Figure 60. Four classes of conditions based on ability to sustain corrosion
 $[\text{°C} = 5(\text{°F}-32)/9]$.

The following procedure was used to determine whether a particular set of climatic conditions is corrosive to reinforcing steel in concrete. A weekly average (based on the changes observed in the cyclic exposures plotted in figures 37 and 38) was used in this analysis. It should be noted that the changes in figures 37 and 38 were observed for a concrete cover of 19 mm (0.75 in); a greater cover would result in an even slower response to an environmental change. However, for this analysis, weekly averages for climatic conditions are assumed to be sufficient to characterize the effects of corrosion in concrete. The following data is required:

- The average weekly temperature and relative humidity are calculated for a 12-month period.
- The number of weeks for which the temperature falls within the above four classifications is calculated.

STEP 2 – CORROSIVE NATURE OF AVERAGE CLIMATE

Typically, any given location will experience a range of climatic conditions that will encompass one of the corrosion conditions at least part of the year. For corrosion to be considered a problem, the following rules are proposed:

- Rule 1. ≥ 6 percent of the year conditions must meet Class IV, or
 Rule 2. ≥ 15 percent of the year conditions must meet Class III or greater, or
 Rule 3. ≥ 50 percent of the year conditions must meet Class II or greater.

These rules are based on average corrosion rates for each class and the requirement that corrosion is considered to be a problem when the first cracks appear ([2-mil] cumulative corrosion) within 40 years. Note that the life of the structure is probably longer than the time to the appearance of the first cracks. The following shows an example calculation:

$$\text{Rule 2: } \% = 2 \text{ [mil]} / (0.325 \text{ [mpy]} \times 40 \text{ [yr]}) = 15\%$$

Based on the above rules, determine whether corrosion is a problem for a particular set of conditions using the average weeks in each classification calculated in Step 1. If the average climatic conditions do not support corrosion, then good-quality concrete can be used with minimal consideration for corrosion of the reinforcing steel. If the average climatic conditions support corrosion, proceed to step 3.

STEP 3 – SELECT CONCRETE MIX

In step 3, the concrete mix is selected based on the availability of mix components, economics, and expected corrosion severity. The models for corrosion and chloride permeability presented in task B can be used for this process. If it is assumed that a continuous supply of chloride will be present, chloride permeability becomes the most critical parameter. With high chloride permeability and a continuous supply of chlorides, the time for corrosion initiation may be short, even for a concrete that has good corrosion resistance properties (relatively low chloride permeability and relatively low corrosion rate following initiation). However, the difference in the corrosion resistance properties of concrete, as defined in task B, makes a significant difference in the life of the structure.

STEP 4 – PREDICTION OF CORROSION AND CHLORIDE PERMEATION

Step 4 is divided into two separate activities: prediction of corrosion rate and prediction of chloride permeation.

Corrosion Rate Prediction

Corrosion Rate of Base Concrete

The corrosion rate for the base concrete exposed to the particular climate conditions is calculated as follows:

1. Record the percentage of time that the climatic conditions exist in the four corrosion classifications (calculations from step 1).
2. Multiply the percentage of time in each classification by the average corrosion rate in each classification and sum. This gives the expected average annual corrosion rate for the particular climatic conditions.

Table 57 gives an example calculation for determining the corrosion rate of the base concrete exposed to the climatic conditions established in step 1. The percentage of times in each classification were assumed to be the values in table 57. In an actual analysis, these values would have to be determined for each particular climatic condition. Note that rules 2 and 3 (step 2) are met for defining corrosive climatic conditions since percentage of time in class III plus class IV equals 25 percent (Rule 2 = ≥ 15 percent) and percentage of time in class IV plus class III plus class II equals 55 percent (rule 3 = ≥ 50 percent).

Table 57. Example calculation for step 4 under "Corrosion Rate of Base Concrete" [1 mpy = 0.0254 mm/yr].

Class	Percentage Time in Class	Average Corrosion Rate for Class* (mpy)	Total Corrosion
I	45%	0.02	0.009
II	30%	0.10	0.030
III	20%	0.33	0.065
IV	5%	0.75	0.038
Total Corrosion Rate (mpy)			0.142

*: Averages for each class (see discussion in step 1 for corrosion rates in each class); 0.02 mpy was used for class I and 0.75 mpy was used for class IV.

Corrosion Rate Index for Base Concrete

The calculation in step 4 under “Corrosion Rate of Base Concrete” gives the average corrosion rate for the base concrete. The following calculation normalizes this value and permits the calculation of the selected concrete mix from step 3 for the particular climatic conditions to be calculated.

The base concrete used in task A (concrete A-5) had the following mix properties:

- Water-cement ratio: 0.45.
- Coarse aggregate: quartz.
- Fine aggregate: quartz.
- Mineral admixture: none.
- Cement type: type I portland – cement A in task B.

Based on the corrosion resistance ratings of the base concrete components, the base concrete is a relatively corrosion-resistant concrete. The task B model (given in table 28) for corrosion rate is used to provide a corrosion rate index for this base concrete. The base concrete had a corrosion rate index of -0.44 (see calculation in table 58). This value will be used in all calculations. It is the corrosion index for the concrete used in the environment model (figure 60).

Corrosion Rate Index of Design Concrete Mix (Step 3)

Using the corrosion rate model previously given in table 28 and partially repeated in table 58, the corrosion rate index for the design concrete is calculated. The cement type for the design may not be specifically represented in the model, but the closest representative cement must be selected.

Table 58. Corrosion rate index calculation for base concrete and design concrete example (see table 28) [1 mpy = 0.0254 mm/yr].

Parameter	Level	Estimate (mpy)	Base Concrete		Design Concrete	
			Level	Index Calculation	Level	Index Calculation
Intercept		4.52		4.52		4.52
Water-Cement Ratio	0.3	-1.92	0.45*	-0.535	0.45*	-0.535
	0.4	-1.07				
	0.5	0.00				
Coarse Aggregate	Limestone	1.32	Quartz	0	Limestone	1.32
	Quartz	0.00				
Fine Aggregate	Glacial Sand	2.19	Quartz	0	Glacial Sand	2.19
	Quartz	0.00				
Mineral Admixture	Silica Fume	-4.11	None	-2.04	None	-2.04
	None	-2.04				
	Class C Flyash	-0.29				
	GGBF Slag	0.00				
	Class F Flyash	-1.44				
Cement Type	Type I Low C3A	E -2.23	A	-2.39	A	-2.39
	Type I Low Alkali	C -2.38				
	Type I High C3A	D -0.56				
	Type I High Alkali	A -2.39				
	Calcium Aluminate	B 2.98				
	Mag Phosphate	F 0.00				
			Index	-0.445	Index	3.07

*: Average from table 28.

As an example, it is assumed that the concrete design is the same as the base concrete except that more porous fine (glacial sand instead of quartz) and coarse (limestone instead of quartz) aggregates were used. The corrosion index for this concrete (calculated based on model estimates and shown in table 58) is 3.07.

Corrosion Index Factor

A corrosion index factor (CIF) can now be calculated to normalize the corrosion rate calculated in step 4 under “Corrosion Rate of Base Concrete” to a corrosion rate of the designed concrete (step 3) in the particular climatic conditions established in step 1.

The CIF is calculated using the following equation:

$$\text{CIF} = (\text{base index} - \text{designed concrete index}) / \text{base index}$$

The base index is always -0.44 (step 4 under “Corrosion Rate Index for Base Concrete”). Therefore, the equation for the corrosion index factor becomes:

$$\text{CIF} = (-0.44 - \text{designed concrete index}) / -0.44$$

The calculation for the CIF of the design concrete example is given below:

$$\text{CIF} = [(-0.44) - (3.07)] / -0.44 = 8.0$$

Corrosion Rate of the Designed Concrete

A positive value of the CIF indicates that the corrosion rate calculated in step 4 under “Corrosion Rate of Base Concrete” must be increased (multiplied) by a factor equal to the magnitude of CIF. A negative CIF indicates that the corrosion rate must be decreased (divided) by a factor equal to the magnitude of CIF. For the example calculation, the value of CIF is +8.0. Therefore, for the climatic conditions established in step 1, the corrosion rate calculated in step 4 under “Corrosion Rate of Base Concrete” is multiplied by 8.0 to get the corrosion rate of the designed concrete.

For the example calculation, the base corrosion rate established in step 4 under “Corrosion Rate of Base Concrete” (0.14 mpy) is multiplied by 8.0 (CIF) to give a predicted corrosion rate of 1.1 mpy (0.028 mm/yr) for the designed concrete in the particular climate established in step 1 (table 58).

Chloride Permeation

Chloride permeation can be calculated in different ways. One way is to determine a permeation coefficient (diffusion coefficient) and relate chloride concentration and time through conventional diffusion equations. In the following, a different approach is taken based on the experimental data from task C and the relationship to rapid chloride permeability (figure 56).

Chloride Permeability

The rapid chloride permeability model (table 25) is used to calculate the chloride permeability for the concrete selected in step 3. Table 59 gives the model estimates along with the prediction for the example concrete. For the example concrete defined under in step 4 under “Corrosion Rate Index of Design concrete Mix (Step 3), the chloride permeation model predicted a value of 3,082 C.

Table 59. Prediction model for rapid chloride permeability.

Parameter	Level	Estimate (coulombs)	Example Concrete	
			Level	Estimate
Intercept		3,011		3,011
Water-Cement Ratio	0.3	-1,894	0.45	-628
	0.4	-1,255		
	0.5	0		
Coarse Aggregate	Limestone	2,177	Quartz	0
	Quartz	0		
Fine Aggregate	Glacial Sand	1,288	Quartz	0
	Quartz	0		
Mineral Admixture	Silica Fume	-734	None	2,128
	None	2,128		
	Class C Flyash	-431		
	GGBF Slag	0		
	Class F Flyash	1,279		
Cement Type	Type III Low C3A	E -3,118	A	-1,430
	Type I Low Alkali	C -2,414		
	Type I High C3A	D -1,743		
	Type I High Alkali	A -1,430		
	Calcium Aluminate	B -2,783		
	Mag Phosphate	F 0		
			Value (C)	3,081

Chloride Concentration per Cycle

Figure 56 related rapid chloride permeability calculated from the model prediction (table 25) to chloride measured at the reinforcing steel level in task C concretes following approximately 33 wet-dry cycles. The wet-dry cycles consisted of 14 days wet followed by 7 days dry. From figure 56, the average chloride concentration per cycle can be calculated as a function of the task B model prediction for the rapid chloride permeability.

Figure 56 was based on tests performed at a high temperature (38 °C [100 °F]) and relatively low depth of cover (19 mm [0.75 in]) during task C. Intuition would indicate that for the lower temperature of typical salt applications (non-marine) and typically greater depth of cover for many concrete structures, a factor to decrease the chloride per cycle is warranted. In going from 38 to 0 °C, the diffusion coefficient in a typical concrete composition would be expected to decrease by a factor of 17.⁴ The time for diffusion of a given chloride concentration to a given depth is related to the square of the depth. Therefore, a factor of two to three increase in depth would increase the diffusion time to achieve the same chloride concentration by a factor of four to nine.

⁴ N.S. Berke and M.C. Hicks, "Predicting Chloride Profiles in Concrete," *Corrosion*, Vol. 50 (3), 1994, P. 234-239.

Also, in the laboratory tests, the salt solution remained on the concrete surface for a continuous 7 day period, which is a much greater time than that expected on a concrete structure. This would also lead to a greater chloride concentration in the concrete for the laboratory tests than expected on a concrete structure. A factor of seven decrease in the chloride concentration per cycle was applied to account for these differences in the laboratory exposures and actual applications. Although the factor of seven adjustment is not fully explained by fundamental principles, it does not detract from the usefulness of the model predictions in comparing concrete mix designs. This factor should be revisited upon field validation of the model prediction.

Taking into account that the number of cycles in the test data was 33 and that a factor of 7 decrease in chloride concentration is expected due to differences in test and actual exposure conditions, figure 61 (calculated from figure 56) provides the chloride concentration per cycle versus rapid permeability model predictions (table 25).

The chloride concentration per cycle is calculated using figure 61. For the example concrete with a chloride permeability of 3,082 coulomb, figure 61 gives a chloride concentration of 0.044 kg/m³ (0.073 lb/yd³) per cycle. The following gives the example calculation:

$$\text{Chloride Concentration} = (3,082 + 2,500) / 76,185 = 0.073 \text{ lb/yd}^3 \text{ per cycle}$$

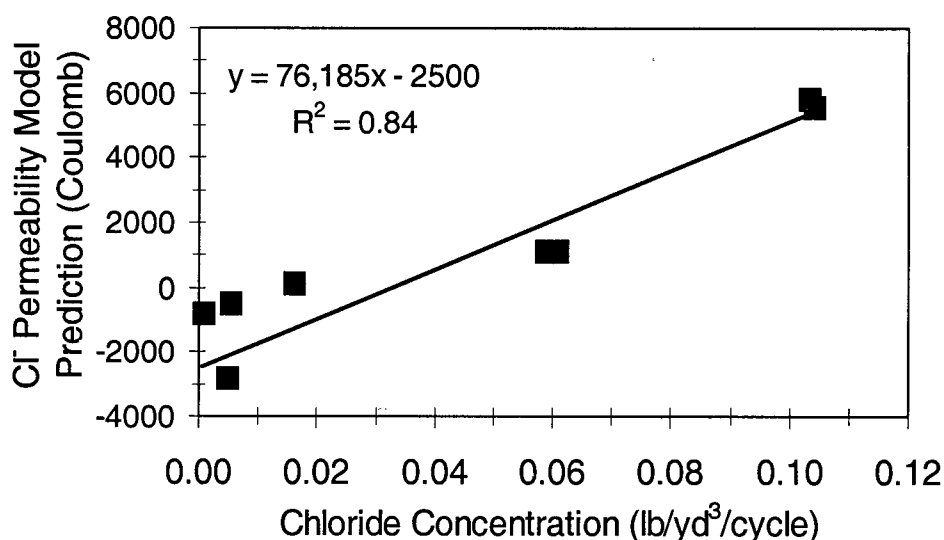


Figure 61. Chloride permeability model prediction versus chloride concentration per cycle [1 lb/yd³ = 0.6 kg/m³].

Chloride at the Reinforcing Steel Level

The chloride at the reinforcing steel level can simply be calculated by multiplying the number of cycles expected for a particular application by the chloride concentration

per cycle calculated in step 4 under “Chloride Concentration per Cycle”. A cycle is considered a 3-week period in which one or more salt applications were applied. For example, if three salt applications were made on a structure over a 2-week period, this would still count as only one cycle. It should be realized that several variables are being averaged together:

- Amount of salt per application.
- Frequency of application over a 3-week cycle.
- Precipitation prior to or after salt application (dilution effect of the salt concentration).

In comparing this approach to a pure diffusion approach, it must be realized that the above considerations are a concern in any approach. Also, ingress of chlorides into the concrete is not solely a diffusion process; however, because of the drying out of the concrete surface, it is accomplished through absorption of chlorides during subsequent wetting.

For the example being discussed, it is assumed that three cycles per year is expected. This would give a chloride concentration of 0.13 kg/m^3 (0.22 lb/yd^{30}) (0.072 /cycle times 3 cycles) for each year of exposure.

STEP 5 – LIFE PREDICTION

The useful life of a concrete structure is governed by the rates of the three processes given below:

- Rate of chloride ion permeation through the concrete.
- Rate of corrosion (once initiated).
- Rate of the development of cracking/spalling damage.

Three phases are identified in the life of a structure.

- Phase I — Corrosion Initiation. In Phase I, the corrosion rate of the reinforcing steel is negligible and a critical chloride level for corrosion initiation has not yet been obtained.
- Phase II — Corrosion Propagation Without Damage. In Phase II, the critical chloride level for corrosion initiation is exceeded. Corrosion is occurring at some rate; however, no damage of the concrete is apparent. The beginning of damage to the concrete signifies the end of Phase II. In this analysis, this is signified by the appearance of the first visual cracks.
- Phase III — Damage to the Structure. In Phase III, corrosion along with damage continues until the damage becomes so great that the useful life of the structure ends.

In this study, Phase II is defined as the time to crack initiation (visual cracks observed in the concrete test slabs. Useful life of the structure is a very difficult prediction to make. This Phase III life greatly depends on other parameters, such as maintenance and repair procedures and other mitigation procedures employed, such as cathodic protection, chloride removal, inhibitor treatment, overlays, etc. Therefore, in this analysis, only Phases I and II life of the structure are considered.

Phase I — Corrosion Initiation

The predictive model proposed here is a simplified version of the above more detailed model. Both tasks A and B predict relatively low, but measurable, corrosion rates at 1.8 kg/m^3 (3 lb/yd^3) chloride (mean for all data = 0.0022 mm/yr [0.09 mpy]) and a much higher corrosion rate for 6 kg/m^3 (10 lb/yd^3) chloride (mean for all data = 0.058 mm/yr [2.3 mpy]). It should be noted that the portland cement materials had a lower mean corrosion rate than given above. The chloride threshold for corrosion initiation was approximately 1.5 kg/m^3 (2.5 lb/yd^3) based on figure 23 (task B data). For this analysis, a chloride concentration of 1.5 kg/m^3 (2.5 lb/yd^3) is assumed to be the critical level for corrosion initiation. Since task B indicated that the threshold is dependent on concrete mix design, specific concrete data for the threshold for corrosion initiation could be substituted for the above-proposed value of 1.5 kg/m^3 (2.5 lb/yd^3), if available.

The time for Phase I is simply calculated by taking the threshold value for corrosion divided by the chloride concentration (lb/yd^3 per yr) at the steel level (step 4). In the example being carried through this analysis, Phase I would last for 11 years (1.5 kg/m^3 [2.5 lb/yd^3] divided by 0.13 kg/m^3 [0.22 lb/yd^3 per yr]).

Phase II — Corrosion Propagation Until Initial Damage

For the simplified model used here, the life of the structure is predicted through Phase II. It is further assumed that the end of Phase II life is defined as time to the appearance of visual cracking. For this study, this was determined to be 0.05 to 0.18 mm (2 to 7 mil) of cumulative corrosion depending on the concrete's microstructure and exposure conditions (table 45). It was also observed that the cyclic exposure permitted more cumulative corrosion prior to cracking. The value selected for this model is that the total cumulative corrosion prior to cracking (end of life) is 0.13 mm (5 mil).

To calculate the length of time for Phase II, the cumulative corrosion prior to cracking is divided by the corrosion rate from step 4 under "Corrosion Rate of the Designed Concrete". For the example being carried through this analysis, the time for Phases II and III is 4.5 years (5 mil divided by 1.1 mpy).

The life of the structure is simply the sum of time of Phase I and Phase II. For the example, the Phase I and Phase II life of the example concrete is predicted to be 15.5 years. This, of course, does not define useful operating life of an actual structure since Phase III life is not considered in this analysis.

STEP 6 – ECONOMIC ANALYSIS

In the economic analysis, the cost of construction, maintenance, materials, environmental impact, etc. are offset by the life of the structure. A detailed economic analysis is not provided here, but the example is followed through to show how the optimization of the concrete can be performed. It is assumed that an economic analysis would indicate that for the environmental conditions (climate and chloride cycles), the Phases I and II life predicted of 15.5 years for the example concrete is not economically acceptable.

The process is to go back to step 3 and redesign the concrete mix to improve performance. Several different concrete designs can be carried through simultaneously to provide several options in the final economic analysis. Tables 59 and 60 show the previously described example design concrete (no. 1) and five additional examples. The concrete mix design can have a profound effect on the predicted Phases I and II life of the concrete structure. Also, the life extension can be a result of a lower corrosion rate, lower chloride permeability, or both.

The economic analysis can be performed on a number of possible mix combinations to optimize performance and costs.

Table 60. Corrosion rate predictions for several example concretes
[1 mpy = 0.0254 mm/yr].

Design Concrete	Concrete Mix Design					CR Base Concrete ^(a)	Corrosion Index Base Concrete ^(b)	Corrosion Index Design Concrete ^(c)	CIF ^(d)	CR Designed Concrete ^(e)
	W-C Ratio	Coarse Aggregate	Fine Aggregate	Mineral Admixture	Cement Type	(mpy)				(mpy)
1	0.45	Limestone	Glacial	none	A	0.14	-0.44	3.06	8.0	1.11
2	0.4	Limestone	Glacial	Class F FA	E	0.14	-0.44	3.29	8.5	1.19
3	0.4	Limestone	Glacial	Silica Fume	A	0.14	-0.44	0.46	2.0	0.29
4	0.4	Quartz	Quartz	none	A	0.14	-0.44	-0.98	-1.2	0.11
5	0.4	Quartz	Quartz	Class C FA	E	0.14	-0.44	0.93	3.1	0.44
6	0.4	Quartz	Quartz	Silica Fume	E	0.14	-0.44	-2.89	-5.6	0.025

^(a) Specific to climate conditions.

^(b) Constant for model.

^(c) Specific to designed concrete mix.

^(d) Corrosion Index Factor.

^(e) Corrosion rate of designed concrete.

Table 61. Phases I and II life predictions for example concretes
[1 lb/yd³ = 0.6 kg/m³].

Design Concrete	Cl ⁻ Permeability ^(a) (C)	Cl ⁻ Concentration per Cycle ^(b) (lb/yd ³ /cy)	Cl ⁻ at Steel Level ^(c) (lb/yd ³ /yr)	Phase I Life ^(d) (yr)	Phase II Life ^(e) (yr)	Phases I and II Life Prediction ^(f) (yr)
1	3082	0.073	0.220	11.4	4.5	16
2	3382	0.077	0.232	10.8	4.2	15
3	3057	0.073	0.219	11.4	17.5	29
4	2454	0.065	0.195	12.8	43.8	57
5	-1793	0.009	0.028	90	11.5	101
6	-2096	0.005	0.016	157	199	356

(a) Model prediction for chloride permeation.

(b) Chloride concentration per cycle .

(c) Chloride at steel reinforcing level .

(d) Phase I life .

(e) Phase II life .

(f) Cracking observed.

SUMMARY: TASK D — IMPLEMENTATION

The results of tasks A, B, and C were consolidated to develop a concrete mix design optimization model based on environment, concrete mix, expected life, and economics. This was accomplished by using a six-step process and it permits life prediction of a concrete mix design based on the following:

- Concrete mix components/parameters.
- Climatic conditions.
- Frequency of salt applications.

Depending on the concrete mix design, the concrete deterioration resistance can be dominated by slow chloride permeation (Phase I) or low corrosion rate (Phases II and III) or both. However, even a low-permeability, high-corrosion-resistant concrete alone will not necessarily extend the life of a concrete structure to the 100+-year life predicted above. Construction practices, concrete cover depth for the steel bar, and the natural cracking tendency of the concrete over time due to fatigue loading and wear can significantly affect the actual life of a structure. Although the concrete is the first line of defense against corrosion, other options are also available for consideration, such as: (1) coating the steel bar, (2) corrosion-inhibiting admixtures, and (3) the design of the structure to permit the addition of cathodic protection when necessary. The model above has attempted to provide the ability to optimize the concrete mix design, which is a first step for achieving the structure's designed service life without maintenance.

CHAPTER 7. CONCLUSIONS

The research was structured to address the three principal rate phenomena that control corrosion-induced deterioration of concrete bridge components. These phenomena were identified as:

- Ingress of chloride ions to the level of the reinforcing steel (chloride permeation rate).
- Corrosion of the reinforcing steel once passivity has been destroyed by the presence of the chloride ion (rate of corrosion).
- Cracking/spalling distress in the concrete as a result of the build-up of steel corrosion products (rate of deterioration).

CHLORIDE PERMEATION RATE

- Low-chloride permeability is critical to achieving the desired life of a concrete structure.
- It was shown that the rapid chloride permeability test results were inversely proportional to electrical resistivity for portland cement-based concrete.
- A predictive model was developed to estimate the rapid chloride permeability as a function of concrete mix design.
- The concrete mix components that had a significant effect on chloride permeability (as measured by the rapid chloride permeability test) were, in order of greatest effect:
 1. Mineral admixture.
 2. Coarse aggregate.
 3. Water-cement ratio.
 4. Cement chemistry (based on portland cements tested).
 5. Fine aggregate.
- Mineral admixture had nearly twice the effect of other concrete mix variables on the chloride permeability. The addition of any of the mineral admixtures tested tended to decrease the chloride permeability. Silica fume was the most effective.
- A relationship was established that relates the rapid chloride permeability model predictions to the amount of chloride ingress to the steel bar level as a function of the number of chloride ponding cycles.

CORROSION RATE

- Corrosion rate is dependent on the environmental variables of temperature, relative humidity, and chloride concentration and, over the range tested, each variable is equally important in establishing the corrosion rate of steel.

- Corrosion rates of steel in mortar are significantly greater than in concrete having the same cement type, cement-to-fine-aggregate ratio, and water-cementitious material ratio.
- Corrosion rate of prestressing steel tendons is less than conventional reinforcing steel in the portland type I cement mortar tested.
- Corrosion rate maps for a specific portland type I concrete were developed as a function of temperature and relative humidity at three different chloride concentrations (0.6 kg/m^3 [1 lb/yd^3], 1.8 kg/m^3 [3 lb/yd^3], and 6 kg/m^3 [10 lb/yd^3]).
- Corrosion resistance of concrete is critical to achieving the desired life of a concrete structure. Assuming that chlorides can be prevented from permeating to the steel bar level is not realistic. Concrete mix designs can have a significant influence on the corrosion resistance of a concrete structure.
- A predictive model was developed to estimate the corrosion rate of steel as a function of concrete mix design. This predictive model was used to determine a "corrosion index" that permitted corrosion rate predictions as a function of temperature, relative humidity, and chloride ponding for a specific concrete mix design.
- The concrete mix components that had a significant effect on corrosion behavior were (in order of greatest effect):
 1. Mineral admixture.
 2. Fine aggregate.
 3. Water-cement ratio.
 4. Cement chemistry (based on portland cement tested).
 5. Coarse aggregate.
 6. Air content.
- Mineral admixture had nearly twice the effect of other concrete mix variables on the corrosion behavior of steel. Only silica fume decreased the corrosion rate to lower values than having no mineral admixture. The addition of Class C flyash, Class F flyash, and GGBF slag increased the corrosion rate compared to no mineral admixture.

DAMAGE

- No quantitative prediction model for damage as a function of cumulative corrosion was established based on the concrete mix design parameters.
- Based on a limited data sample, the rate of damage (cracking/spalling) is related to the amount of corrosion product that can diffuse into the concrete matrix (i.e., the less the diffusion into the concrete matrix, the greater the rate of damage). Diffusion into the concrete matrix is dependent on:

1. Porosity of the cementitious phase and entrained air voids (water-cement ratio and air content).
 2. Accessible porosity of the aggregate.
- Although based on limited data, a good correlation was shown between cumulative corrosion prior to cracking and modulus of elasticity of the concrete. The lower the modulus of elasticity, the more the cumulative corrosion prior to cracking. Although beneficial based on life prediction, the value of this relationship is limited because other critical properties suffer as modulus of elasticity decreases.
 - A predictive model based on concrete mix design parameters of the type presented in this report for compressive strength should be developed for modulus of elasticity. Combining the predictive model to the existing correlation presented in this report, cumulative corrosion prior to cracking could be incorporated in the final optimization model. The range of values for cumulative corrosion prior to cracking for the concretes tested in this study were significant (0.051 to 0.191 mm [2 to 7.5 mil]).

CONCRETE OPTIMIZATION MODEL

- The statistical models developed in task B for predicting corrosion and chloride permeability were validated through the concrete slab tests performed in task C.
- A six-step optimization model was proposed for predicting the Phases I and II life of a concrete structure, aiding in economic analysis and optimization of resources.
- The model is based on prediction models developed in this research and requires input of the following by the bridge designer.
 1. Concrete mix components/parameters.
 2. Climatic conditions.
 3. Frequency of salt applications.
- The proposed model was not verified on existing structures. Before this model can be used with confidence, the model must be verified and revised based on actual performance data from operating bridge structures.

RECOMMENDATIONS

The data produced in this study have provided significant advancement in the understanding of: (1) the interaction of concrete mix components and environmental variables on the corrosion resistance properties of concrete and (2) the effect of mix component variables on the mechanical and chloride permeability properties. The prediction models have the ability to incorporate specific climatic conditions and salting procedures, as well as concrete mix components. However, there remain a few areas that require additional work to elaborate on the models or to verify their performance. These include the following:

Improved relationships between concrete mechanical property data and concrete damage as a function of corrosive conditions. Recent work by Liu and Weyers⁵ on modeling time to cracking could provide significant input to this problem. However, work is required to either incorporate that work into the present model and/or develop additional data to establish the relationships needed. For the life prediction model, the mechanical properties of the concrete should permit a prediction of the cumulative corrosion to cracking. One specific area that is missing from the present study is a prediction model for the modulus of elasticity as a function of concrete mix components (similar to the one developed for compressive strength).

Verification of model predictions. Several assumptions were necessary to complete the model predictions for Phases I and II life of a specifically designed concrete, for a specific set of climatic conditions, and with a specified average salting practice. The model predictions should be verified on actual structures. A program should be developed to utilized structures that have already been characterized. This new (or follow-on) project would develop the necessary data set for verifying the model predictions. It would be necessary to select several sites with varying climatic conditions and concrete mix properties. Finally, it is necessary to develop a user-friendly format for the prediction model that prompts the user for the required information, automatically calculates the results, and presents the findings.

⁵ Y. Liu and R.E. Weyers, "Modeling the Time-to-Corrosion Cracking in Chloride-Contaminated Reinforced Concrete Structures," *ACI Materials Journal*, November-December 1998, p .675.

APPENDIX A — CORROSION RATE, CORROSION POTENTIAL, AND CHLORIDE CONCENTRATIONS FOR TASK B EXPERIMENTS

Table 62. Concrete nos. 1, 2, 3, 4, 5R, 6 and 7
[1 lb/yd³ = 0.6 kg/m³; 1 mpy = 0.0254 mm/yr].

Concrete Mix	Cell	Target Cl (lb/yd ³)	Actual Cl (lb/yd ³)	Corrosion Rate (mpy)	Corrosion Potential (V)
1	1	10	0.84	0.144	-0.375
1	2	10	3.99	0.755	-0.336
1	3	10	0.6	0.113	-0.249
1	4	3	0.16	0.009	-0.289
1	5	3	2.51	0.002	-0.119
1	6	3	2.35	0.210	-0.265
2	1	10	5.96	0.724	-0.282
2	2	10	6.21	0.542	-0.272
2	3	10	6.39	1.136	-0.265
2	4	3	2.27	0.020	-0.140
2	5	3	2.06	0.041	-0.117
2	6	3	1.14	0.019	-0.135
3	1	10	11.01	0.544	-0.380
3	2	10	5.87	0.154	-0.288
3	3	10	10.13	0.281	-0.525
3	4	3	0.99	0.012	-0.201
3	5	3	1.94	0.006	-0.232
3	6	3	0.69	0.002	-0.039
4	1	10	10.94	11.939	-0.268
4	2	10	9.13	17.269	-0.334
4	3	10	10.83	18.834	-0.364
4	4	3	2.41	0.059	-0.259
4	5	3	1.92	0.019	-0.189
4	6	3	2.68	0.683	-0.226
5R	1	10	11.2	0.423	-0.071
5R	-2	10	12.69	1.177	-0.068
5R	-3	10	12.77	0.125	-0.342
5R	-4	3	0.47	0.125	-0.342
5R	-5	3	0.78	0.003	-0.294
5R	-6	3	4.11	0.003	-0.212
6	1	10	9.07	0.607	-0.552
6	2	10	12.95	1.181	-0.422
6	3	10	10.78	0.373	-0.398
6	4	3	1.05	0.010	-0.141
6	5	3	1.71	0.005	-0.042
6	6	3	1.86	0.008	-0.125
7	1	10	6.88	0.331	-0.566
7	2	10	5.92	0.188	-0.630
7	3	10	7.91	0.126	-0.720
7	4	3	1.58	0.035	-0.490
7	5	3	1.99	0.021	-0.493
7	6	3	2.21	0.026	-0.483

Table 63. Concrete nos. 8, 9, 10, 11, 12, 13, and 15R
 [1 lb/yd³ = 0.6 kg/m³; 1 mpy = 0.0254 mm/yr].

Concrete Mix	Cell	Target Cl lb/yd ³	Actual Cl lb/yd ³	Corrosion Rate (mpy)	Corrosion Potential (V)
8	1	10	4.82	0.331	-0.543
8	2	10	6.14	0.306	-0.591
8	3	10	5.96	0.523	-0.568
8	4	3	3.34	0.212	-0.479
8	5	3	2.69	0.085	-0.467
8	6	3	2.43	0.085	-0.509
9	1	10	2.79	0.800	-0.230
9	2	10	6.26	1.906	-0.192
9	3	10	2.11	0.033	-0.298
9	4	3	0.23	0.004	-0.110
9	5	3	0.87	0.016	-0.188
9	6	3	0.83	0.004	-0.018
10	1	10	1.33	0.148	-0.389
10	3	10	4.56	2.152	-0.378
10	4	3	0.04	0.007	-0.050
10	5	3	0.07	0.026	-0.206
10	6	3	0.04	0.021	-0.126
11	1	10	3.23	0.019	-0.504
11	2	10	6.93	0.056	-0.414
11	3	10	3.47	0.051	-0.372
11	4	3	1.99	0.014	-0.329
11	5	3	0.51	0.009	-0.289
11	6	3	1.95	0.006	-0.302
12	1	10	4.14	11.527	-0.278
12	2	10	6	1.035	-0.161
12	3	10	5.43	1.021	-0.282
12	4	3	1.43	0.015	-0.226
12	5	3	1.54	0.029	-0.215
12	6	3	1.71	0.030	-0.229
13	1	10	10.11	0.228	-0.388
13	2	10	11.65	0.351	-0.507
13	3	10	13.55	0.686	-0.540
13	4	3	2.13	0.003	0.050
13	5	3	2.36	0.002	-0.072
13	6	3	2.36	0.005	-0.026
15R	1	10	8.96	0.618	-0.536
15R	2	10	6.72	0.535	-0.480
15R	3	10	9.41	0.277	-0.515
15R	4	3	1.79	0.010	-0.101
15R	5	3	3.17	0.034	-0.174
15R	6	3	1.61	0.012	-0.088

Table 64. Concrete nos. 16, 17, 18, 19, 20, 21, and 22
 [1 lb/yd³ = 0.6 kg/m³; 1 mpy = 0.0254 mm/yr].

Concrete Mix	Cell	Target Cl lb/yd ³	Actual Cl lb/yd ³	Corrosion Rate (mpy)	Corrosion Potential (V)
16	1	10	9.71	3.049	-0.404
16	2	10	8.63	1.221	-0.337
16	3	10	9.59	5.343	-0.379
16	4	3	1.44	0.012	-0.119
16	5	3	1.56	0.005	0.102
16	6	3	1.28	0.007	-0.057
17	1	10	not available	3.744	-0.352
17	2	10	12.3	3.088	-0.280
17	3	10	11.39	1.003	-0.286
17	4	3	2.95	0.014	-0.216
17	5	3	3.71	0.014	-0.172
17	6	3	3.71	0.021	-0.271
18	1	10	1.08	0.411	-0.236
18	2	10	0.9	0.136	-0.238
18	3	10	0.75	0.134	-0.162
18	4	3	0.19	0.023	-0.082
18	5	3	0.19	0.031	-0.144
18	6	3	0.19	0.020	-0.090
19	1	10	10.89	0.739	-0.196
19	2	10	14.43	2.367	-0.308
19	3	10	14.95	2.571	-0.239
19	4	3	5.48	0.010	-0.238
19	5	3	4.1	0.009	-0.116
19	6	3	3.39	0.006	-0.051
20	1	10	8.43	1.871	-0.511
20	2	10	7.05	8.195	-0.444
20	3	10	5.28	24.209	-0.307
20	4	3	3.29	0.609	-0.532
20	5	3	2.68	0.660	-0.397
20	6	3	3.36	2.271	-0.363
21	1	10	9	8.795	-0.433
21	2	10	14	6.747	-0.569
21	3	10	11.67	3.828	-0.383
21	4	3	2.98	0.070	-0.072
21	5	3	3.1	0.033	-0.067
21	6	3	2.37	0.044	-0.076
22	1	10	6.23	13.882	-0.179
22	2	10	6.91	11.986	-0.228
22	3	10	8.85	4.911	-0.168
22	4	3	2.5	0.009	-0.133
22	5	3	2.43	0.003	-0.075
22	6	3	2.39	0.019	-0.237

Table 65. Concrete nos. 23, 24, 25, 26, 27, 28, 29, and 30
[1 lb/yd³ = 0.6 kg/m³; 1 mpy = 0.0254 mm/yr].

Concrete Mix	Cell	Target Cl lb/yd ³	Actual Cl lb/yd ³	Corrosion Rate (mpy)	Corrosion Potential (V)
23	1	10	1.78	0.054	-0.267
23	2	10	1.78	0.137	-0.232
23	3	10	5.23	0.302	-0.149
23	4	3	1.28	0.011	-0.064
23	5	3	0.78	0.004	-0.110
23	6	3	2.05	0.038	-0.088
24	1	10	2.67	2.975	-0.369
24	2	10	5.08	1.140	-0.428
24	3	10	5.26	0.272	-0.328
24	4	3	0.32	0.002	0.002
24	5	3	1.44	0.002	-0.007
24	6	3	1.04	0.003	-0.003
25	1	10	5.28	0.389	-0.303
25	4	10	8.3	2.226	-0.478
25	5	3	1.37	0.012	-0.582
25	6	3	1.29	0.069	-0.472
26	1	10	7.77	1.033	-0.261
26	2	10	7.96	0.220	-0.252
26	3	10	8.00	1.888	-0.244
26	4	3	0.77	0.002	-0.091
26	5	3	0.46	0.005	-0.104
26	6	3	0.77	0.016	-0.241
27	1	10	2.96	0.907	-0.162
27	2	10	4.74	1.125	-0.141
27	3	10	3.54	0.710	-0.265
27	4	3	0.65	0.001	0.008
27	5	3	0.11	0.003	-0.046
27	6	3	0.51	0.001	-0.009
28	1	10	5.82	0.921	-0.179
28	2	10	6.73	0.804	-0.253
28	3	10	6.69	1.013	-0.229
28	4	3	3.64	0.263	0.155
28	5	3	0.99	0.042	-0.094
28	6	3	1.34	0.042	-0.134
29	1	10	7.16	3.730	-0.406
29	2	10	7.69	0.105	-0.428
29	3	10	9.77	0.372	-0.436
29	4	3	1.55	0.014	-0.271
29	5	3	2.08	0.007	-0.006
29	6	3	1.23	0.004	-0.212
30	1	10	3.08	0.012	-0.416
30	2	10	6.97	0.103	-0.517
30	3	10	6.85	0.161	-0.615
30	4	3	5.45	0.008	-0.184
30	5	3	3.31	0.022	-0.139
30	6	3	3.31	0.019	-0.181

**APPENDIX B — COUPLED CURRENTS FOR SELECTED TASK C
CONCRETES (Nos. 1, 3, 31, 37, and 38).**

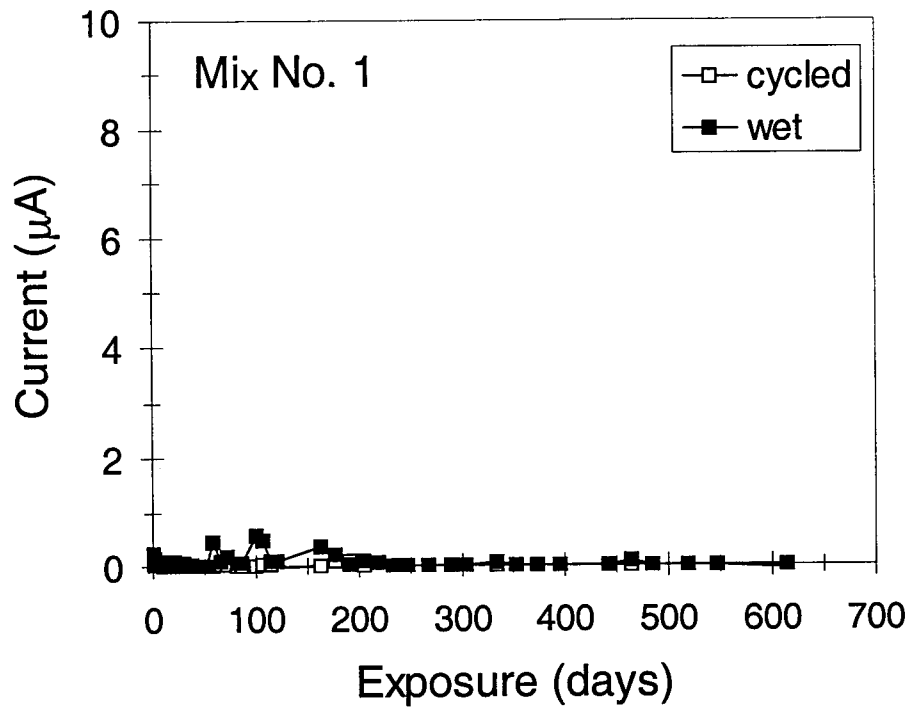


Figure 62. Coupled current versus time for concrete no. 1.

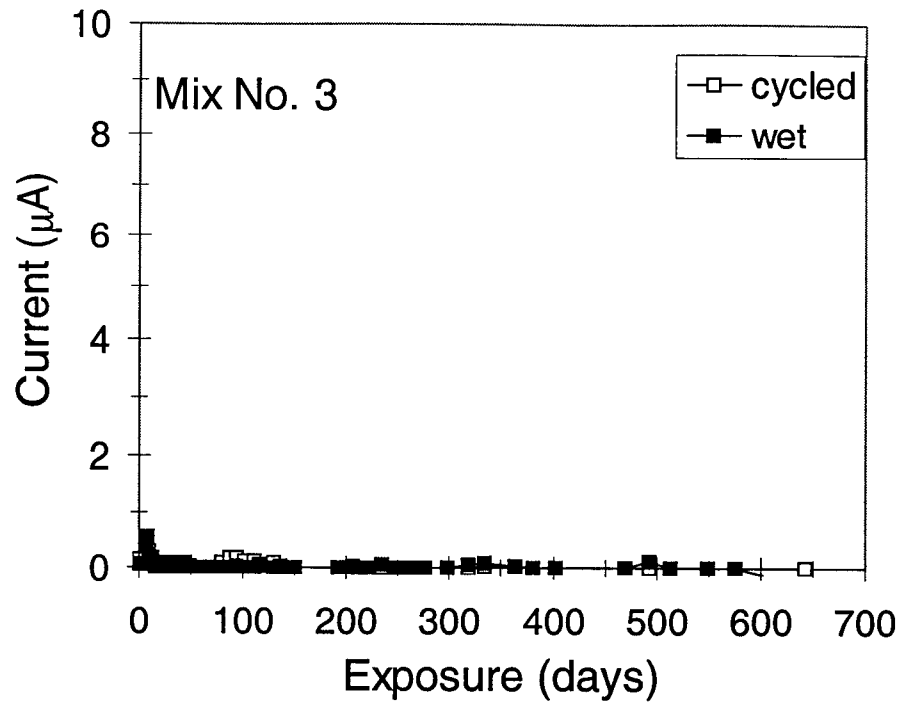


Figure 63. Coupled current versus time for concrete no. 3.

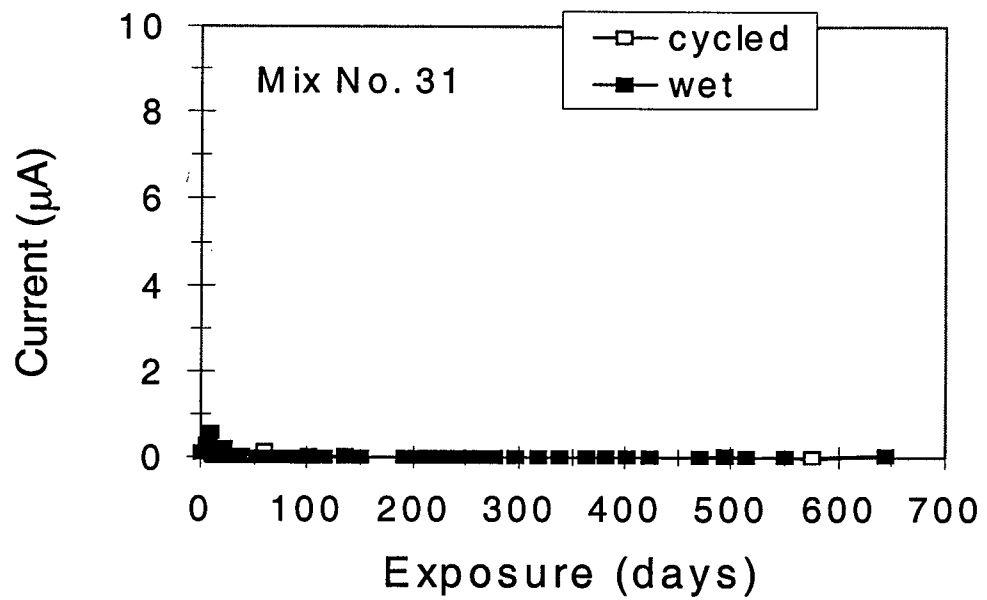


Figure 64. Coupled current versus time for concrete no. 31.

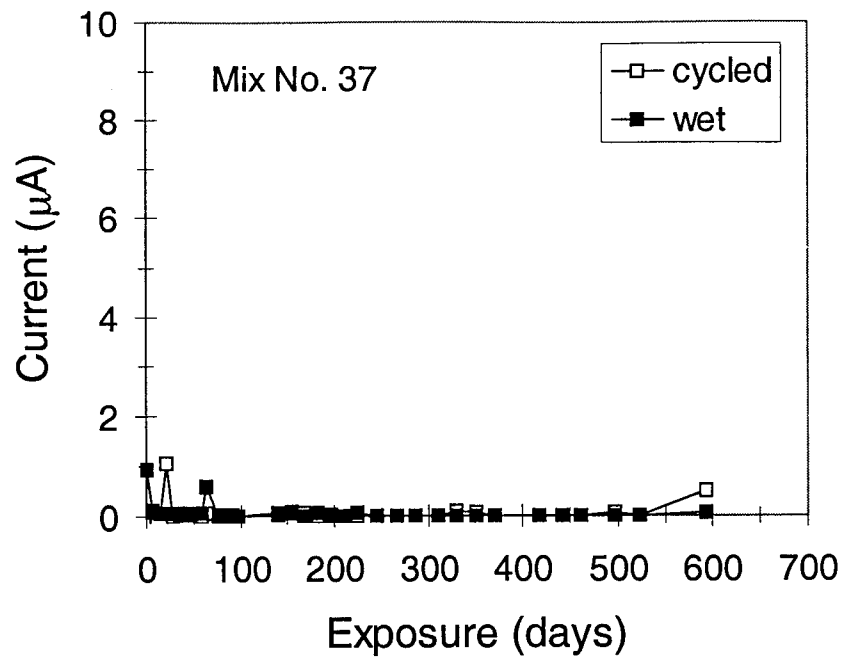


Figure 65. Coupled current versus time for concrete no. 37.

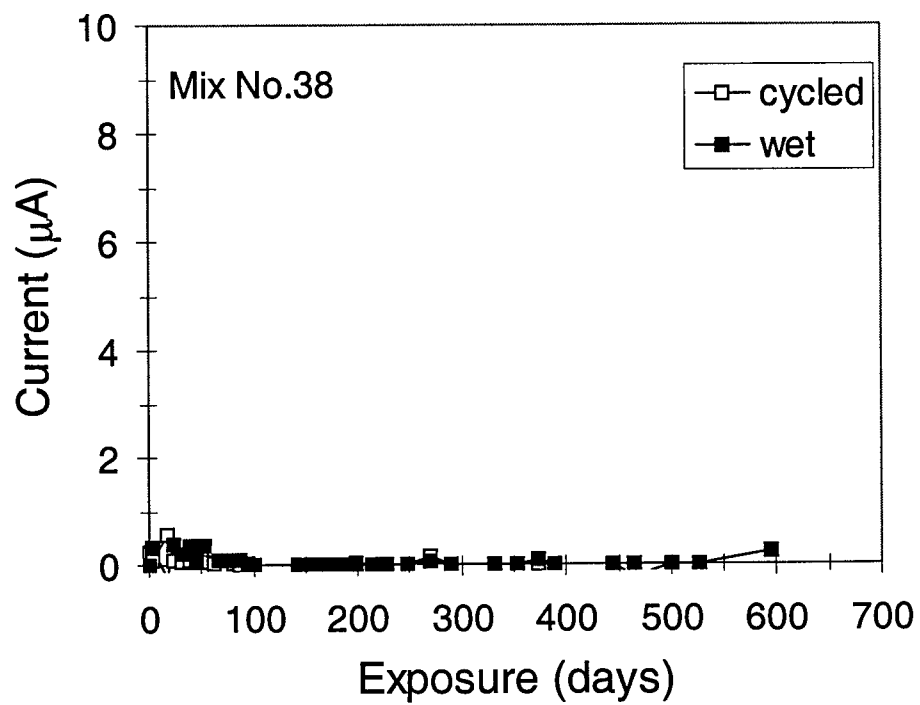


Figure 66. Coupled current versus time for concrete no. 38.

APPENDIX C — COMPLETE LPR CORROSION RATE AND POTENTIAL DATA FOR ALL SPECIMENS FOR TASK C STANDARD CONCRETES

Table 66. Concrete no. 1 [1 mpy = 0.0254 mm/yr].

Concrete	Exposure	Slab	Steel Location	Potential (mV, CSE)	Corrosion Rate (mpy)
No. 1	Cycled	A	Left	-132	0.00
No. 1	Cycled	A	Center	-106	0.01
No. 1	Cycled	A	Right	-140	0.00
No. 1	Cycled	B	Left	-109	0.01
No. 1	Cycled	B	Center	-101	0.02
No. 1	Cycled	B	Right	-108	0.01
No. 1	Cycled	C	Left	-100	0.01
No. 1	Cycled	C	Center	-95	0.01
No. 1	Cycled	C	Right	-96	0.01
No. 1	Cycled	D	Left	-112	0.01
No. 1	Cycled	D	Center	-106	0.01
No. 1	Cycled	D	Right	-94	0.01
No. 1	Cycled	Avg	Left	-113	0.01
No. 1	Cycled	Avg	Center	-102	0.01
No. 1	Cycled	Avg	Right	-109	0.01
No. 1	Wet	E	Left	-101	0.01
No. 1	Wet	E	Center	-102	0.01
No. 1	Wet	E	Right	-112	0.01
No. 1	Wet	F	Left	-85	0.01
No. 1	Wet	F	Center	-85	0.01
No. 1	Wet	F	Right	-104	0.01
No. 1	Wet	G	Left	-89	0.01
No. 1	Wet	G	Center	-76	0.01
No. 1	Wet	G	Right	-114	0.01
No. 1	Wet	H	Left	-89	0.01
No. 1	Wet	H	Center	-84	0.01
No. 1	Wet	H	Right	-104	0.01
No. 1	Wet	Avg	Left	-91	0.01
No. 1	Wet	Avg	Center	-87	0.01
No. 1	Wet	Avg	Right	-109	0.01

Table 67. Concrete no. 3 [1 mpy = 0.0254 mm/yr].

Concrete	Exposure	Slab	Steel Location	Potential (mV, CSE)	Corrosion Rate (mpy)
No. 3	Cycled	A	Left	-141	0.00
No. 3	Cycled	A	Center	-142	0.01
No. 3	Cycled	A	Right	-146	0.00
No. 3	Cycled	B	Left	-138	0.00
No. 3	Cycled	B	Center	-143	0.01
No. 3	Cycled	B	Right	-123	0.00
No. 3	Cycled	C	Left	-113	0.00
No. 3	Cycled	C	Center	-111	0.01
No. 3	Cycled	C	Right	-112	0.00
No. 3	Cycled	D	Left	-123	0.00
No. 3	Cycled	D	Center	-128	0.01
No. 3	Cycled	D	Right	-117	0.00
No. 3	Cycled	Avg	Left	-129	0.00
No. 3	Cycled	Avg	Center	-131	0.01
No. 3	Cycled	Avg	Right	-124	0.00
No. 3	Wet	E	Left	-61	0.01
No. 3	Wet	E	Center	-60	0.01
No. 3	Wet	E	Right	-50	0.00
No. 3	Wet	F	Left	-57	0.04
No. 3	Wet	F	Center	-63	0.01
No. 3	Wet	F	Right	-80	0.01
No. 3	Wet	G	Left	-68	0.01
No. 3	Wet	G	Center	-70	0.01
No. 3	Wet	G	Right	-75	0.01
No. 3	Wet	H	Left	-58	0.01
No. 3	Wet	H	Center	-52	0.01
No. 3	Wet	H	Right	-54	0.00
No. 3	Wet	Avg	Left	-61	0.02
No. 3	Wet	Avg	Center	-61	0.01
No. 3	Wet	Avg	Right	-65	0.01

Table 68. Concrete no. 11 [1 mpy = 0.0254 mm/yr].

Concrete	Exposure	Slab	Steel Location	Potential (mV, CSE)	Corrosion Rate (mpy)
No. 11	Cycled	A	Left	-263	0.02
No. 11	Cycled	A	Center	-467	1.57
No. 11	Cycled	A	Right	-481	0.37
No. 11	Cycled	B	Left	-150	0.02
No. 11	Cycled	B	Center	-309	1.11
No. 11	Cycled	B	Right	-187	0.06
No. 11	Cycled	C	Left	-194	0.02
No. 11	Cycled	C	Center	-228	0.12
No. 11	Cycled	C	Right	-500	3.76
No. 11	Cycled	D	Left	-167	0.02
No. 11	Cycled	D	Center	-249	0.27
No. 11	Cycled	D	Right	-528	3.38
No. 11	Cycled	Avg	Left	-194	0.02
No. 11	Cycled	Avg	Center	-313	0.77
No. 11	Cycled	Avg	Right	-424	1.89
No. 11	Wet	E	Left	-26	0.01
No. 11	Wet	E	Center	-222	0.07
No. 11	Wet	E	Right	-496	0.48
No. 11	Wet	F	Left	-87	0.00
No. 11	Wet	F	Center	-457	0.14
No. 11	Wet	F	Right	-113	0.00
No. 11	Wet	G	Left	-133	0.01
No. 11	Wet	G	Center	-325	0.06
No. 11	Wet	G	Right	-282	0.05
No. 11	Wet	H	Left	-38	0.01
No. 11	Wet	H	Center	-501	1.15
No. 11	Wet	H	Right	-659	4.41
No. 11	Wet	Avg	Left	-71	0.01
No. 11	Wet	Avg	Center	-377	0.36
No. 11	Wet	Avg	Right	-388	1.24

Table 69. Concrete no. 15R [1 mpy = 0.0254 mm/yr].

Concrete	Exposure	Slab	Steel Location	Potential (mV, CSE)	Corrosion Rate (mpy)
No. 15R	Cycled	A	Left	90	0.00
No. 15R	Cycled	A	Center	-334	0.60
No. 15R	Cycled	A	Right	-302	0.01
No. 15R	Cycled	B	Left	6	0.01
No. 15R	Cycled	B	Center	-353	1.54
No. 15R	Cycled	B	Right	-317	0.03
No. 15R	Cycled	C	Left	-11	0.01
No. 15R	Cycled	C	Center	-295	0.18
No. 15R	Cycled	C	Right	-236	0.01
No. 15R	Cycled	D	Left	-71	0.01
No. 15R	Cycled	D	Center	-340	0.37
No. 15R	Cycled	D	Right	-244	0.01
No. 15R	Cycled	Avg	Left	4	0.01
No. 15R	Cycled	Avg	Center	-330	0.67
No. 15R	Cycled	Avg	Right	-275	0.02
No. 15R	Wet	E	Left	-138	0.01
No. 15R	Wet	E	Center	-341	0.19
No. 15R	Wet	E	Right	-480	0.31
No. 15R	Wet	F	Left	-114	0.07
No. 15R	Wet	F	Center	-263	0.01
No. 15R	Wet	F	Right	-269	0.00
No. 15R	Wet	G	Left	-244	0.00
No. 15R	Wet	G	Center	350	0.02
No. 15R	Wet	G	Right	-302	0.01
No. 15R	Wet	H	Left	-193	0.04
No. 15R	Wet	H	Center	-356	0.15
No. 15R	Wet	H	Right	-520	1.28
No. 15R	Wet	Avg	Left	-172	0.03
No. 15R	Wet	Avg	Center	-153	0.09
No. 15R	Wet	Avg	Right	-393	0.40

Table 70. Concrete no. 22 [1 mpy = 0.0254 mm/yr].

Concrete	Exposure	Slab	Steel Location	Potential (mV, CSE)	Corrosion Rate (mpy)
No. 22	Cycled	A	Left	-278	0.08
No. 22	Cycled	A	Center	-444	0.14
No. 22	Cycled	A	Right	-454	2.72
No. 22	Cycled	B	Left	-292	0.01
No. 22	Cycled	B	Center	-463	2.48
No. 22	Cycled	B	Right	-590	7.58
No. 22	Cycled	C	Left	-121	0.06
No. 22	Cycled	C	Center	-400	5.26
No. 22	Cycled	C	Right	-425	0.22
No. 22	Cycled	D	Left	-413	0.01
No. 22	Cycled	D	Center	-541	9.43
No. 22	Cycled	D	Right	-528	1.37
No. 22	Cycled	Avg	Left	-276	0.04
No. 22	Cycled	Avg	Center	-462	4.33
No. 22	Cycled	Avg	Right	-499	2.97
No. 22	Wet	E	Left	-205	0.02
No. 22	Wet	E	Center	-395	1.11
No. 22	Wet	E	Right	-481	0.50
No. 22	Wet	F	Left	-246	0.00
No. 22	Wet	F	Center	-466	1.65
No. 22	Wet	F	Right	-490	0.69
No. 22	Wet	G	Left	-88	0.15
No. 22	Wet	G	Center	-510	9.70
No. 22	Wet	G	Right	-417	1.75
No. 22	Wet	H	Left	-292	0.03
No. 22	Wet	H	Center	-426	1.81
No. 22	Wet	H	Right	-572	0.73
No. 22	Wet	Avg	Left	-207	0.05
No. 22	Wet	Avg	Center	-449	3.57
No. 22	Wet	Avg	Right	-490	0.92

Table 71. Concrete no. 24 [1 mpy = 0.0254 mm/yr].

Concrete	Exposure	Slab	Steel Location	Potential (mV, CSE)	Corrosion Rate (mpy)
No. 24	Cycled	A	Left	39	0.01
No. 24	Cycled	A	Center	-133	0.01
No. 24	Cycled	A	Right	-135	0.01
No. 24	Cycled	B	Left	102	0.01
No. 24	Cycled	B	Center	-125	0.01
No. 24	Cycled	B	Right	-132	0.01
No. 24	Cycled	C	Left	50	0.01
No. 24	Cycled	C	Center	-131	0.01
No. 24	Cycled	C	Right	-145	0.01
No. 24	Cycled	D	Left	74	0.01
No. 24	Cycled	D	Center	-126	0.01
No. 24	Cycled	D	Right	-124	0.01
No. 24	Cycled	Avg	Left	66	0.01
No. 24	Cycled	Avg	Center	-129	0.01
No. 24	Cycled	Avg	Right	-134	0.01
No. 24	Wet	E	Left	-318	0.01
No. 24	Wet	E	Center	-513	0.20
No. 24	Wet	E	Right	-113	0.01
No. 24	Wet	F	Left	3	0.01
No. 24	Wet	F	Center	-116	0.01
No. 24	Wet	F	Right	-121	0.01
No. 24	Wet	G	Left	-9	0.01
No. 24	Wet	G	Center	-20	0.01
No. 24	Wet	G	Right	-129	0.01
No. 24	Wet	H	Left	-59	0.01
No. 24	Wet	H	Center	-96	0.01
No. 24	Wet	H	Right	-224	0.02
No. 24	Wet	Avg	Left	-95	0.01
No. 24	Wet	Avg	Center	-186	0.06
No. 24	Wet	Avg	Right	-147	0.01

Table 72. Concrete no. 29 [1 mpy = 0.0254 mm/yr].

Concrete	Exposure	Slab	Steel Location	Potential (mV, CSE)	Corrosion Rate (mpy)
No. 29	Cycled	A	Left	-377	0.03
No. 29	Cycled	A	Center	-393	6.04
No. 29	Cycled	A	Right	-489	7.90
No. 29	Cycled	B	Left	-417	0.14
No. 29	Cycled	B	Center	-348	5.89
No. 29	Cycled	B	Right	-468	5.03
No. 29	Cycled	C	Left	-575	0.08
No. 29	Cycled	C	Center	-494	1.15
No. 29	Cycled	C	Right	-516	14.19
No. 29	Cycled	D	Left	-390	5.71
No. 29	Cycled	D	Center	-389	2.69
No. 29	Cycled	D	Right	-462	5.86
No. 29	Cycled	Avg	Left	-440	1.49
No. 29	Cycled	Avg	Center	-406	3.94
No. 29	Cycled	Avg	Right	-484	8.25
No. 29	Wet	E	Left	-251	0.02
No. 29	Wet	E	Center	-181	1.51
No. 29	Wet	E	Right	-349	2.59
No. 29	Wet	F	Left	-48	0.02
No. 29	Wet	F	Center	-310	4.86
No. 29	Wet	F	Right	-282	2.21
No. 29	Wet	G	Left	NA	NA
No. 29	Wet	G	Center	-176	1.44
No. 29	Wet	G	Right	-319	10.74
No. 29	Wet	H	Left	-96	0.00
No. 29	Wet	H	Center	-185	3.89
No. 29	Wet	H	Right	-160	0.12
No. 29	Wet	Avg	Left	-132	0.01
No. 29	Wet	Avg	Center	-213	2.93
No. 29	Wet	Avg	Right	-277	3.92

Table 73. Concrete no. 31 [1 mpy = 0.0254 mm/yr].

Concrete	Exposure	Slab	Steel Location	Potential (mV, CSE)	Corrosion Rate (mpy)
No. 31	Cycled	A	Left	78	0.00
No. 31	Cycled	A	Center	98	0.00
No. 31	Cycled	A	Right	-115	0.00
No. 31	Cycled	B	Left	-130	0.00
No. 31	Cycled	B	Center	-125	0.01
No. 31	Cycled	B	Right	-106	0.00
No. 31	Cycled	C	Left	75	0.01
No. 31	Cycled	C	Center	-118	0.01
No. 31	Cycled	C	Right	-92	0.00
No. 31	Cycled	D	Left	130	0.04
No. 31	Cycled	D	Center	-94	0.01
No. 31	Cycled	D	Right	-103	0.00
No. 31	Cycled	Avg	Left	38	0.01
No. 31	Cycled	Avg	Center	-60	0.01
No. 31	Cycled	Avg	Right	-104	0.00
No. 31	Wet	E	Left	78	0.01
No. 31	Wet	E	Center	-68	0.01
No. 31	Wet	E	Right	-38	0.01
No. 31	Wet	F	Left	-15	0.01
No. 31	Wet	F	Center	-47	0.01
No. 31	Wet	F	Right	-41	0.01
No. 31	Wet	G	Left	72	0.01
No. 31	Wet	G	Center	2	0.01
No. 31	Wet	G	Right	-7	0.01
No. 31	Wet	H	Left	-43	0.00
No. 31	Wet	H	Center	-69	0.00
No. 31	Wet	H	Right	-63	0.01
No. 31	Wet	Avg	Left	23	0.01
No. 31	Wet	Avg	Center	-45	0.01
No. 31	Wet	Avg	Right	-37	0.01

Table 74. Concrete no. 37 [1 mpy = 0.0254 mm/yr].

Concrete	Exposure	Slab	Steel Location	Potential (mV, CSE)	Corrosion Rate (mpy)
No. 37	Cycled	A	Left	11	0.01
No. 37	Cycled	A	Center	-133	0.01
No. 37	Cycled	A	Right	-82	0.00
No. 37	Cycled	B	Left	43	0.01
No. 37	Cycled	B	Center	7	0.02
No. 37	Cycled	B	Right	-182	0.01
No. 37	Cycled	C	Left	-2	0.01
No. 37	Cycled	C	Center	-36	0.01
No. 37	Cycled	C	Right	-200	0.01
No. 37	Cycled	D	Left	39	0.01
No. 37	Cycled	D	Center	-185	0.01
No. 37	Cycled	D	Right	-197	0.00
No. 37	Cycled	Avg	Left	23	0.01
No. 37	Cycled	Avg	Center	-87	0.01
No. 37	Cycled	Avg	Right	-165	0.01
No. 37	Wet	E	Left	79	0.01
No. 37	Wet	E	Center	-97	0.01
No. 37	Wet	E	Right	-65	0.01
No. 37	Wet	F	Left	-3	0.01
No. 37	Wet	F	Center	-100	0.02
No. 37	Wet	F	Right	-105	0.01
No. 37	Wet	G	Left	-8	0.01
No. 37	Wet	G	Center	-94	0.02
No. 37	Wet	G	Right	-113	0.01
No. 37	Wet	H	Left	42	0.01
No. 37	Wet	H	Center	-12	0.01
No. 37	Wet	H	Right	-27	0.01
No. 37	Wet	Avg	Left	27	0.01
No. 37	Wet	Avg	Center	-76	0.02
No. 37	Wet	Avg	Right	-77	0.01

Table 75. Concrete no. 38 [1 mpy = 0.0254 mm/yr].

Concrete	Exposure	Slab	Steel Location	Potential (mV, CSE)	Corrosion Rate (mpy)
No. 38	Cycled	A	Left	-53	0.01
No. 38	Cycled	A	Center	-158	0.01
No. 38	Cycled	A	Right	-165	0.01
No. 38	Cycled	B	Left	-35	0.01
No. 38	Cycled	B	Center	-166	0.00
No. 38	Cycled	B	Right	-164	0.01
No. 38	Cycled	C	Left	-106	0.02
No. 38	Cycled	C	Center	-131	0.01
No. 38	Cycled	C	Right	-179	0.00
No. 38	Cycled	D	Left	-31	0.01
No. 38	Cycled	D	Center	-142	0.01
No. 38	Cycled	D	Right	-147	0.01
No. 38	Cycled	Avg	Left	-56	0.01
No. 38	Cycled	Avg	Center	-149	0.01
No. 38	Cycled	Avg	Right	-164	0.01
No. 38	Wet	E	Left	44	0.01
No. 38	Wet	E	Center	-97	0.02
No. 38	Wet	E	Right	-130	0.01
No. 38	Wet	F	Left	-9	0.01
No. 38	Wet	F	Center	-108	0.02
No. 38	Wet	F	Right	-108	0.01
No. 38	Wet	G	Left	-19	0.01
No. 38	Wet	G	Center	-110	0.02
No. 38	Wet	G	Right	-88	0.01
No. 38	Wet	H	Left	4	0.01
No. 38	Wet	H	Center	-27	0.01
No. 38	Wet	H	Right	-25	0.01
No. 38	Wet	Avg	Left	5	0.01
No. 38	Wet	Avg	Center	-85	0.02
No. 38	Wet	Avg	Right	-88	0.01

APPENDIX D – RESULTS OF INDIVIDUAL POST-TEST EXAMINATIONS OF TASK C CONCRETES

Table 76. Percentage of corrosion coverage for task C concretes.

Concrete Mix	Exposure	Slab	Bar Condition (% Corrosion)			Slab	Bar Condition (% Corrosion)			Slab	Bar Condition (% Corrosion)			Slab	Bar Condition (% Corrosion)		
			Center	Right	Left		Center	Right	Left		Center	Right	Left		Center	Right	Left
1	cycled	A	0	0	0	B	-	-	-	C	-	-	-	D	-	-	-
1	wet	E	-	-	-	F	-	-	-	G	-	-	-	H	-	-	-
3	cycled	A	0	0	0	B	-	-	-	C	-	-	-	D	-	-	-
3	wet	E	-	-	-	F	-	-	-	G	-	-	-	H	-	-	-
11	cycled	A	a	a	a	B	75	50	0	C	b	b	b	D	50	100	0
11	wet	E	25	100	0	F	25	25	10	G	25	25	<10	H	50	75	0
15R	cycled	A	50	<10	0	B	a	a	a	C	50	10	10	D	50	10	0
15R	wet	E	25	10	0	F	25	25	25	G	10	<10	<10	H	<10	25	<10
22	cycled	A	b	b	b	B	a	a	a	C	b	b	b	D	100	100	<10
22	wet	E	75	100	<10	F	100	75	<10	G	100	100	<10	H	75	100	10
24	cycled	A	<10	<10	<10	B	<10	<10	<10	C	10	<10	<10	D	<10	<10	<10
24	wet	E	10	0	0	F	<10	<10	<10	G	<10	<10	<10	H	<10	10	<10
29	cycled	A	a	a	a	B	75	100	<10	C	50	75	<10	D	75	100	50
29	wet	E	100	100	<10	F	100	75	10	G	100	100	0	H	100	100	<10
31	cycled	A	a	a	a	B	0	0	0	C	-	-	-	D	-	-	-
31	wet	E	-	-	-	F	-	-	-	G	-	-	-	H	-	-	-
37	cycled	A	0	<10	<10	B	-	-	-	C	-	-	-	D	-	-	-
37	wet	E	-	-	-	F	-	-	-	G	-	-	-	H	-	-	-
38	cycled	A	0	0	0	B	-	-	-	C	-	-	-	D	-	-	-
38	wet	E	0	<10	0	F	-	-	-	G	-	-	-	H	-	-	-

a: Slab used for petrographic analysis.

b: Slab not available.

-: Slab not examined.

% Corrosion: 0% - No visible sign of corrosion.
 <10% - Possible very light corrosion, but difficult to determine (negligible).
 10% - Very light corrosion and minimal coverage.
 25% - Approximately 25% coverage of corrosion.
 50% - Approximately 50% coverage of corrosion with some pitting.
 75% - Approximately 75% coverage of corrosion, typically some deep pitting.
 100% - Entire surface covered with corrosion, typically some very deep pitting.

Table 77. Concrete surface condition of task C concretes.

Mix Concrete	Exposure	Slab	Concrete Condition	Slab	Concrete Condition	Slab	Concrete Condition	Slab	Concrete Condition
1	cycled	A	Good	B	Good	C	Good	D	Good
1	wet	E	Good	F	Good	G	Good	H	Good
3	cycled	A	Good	B	Good	C	Good	D	Good
3	wet	E	Good	F	Good	G	Good	H	Good
11	cycled	A	Good	B	Good	C	b	D	Good
11	wet	E	Good	F	Good	G	Good	H	Good
15R	cycled	A	Good	B	Good	C	Good	D	Good
15R	wet	E	Good	F	Good	G	Good	H	Good
22	cycled	A	b	B	Chalky	C	b	D	Chalky
22	wet	E	Chalky	F	Chalky	G	Chalky	H	Chalky
24	cycled	A	Good	B	Good	C	Good	D	Good
24	wet	E	Good	F	Good	G	Good	H	Good
29	cycled	A	Rough, Powdery	B	Rough, Powdery	C	Rough, Powdery	D	Rough, Powdery
29	wet	E	Rough, Powdery	F	Rough, Powdery	G	Rough, Powdery	H	Rough, Powdery
31	cycled	A	Good	B	Good	C	Good	D	Good
31	wet	E	Good	F	Good	G	Good	H	Good
37	cycled	A	Good	B	Good	C	Good	D	Good
37	wet	E	Good	F	Good	G	Good	H	Good
38	cycled	A	Good	B	Good	C	Good	D	Good
38	wet	E	Good	F	Good	G	Good	H	Good

b: Slab not available.

APPENDIX E — COMPLETE LPR CORROSION RATE AND POTENTIAL DATA FOR ALL SPECIMENS FOR TASK C REPAIR MATERIALS

Table 78. Repair material no. 40 standard slab [1 mpy = 0.0254 mm/yr].

Concrete	Exposure	Slab	Steel Location	Potential (mV, CSE)	Corrosion Rate (mpy)
No. 40	Wet	A	Left	-255	0.00
No. 40	Wet	A	Center	-290	0.09
No. 40	Wet	A	Right	-570	0.15
No. 40	Wet	B	Left	-249	0.00
No. 40	Wet	B	Center	-223	0.05
No. 40	Wet	B	Right	-408	0.06
No. 40	Wet	C	Left	-305	0.00
No. 40	Wet	C	Center	-370	0.18
No. 40	Wet	C	Right	-610	0.63
No. 40	Wet	D	Left	-285	0.02
No. 40	Wet	D	Center	-214	0.10
No. 40	Wet	D	Right	-541	0.91
No. 40	Wet	Avg	Left	-273	0.01
No. 40	Wet	Avg	Center	-274	0.11
No. 40	Wet	Avg	Right	-532	0.44

Table 79. Repair material no. 41 standard slab [1 mpy = 0.0254 mm/yr].

Concrete	Exposure	Slab	Steel Location	Potential (mV, CCS)	Corrosion Rate (mpy)
No. 41	Wet	A	Left	-67	0.05
No. 41	Wet	A	Center	-185	3.08
No. 41	Wet	A	Right	-176	2.26
No. 41	Wet	B	Left	-402	1.17
No. 41	Wet	B	Center	-207	0.97
No. 41	Wet	B	Right	-152	1.49
No. 41	Wet	C	Left	-217	1.15
No. 41	Wet	C	Center	-327	0.05
No. 41	Wet	C	Right	-207	6.39
No. 41	Wet	D	Left	-235	0.68
No. 41	Wet	D	Center	-295	0.79
No. 41	Wet	D	Right	-254	5.20
No. 41	Wet	Avg	Left	-230	0.76
No. 41	Wet	Avg	Center	-254	1.22
No. 41	Wet	Avg	Right	-197	3.83

Table 80. Repair material no. 42 standard slab [1 mpy = 0.0254 mm/yr].

Concrete	Exposure	Slab	Steel Location	Potential (mV, CSE)	Corrosion Rate (mpy)
No. 42	Wet	E	Left	-101	0.01
No. 42	Wet	E	Center	-102	0.01
No. 42	Wet	E	Right	-112	0.01
No. 42	Wet	F	Left	-85	0.01
No. 42	Wet	F	Center	-85	0.01
No. 42	Wet	F	Right	-104	0.01
No. 42	Wet	G	Left	-89	0.01
No. 42	Wet	G	Center	-76	0.01
No. 42	Wet	G	Right	-114	0.01
No. 42	Wet	H	Left	-89	0.01
No. 42	Wet	H	Center	-84	0.01
No. 42	Wet	H	Right	-104	0.01
No. 42	Wet	Avg	Left	-91	0.01
No. 42	Wet	Avg	Center	-87	0.01
No. 42	Wet	Avg	Right	-109	0.01

Table 81. Repair material no. 43 standard slab [1 mpy = 0.0254 mm/yr].

Concrete	Exposure	Slab	Steel Location	Potential (mV, CSE)	Corrosion Rate (mpy)
No. 43	Wet	E	Left	78	0.01
No. 43	Wet	E	Center	-68	0.01
No. 43	Wet	E	Right	-38	0.01
No. 43	Wet	F	Left	-15	0.01
No. 43	Wet	F	Center	-47	0.01
No. 43	Wet	F	Right	-41	0.01
No. 43	Wet	G	Left	72	0.01
No. 43	Wet	G	Center	2	0.01
No. 43	Wet	G	Right	-7	0.01
No. 43	Wet	H	Left	-43	0.00
No. 43	Wet	H	Center	-69	0.00
No. 43	Wet	H	Right	-63	0.01
No. 43	Wet	Avg	Left	23	0.01
No. 43	Wet	Avg	Center	-45	0.01
No. 43	Wet	Avg	Right	-37	0.01

Table 82. Repair material no. 40 repair slab [1 mpy = 0.0254 mm/yr].

Concrete	Exposure	Slab	Steel Location	Potential (mV, CCS)	Corrosion Rate (mpy)
No. 40 Repair	Wet	A	Left	-200	44.83
No. 40 Repair	Wet	A	Center	-330	21.96
No. 40 Repair	Wet	A	Right	-583	0.67
No. 40 Repair	Wet	B	Left	-334	5.54
No. 40 Repair	Wet	B	Center	-483	44.83
No. 40 Repair	Wet	B	Right	-396	1.46
No. 40 Repair	Wet	C	Left	-176	NA
No. 40 Repair	Wet	C	Center	-514	NA
No. 40 Repair	Wet	C	Right	-604	NA
No. 40 Repair	Wet	D	Left	-180	0.84
No. 40 Repair	Wet	D	Center	-392	19.82
No. 40 Repair	Wet	D	Right	-398	0.06
No. 40 Repair	Wet	Avg	Left	-223	17.07
No. 40 Repair	Wet	Avg	Center	-430	28.87
No. 40 Repair	Wet	Avg	Right	-495	0.73

Table 83. Repair material no. 41 repair slab [1 mpy = 0.0254 mm/yr].

Concrete	Exposure	Slab	Steel Location	Potential (mV, CCS)	Corrosion Rate (mpy)
No. 41 Repair	Wet	A	Left	-218	1.23
No. 41 Repair	Wet	A	Center	-233	0.89
No. 41 Repair	Wet	A	Right	-234	6.81
No. 41 Repair	Wet	B	Left	-274	5.54
No. 41 Repair	Wet	B	Center	-424	44.83
No. 41 Repair	Wet	B	Right	-341	6.81
No. 41 Repair	Wet	C	Left	-274	0.26
No. 41 Repair	Wet	C	Center	-424	5.04
No. 41 Repair	Wet	C	Right	-341	0.02
No. 41 Repair	Wet	D	Left	-343	0.09
No. 41 Repair	Wet	D	Center	-480	22.27
No. 41 Repair	Wet	D	Right	-343	8.58
No. 41 Repair	Wet	Avg	Left	-277	1.78
No. 41 Repair	Wet	Avg	Center	-390	18.26
No. 41 Repair	Wet	Avg	Right	-315	5.55

Table 84. Repair material no. 42 repair slab [1 mpy = 0.0254 mm/yr].

Concrete	Exposure	Slab	Steel Location	Potential (mV, CCS)	Corrosion Rate (mpy)
No. 42 Repair	Wet	A	Left	-151	0.08
No. 42 Repair	Wet	A	Center	-461	5.09
No. 42 Repair	Wet	A	Right	-156	0.00
No. 42 Repair	Wet	B	Left	-392	0.17
No. 42 Repair	Wet	B	Center	-464	27.80
No. 42 Repair	Wet	B	Right	-102	0.01
No. 42 Repair	Wet	C	Left	-236	0.42
No. 42 Repair	Wet	C	Center	-406	6.74
No. 42 Repair	Wet	C	Right	-230	0.00
No. 42 Repair	Wet	D	Left	-465	5.22
No. 42 Repair	Wet	D	Center	-525	10.59
No. 42 Repair	Wet	D	Right	-309	0.00
No. 42 Repair	Wet	Avg	Left	-311	1.47
No. 42 Repair	Wet	Avg	Center	-464	12.56
No. 42 Repair	Wet	Avg	Right	-200	0.00

Table 85. Repair material no. 43 repair slab [1 mpy = 0.0254 mm/yr].

Concrete	Exposure	Slab	Steel Location	Potential (mV, CCS)	Corrosion Rate (mpy)
No. 43 Repair	Wet	A	Left	-232	0.84
No. 43 Repair	Wet	A	Center	-300	2.46
No. 43 Repair	Wet	A	Right	-224	0.01
No. 43 Repair	Wet	B	Left	-279	2.16
No. 43 Repair	Wet	B	Center	-161	0.70
No. 43 Repair	Wet	B	Right	-194	0.01
No. 43 Repair	Wet	C	Left	-233	0.23
No. 43 Repair	Wet	C	Center	-205	0.38
No. 43 Repair	Wet	C	Right	-180	0.01
No. 43 Repair	Wet	D	Left	-050	0.13
No. 43 Repair	Wet	D	Center	-234	NA
No. 43 Repair	Wet	D	Right	-100	0.01
No. 43 Repair	Wet	Avg	Left	-248	0.84
No. 43 Repair	Wet	Avg	Center	-225	1.18
No. 43 Repair	Wet	Avg	Right	-175	0.01